Doctoral Dissertation

Optical Code Division Multiple Access Based Long Reach Passive Optical Network

Satoshi Yoshima

July 2013

Division of Electrical, Electronic, and Information Engineering

Graduate School of Engineering

Osaka University

Preface

This dissertation treats a long reach passive optical network (PON) using optical code division multiple access (OCDMA) technologies based on research the author carried out during his Ph. D. studies in the Division of Electrical, Electronic, and Information Engineering, Graduate School of Engineering, Osaka University, and his tenure at the Mitsubishi Electric Corporation.

Chapter 1 is an introduction of the thesis and presents the background and purpose of the study. The historical perspective and recent investigations on access networks are summarized. Optical access network technologies for high-speed, highly flexible, and long-reach transmission are then introduced. Finally, the motivation behind this study, including the reason for focusing on optical code division multiplexing (OCDM)/OCDMA, is presented.

Chapter 2 gives an overview of optical encoding/decoding techniques. Optical devices for optical encoding/decoding are also described in this chapter. Here, the pros and cons are discussed from the viewpoints of the difference in characteristics for optical encoding/decoding schemes. Finally, we introduce the properties of a multi-port encoder/decoder that can simultaneously process several optical codes (OCs).

Chapter 3 deals with 10-Gb/s burst-mode transmission. First, a 10-Gb/s burst-mode transmitter for an optical network unit (ONU) is introduced. The impedance controlled DC-coupled transmission line between a laser diode (LD) driver and a distributed feedback LD (DFB-LD) enables both a fast turn-on/off time and high-launched optical power. Next, a 10-Gb/s burst-mode receiver for an optical line terminal (OLT) is described. To meet the demand for wide dynamic range and good receiver sensitivity, continuous automatic gain control (AGC) and automatic threshold control (ATC) functions are adopted for the burst-mode receiver. In addition, the configuration of an 1/10-Gb/s dual-rate burst-mode receiver, which can be realized by utilizing a serial type transimpedance amplifier (TIA) and limiting amplifier (LIA), is described. The TIA and LIA switch their transimpedance gain, noise equivalent bandwidth, and transient response time by an external rate select signal. The results described in Chapter 3 have been published in II-1, II-6, III-1, III-4, and III-5 that are shown in the list of publications by the author.

Chapter 4 extends the 10-Gb/s time division multiplexing (TDM) PON system over OCDMA (10G-TDM-OCDM-PON) using a super-structured fiber Bragg grating (SSFBG) encoder for the ONU, a

multi-port decoder, and a 10-Gb/s burst-mode receiver for the OLT. Then, we experimentally demonstrate TDM × OCDM uplink transmission. With the assistance of forward error correction (FEC), error-free operation can be achieved in all data of the 10G-TDM-OCDM-PON. In addition, we show that the key to unprecedented symmetric uplink bandwidth is a multi-level phase-shifted encoding/decoding whereby an auto-correlation output can be preferably adopted in the burst-mode receiver. The uplink throughput performances of the 10G-TDM-OCDM-PON are also discussed. The results described in Chapter 4 have been published in I-1, II-2, II-3, II-4, III-2, and III-3 that are shown in the list of publications by the author.

Chapter 5 proposes long reach 10G-TDM-OCDM-PON systems. To achieve long reach transmission over a 65-km single mode fiber (SMF), three schemes are newly adopted in addition to 10G-TDM-OCDM-PON. First, a narrow band optical band pass filter (NB-OBPF), which can tailor the OC spectrum, is applied for the output of the multi-port encoder to transmit OC signals without dispersion compensation. Second, long reach 10G-TDM-OCDM-PON can be scaled up by aggregating 10-Gb/s TDM-PON systems using only a multi-port encoder/decoder pair in an OLT and a remote node (RN). The configuration of the ONU becomes simpler than the 10G-TDM-OCDM-PON by eliminating the encoder/decoder at each ONU. Third, an 82.5 Gsample/s over-sampling clock and data recovery (CDR) is used for a burst-mode 3R receiver. The 10-Gb/s burst-mode 3R receiver can recover a pulse width distorted signal after transmission. We experimentally demonstrate full duplex 10G-TDM-OCDM-PON transmission on a single wavelength over a 65-km SMF without dispersion compensation. Error-free operation with a FEC for all uplink and downlink data can be achieved. In addition, we discuss the causes of power penalty. The transmission penalty has been the most pressing issue in the construction of long reach 10G-TDM-OCDM-PON systems because it is the main cause of power penalty. The results described in Chapter 5 have been published in I-2, II-5, and III-6 that are shown in the list of publications by the author.

Chapter 6 summarizes the above results.

Satoshi Yoshima

July 2013

Acknowledgments

The present research has been carried out during my tenure at the Mitsubishi Electric Corporation and my doctorial course at the Department of Information and Communications Technology in the Division of Electrical, Electronic, and Information Engineering, Graduate School of Engineering, Osaka University, under the guidance of Prof. Ken-ichi Kitayama.

First, I would like to express my deepest sense of appreciation to Prof. Ken-ichi Kitayama for his professional instruction, continuous encouragement, and a number of stimulating discussions. His keen insight and wealth of creative ideas have always provided me with precise guiding frameworks for performing my research. I have learned many valuable lessons through my collaboration with him. I have been truly fortunate to have had the opportunity to work with him.

I am profoundly indebted to Prof. Kyo Inoue and Associate Prof. Akihiro Maruta of Electrical, Electronic, and Information Engineering Division for careful reviews and comments, which have improved this dissertation. I greatly thank Associate Prof. Akihiro Maruta for his invaluable guidance throughout the work on this thesis.

I am also greatly indebted to Prof. Tetsuya Takine, Prof. Seiichi Sampei, Prof. Noboru Babaguchi, and Prof. Takashi Washio of Electrical, Electronic, and Information Engineering Division for giving me sufficient basic background for this thesis.

I wish to express my sincere thanks to Associate Prof. Shinichi Miyamoto, Associate Prof. Takahiro Matsuda, and Assistant Prof. Yuki Yoshida of Electrical, Electronic, and Information Engineering Division for providing me with technical advice for this thesis.

I particularly appreciate Dr. Naoya Wada, Mr. Yoshihiro Tomiyama, and Mr. Hiroyuki Sumimoto of the Photonic Network System Laboratory, Photonic Network Research Institute, the National Institute of Information and Communications Technology for their fruitful discussions and great support for experiments. Special thanks go to Dr. Nobuyuki Kataoka, who was with the National Institute of Information and Communications Technology, for his appropriate advice about OCDMA, fruitful discussions, and hearty encouragement.

I wish to express my sincere appreciation for all the past and present colleagues of the Photonic Network

Laboratory in the Division of Electrical, Electronic, and Information Engineering, Graduate School of Engineering, Osaka University. I greatly thank Mr. Naoki Nakagawa and Mr. Yusuke Tanaka for their collaborations through this research. I also would like to thank Dr. Kiyoshi Onohara, Dr. Kensuke Ikeda, Dr. Shoichiro Oda, Dr. Yuji Miyoshi, Mr. Taro Hamanaka, Dr. Takahiro Kodama, and Mr. Ryosuke Matsumoto for fruitful discussions and continuing friendships.

I would like to thank to Prof. Gabriella Cincotti of University Roma Tre for support with the experiments.

I would like to thank Mitsubishi Electric Corporation, in particular the Information Technology R&D Center, for providing invaluable opportunities to devote myself to such exciting technological challenges. A large number of people in this company have helped me in this research.

I am particularly grateful to Dr. Shinya Fushimi for giving me the opportunity to work towards my doctorate and his generous support.

I appreciate Dr. Takashi Mizuochi for providing me with valuable comments from his considerable experience in the area of optical fiber communication, close support, and continuous encouragement. I also appreciate Mr. Masamichi Nogami for his helpful technical advice in theoretical and experimental research on optical transceivers and integrated circuits for optical fiber communication, especially in the area of high-speed burst-mode transmission.

I wish to express my sincere thanks to Dr. Kuniaki Motoshima, Mr. Hiroshi Ichibangase, Mr. Hitoyuki Tagami, Dr. Atsushi Sugitatsu, Mr. Hiroshi Aruga, Mr. Akira Takahashi, Mr. Seiji Kozaki, and Dr. Hiroaki Mukai for their technical advice, comments, and support. Special thanks go to Dr. Junichi Nakagawa for providing me with comments and advice in the area of optical access network.

I would like to express my gratitude to all the past and present colleagues of the Optical Communication Technology Department in the Information Technology R&D Center, Mitsubishi Electric Corporation. Special thanks go to Mr. Masaki Noda, Mr. Naoki Suzuki, Mr. Toshiharu Miyahara, Mr. Satoshi Shirai, Mr. Susumu Ihara, Mr. Nobuo Ohata, Mr. Eitetsu Igawa, Mr. Kenji Ishii, Mr. Ken-ichi Kobiki, Mr. Daisuke Mita, and Mr. Tetsuro Ashida, who provided me with invaluable suggestions and devoted a lot of time to me in fruitful discussions.

Finally, I would like to thank my parents, Yutaka and Mutsuko, my sister, Akiko, my paternal grandmother, Emi, and my maternal grandparents, Yasuo and Yasuyo, for their deep understanding, support, and love during the whole period of my life.

Contents

Chapter 1

Introduction

Developments to fiber-optic communication technologies have been delivering smarter and more comfortable lifestyles to people for the past several decades [1]. In 1981, the first fiber-optic transmission systems featuring a 32-Mb/s capacity were launched in Japan [2]. At first, these systems were applied only for trunk transmission. Soon after that, submarine transmission was realized by fiber-optic communication technologies. Since the first installation of fiber-optic communication systems, remarkable progress of optical fiber transmission technologies has been seen. For example, nowadays fiber-optic transmission systems with 100-Gb/s capacity per one wavelength channel can be realized [3–5], but access networks have been constructed by twisted pairs for a long time.

The remarkable expansion of Internet services, such as video on demand, online video games, file sharing, and music distribution, as well as the numerous social media services, has created a demand for high-speed access networks. In order to meet this demand, optical access networks started being introduced from the end of the 1990s. Of particular note are Gigabit Ethernet passive optical networks (1G-EPON) [6], which can deliver more than 1-Gb/s high-speed transmission and provide low-cost services for residences. Due to the spread of 1G-EPON systems, there were more than 23.2 million fiber-to-the-home (FTTH) subscribers in Japan by the end of September 2012 [7]. This growth of optical access networks comes with the demand for access networks that are higher speed, more flexible, and more intelligent.

In this chapter, historical perspective on access networks, including the architecture of optical access networks, are introduced. More recent and future optical access networks are also reviewed.

1.1 Demand for High-Speed Access Networks

The rise of new content-rich services and the increasing demand for faster services have driven the progress of high-speed access networks. Nowadays, several online services are able to be utilized, including video on demand, online video games, file sharing, and music distribution, as well as numerous social media services. These services require transmitting not only text-based content but also multimedia content including music and video. In order to satisfy the large bandwidth requirements, broadband services were installed toward the end of the 1990s in Japan. Access networks can be mainly classified into four types: copper-based digital subscriber lines (DSLs) [8, 9], which were almost asynchronous DSL (ADSL), hybrid fiber and coaxial (HFC) networks for CATV [10], fiber optic-based fiber-to-the-x (FTTX) [11], and high-speed mobile services including 3.9-generation mobile communication called long-term evolution (LTE) [12] and broadband wireless access (BWA) adopting the 2.5-GHz frequency band [13]. Here, the x of FTTX indicates home (H), building (B), curb (C), and so on, depending on the network architecture. FTTH and FTTB mean that the fiber reaches the boundary for the living space such as the home and the building, respectively. FTTC means that the fiber reaches the street cabinet, which is close to the user's premises, typically within several hundred meters. In all of the FTTX systems, a metallic cable or wireless systems such as wireless local area network (LAN) are used for networks between the optical network unit (ONU) and user terminal such as a personal computer (PC).

Figure 1.1 shows the evolution of the number of broadband service subscribers in Japan [7]. As shown in the figure, ADSL services were commercialized in the early 2000s as the first widespread broadband service to meet the new demand for high-speed data communication networks. The ADSL technologies were able to realize faster data communication services on the installed metal cable than the previous integrated services digital network (ISDN) systems with 64-kb/s. The number of DSL subscribers increased to 14.5 million in the first quarter of 2006. However, there were several issues for realizing high-speed broadband services. One was the limitation of transmission distance. The signal to noise ratio of ADSL services is degraded due to line noise in the metallic cables, which means that only low-speed services are provided for subscribers located a long distance from the central office (CO) of the service provider. The second issue was the limitation of transmission speed.

High-speed ADSL was realized by a multi-level modulation format such as 64 quadrature amplitude modulation (QAM) and high-frequency transmission higher than a normal voice telephony channel. However, the highest transmission speed of ADSL was only several Mb/s due to the transmission frequency limitation of up to several MHz. Therefore, the number of subscribers has been decreasing since 2006.

In contrast, FTTH services started to widely spread from the middle of the 2000s because they can provide symmetric high-speed communication systems more reliably than ADSL services. FTTH systems can provide faster than 100-Mb/s high-speed symmetric transmission services for each subscriber, 20-km long transmission lines, and high-quality services. This style of high-speed access system is paving the way for a new generation of broadband services. As a result, the number of FTTH users exceeded that of ADSL users at the end of June 2008. Nowadays, FTTH is the most popular broadband infrastructure in Japan. At the end of September 2012, the number of FTTH subscribers in Japan was 23.2 million. In addition, the number of subscribers of CATV services has gradually increased. From the beginning of 2012, the number of subscribers of broadband mobile services, including the 3.9G mobile service and BWA, has rapidly increased because mobile phones with more advanced computing and connectivity ("smartphones") can access the Internet easily and from anywhere. These broadband mobile services will play an important role in broadband services in the near future.

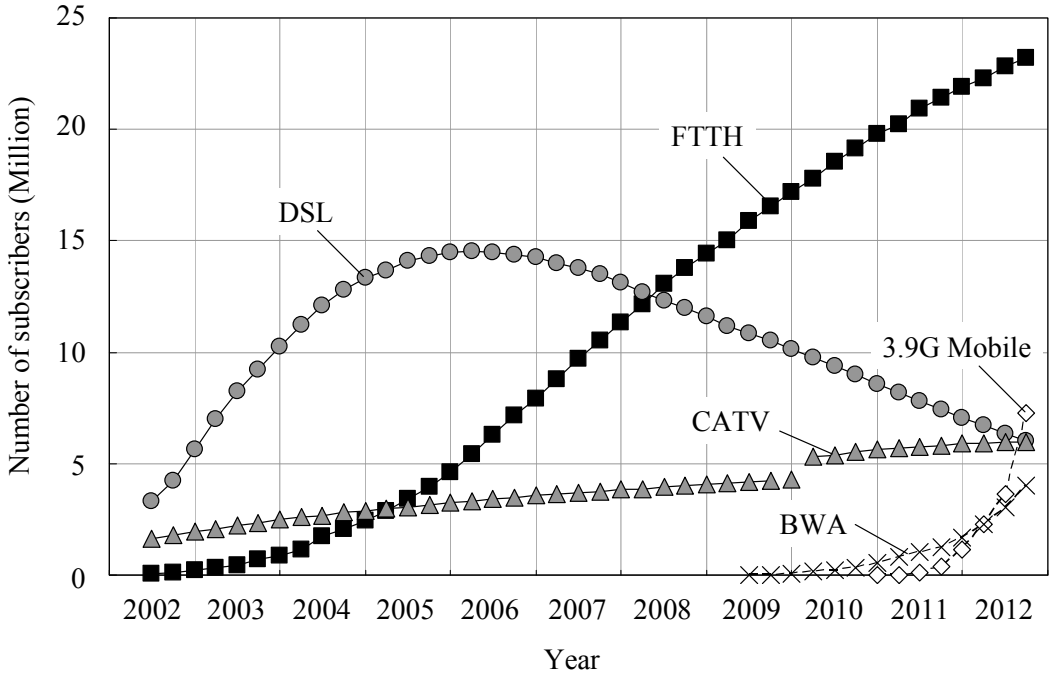

Fig. 1.1: Number of broadband subscribers in Japan.

(Based on Ministry of Internal Affairs and Communications Japanese Government Report)

1.2 Architecture of Optical Access Network

Figure 1.2 shows the topologies of optical access systems [14, 15]. In general, there are three categories of architecture to realize an optical access network. One is the point-to-point (P2P) system shown in Fig. 1.2(a), which is the basic configuration for optical access networks. This system features a CO comprised of several media converters connected to each residential user. In this P2P network, individual fibers run from a CO to each residential home. Another architecture is the point-to-multipoint system (P2MP) with an active switch, which is called active star architecture. In this network, only one fiber is installed between a CO and an active switch, and the CO needs only one media converter to communicate with all residential homes. The total cost of the active star architecture is less than that of the P2P system because there is only one media converter per CO and only one feeder fiber between a CO and an active switch. However, the active switch requires powering and maintenance, and it should be capable of operation over a wide temperature range because it is an outdoor device. The other architecture is the P2MP with passive devices such as optical splitters, which is called passive star architecture or passive optical network (PON). In this architecture, a CO is connected to each residential home via an optical power splitter. In a PON system, subscriber equipment, which is called an ONU, can be accommodated by a single piece of CO equipment called an optical line terminal (OLT). This architecture reduces costs because a splitter requires no power supply and little maintenance. As a result, PON systems currently play the main role in optical access networks.

PON systems feature four optical access technologies: time division multiple access (TDMA) [16], wavelength division multiple access (WDMA) [17], orthogonal frequency division multiple access (OFDMA) [18], and optical code division multiple access (OCDMA) [19]. Figure 1.3 compares these technologies using their schematic representations. In the TDMA, each ONU upstream time slot is controlled by an OLT access controller to avoid collisions. As a result, upstream packets from the ONUs are time-interleaved at the power splitter. The OLT receiver has to adjust its gain, threshold, and clock synchronization to receive burst signals because the transmission loss and time slot of each ONU are different [20–22]. The TDM-PON plays the main role in optical access systems due to low cost capable equipment. Although the cost of a burst-mode receiver and an access controller is higher than that of other equipment, they can be shared by all of the residential users. There has been a tremendous amount of research and development on TDMA systems, going all the way back to the first proposal of TDM-PON systems back in 1987 [23, 24]. Early experiments and field trials were performed using the synchronous transfer mode (STM) and the

asynchronous transfer mode (ATM). In Japan, the first commercial system was launched as a STM-PON with 16-Mb/s in 1997 [25]. After that, the broadband PON (B-PON) with 622-Mb/s [26], 1G-EPON with 1.25-Gb/s [6], and Gigabit-capable PON (G-PON) with 2.5-Gb/s [27] capacities were standardized in 2001, 2004, and 2004, respectively. These systems have also been commercially launched all over the world for use in FTTX systems.

In WDMA networks, a wavelength channel is assigned to each ONU. There is no interaction or coupling between subscribers. As a result, each subscriber gets a dedicated point-to-point path to an OLT. In a typical WDMA, wavelength channels are multiplexed or demultiplexed by an arrayed waveguide grating (AWG) instead of an optical power splitter, as shown in Fig. 1.3(b). WDMA networks require wavelength selected transceivers for each ONU. This "colored" ONU increases the network cost. To resolve this, research on WDMA networks with an injection-locked Fabry-Perot laser diode or a reflective semiconductor optical amplifier (RSOA) as a "colorless" ONU transmitter have been energetically pursued [28–30]. However, at present, there have only been field trials in limited regions such as Korea, and thus far there has been no large scale commercial deployment.

In OFDMA networks, the overall bandwidth is divided into orthogonal subcarriers. Each ONU is allocated one or more subcarriers that can be realized by fast Fourier transform (FFT) and inverse FFT (IFFT). Different modulation formats can be assigned for each subcarrier based on the channel conditions and the transmitter frequency response. In addition, the upstream bandwidth of each ONU can be changed by changing the assigned number of subcarriers. Therefore, OFDMA networks can provide flexibility and scalability for each ONU. OFDMA has functioned as the major access technology in RF communications such as LTE. Nevertheless, its application to optical communication is challenging because high-speed digital signal processing (DPS) is expensive for optical access networks and the synchronization of multiple upstream laser frequency offset from each ONU is difficult. In recent years, several studies have reported methods for realizing OFDMA-PON. In 2007, 10-Gb/s optical OFDMA transmission using a direct modulated laser (DML) in a 2.5-GHz channel bandwidth was experimentally demonstrated offline, for the first time [31]. Recently, real-time 40-Gb/s WDM-OFDMA-PON transmission has been demonstrated using a field programmable gate array (FPGA)-based DSP [32]. In addition, to realize a bandwidth-elastic and power-efficient OFDMA network, coherent interleaved frequency division multiple access (IFDMA) has been proposed and experimentally demonstrated [33, 34].

In an OCDMA network, upstream signal transmission is realized by the optical encoder (ENC) and optical decoder (DEC). OCDMA can multiplex a number of channels on a single wavelength and identical time slot by using different optical codes for each channel, similar to spread-spectrum wireless CDMA [35]. In contrast to the frequency spread/despread, time and/or optical frequency

spread/despread techniques are adopted in OCDMA. OCDMA has been studied and experiments have been performed since the 1980s [36, 37]. Early studies showed promise in overcoming some of the nagging drawbacks in those days, which included laser frequency drift, broad laser line widths, and limited hardware speeds. In recent years, coherent OCDMA has been energetically studied in pursuit of its unique characteristics such as high frequency efficiency, good correlation performance, low signal processing latency, and asynchronous access capacity [19]. Encoding/decoding of a coherent time-spreading (TS)-OCDMA system has been realized by using compact optical passive devices such as a super-structured fiber Bragg grating (SSFBG) [64] and/or a multi-port optical encoder/decoder in an AWG configuration [67]. Recently, a field trial of 3-WDM × 10-OCDMA × 10.71-Gb/s, asynchronous 111-km transmission [97] and an experimental demonstration of asynchronous 4 × 40-Gb/s full-duplex transmission [38] have been achieved.

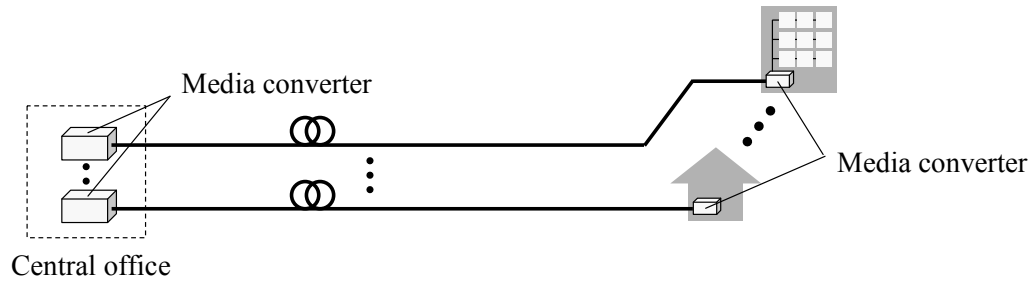

(a) Point-to-point architecture

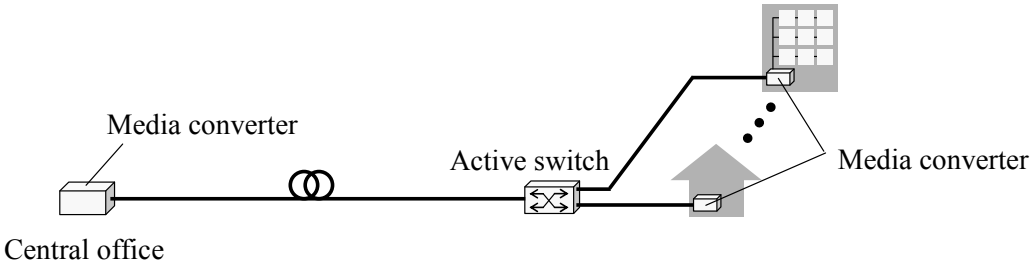

(b) Active star architecture

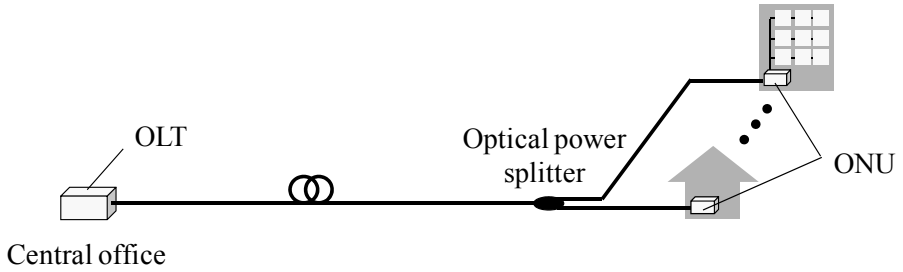

(c) Passive optical network

Fig. 1.2: Architectures of optical access network.

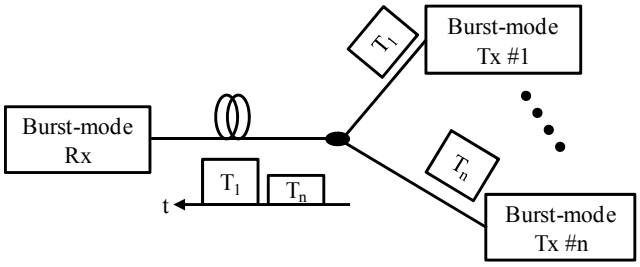

(a) TDMA

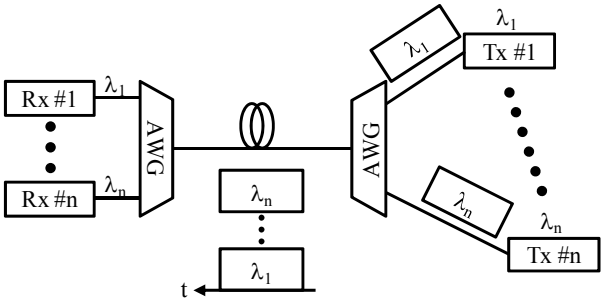

(b) WDMA

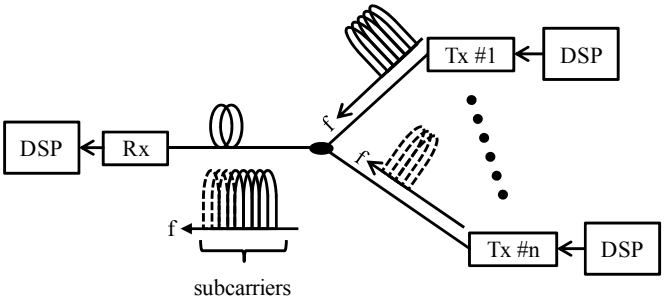

(c) OFDMA

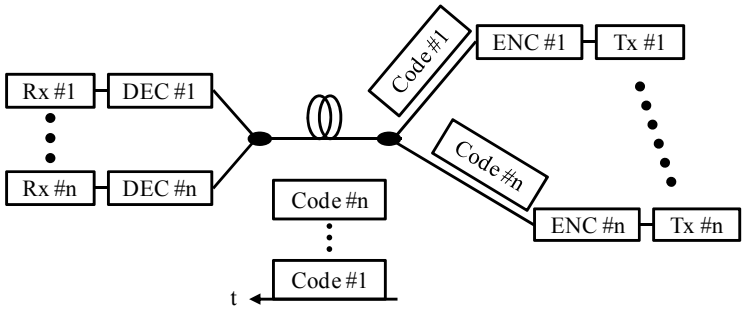

(d) OCDMA

Fig. 1.3: Optical access technologies.

1.3 Roadmap of Optical Access Network

Figure 1.4 shows the roadmap of optical access network technologies [45–50]. Currently, 1-Gb/s TDM-PON systems including 1G-EPON and G-PON have become widely spread thanks to a bit rate higher than 1.25 Gb/s, a possible number of shared users as high as 32, and a transmission length of 20 km. In order to meet the demand for high-speed optical access systems, 10-Gb/s TDM-PON systems including 10-Gigabit Ethernet PON (10G-EPON) [39, 43] and 10-Gigabit-capable PON (XG-PON) [40, 44] were standardized in 2009 and 2010, respectively. These 10-Gb/s TDM-PON systems are called next-generation PON1 (NG-PON1). For NG-PON1, the most crucial challenge is high-speed 10-Gb/s burst-mode transmission. In order to realize 10-Gb/s TDM-PON systems, research on 10-Gb/s burst-mode transmitters [68, 71–73], receivers [69, 74–84], and clock and data recovery (CDR) [86–88] have been pursued. Furthermore, in recent years, 40-Gb/s capable NG-PON2 has been energetically discussed in the full service access network (FSAN) [41]. As a result of this discussion, hybrid TDM and WDM PON (TWDM-PON) systems, which are realized by 4 wavelength channels multiplexed for both upstream and downstream, will be standardized as an NG-PON2 [51, 52, 90]. The reason the TWDM-PON is selected as the NG-PON2 is that TWDM-PON is more cost-effective compared with other proposed methods such as high-speed TDM, orthogonal frequency division multiplexing (OFDM), and so on. On the other hand, several approaches, including high-speed TDM, dense WDM (DWDM), OCDM, and OFDM, have been proposed to realize a capacity larger than 40-Gb/s that is more flexible and enables higher functionality of optical access networks. These high-capacity networks are called NG-PON3.

NG-PON1 is required for the coexistence with the current 1-Gb/s TDM-PON that has been widely installed. In addition, network operators require that NG-PON2 preferably support operation over legacy power splitter-based PONs and possibly aggregate several such legacy PONs in order to reduce total costs of building and operating optical access networks [49]. Moreover, long-reach transmission longer than 40 km and a high splitting ratio of more than 64 are required for NG-PON2 to expand the coverage area. Especially, long-reach transmission is strongly required because metro-access hybrid networks can be costly by aggregating OLT equipment with a metro ring node. Now, standardization activity for NG-PON3 by applying revolutionary technologies has not yet started because NG-PON2 has not been realized by revolutionary technologies as originally envisioned but by the evolutional technologies of TWDM. However, the requirements for NG-PON3 will be increased sooner or later. For NG-PON3, there are two potential approaches in terms of optical distribution network (ODN) migration. One is coexistence on the legacy ODN. The other is a

modified ODN, which means addition to or modification of the ODN outside the OLT site. Coexistence on the same ODN is a preferable alternative, but there is little wavelength region available for NG-PON3. Therefore, high spectral efficiency will be necessary for NG-PON3 in order to coexist with legacy networks.

OCDMA has unique characteristics capable of multiplexing a number of channels on a single wavelength and an identical time slot with up to 40-Gb/s capacity per channel. Especially, OCDMA with multi-level phase shift keying (PSK) optical code theoretically realizes good spectral efficiency. For example, 10G-OCDMA with a 16-level PSK optical code can achieve 0.8 bit/s/Hz when a 16-channel with 12.5-GHz channel spacing is multiplexed within a 200-GHz bandwidth [67]. This spectral efficiency, which is as high as current long-haul WDM systems, can be realized because 40-Gb/s differential quadrature phase shift keying (DQPSK) WDM systems with a 50-GHz channel spacing have 0.8 bit/s/Hz. Therefore, OCDMA is suitable for NG-PON3 because it can realize high spectral efficiency in optical access networks that require multiple access technologies.

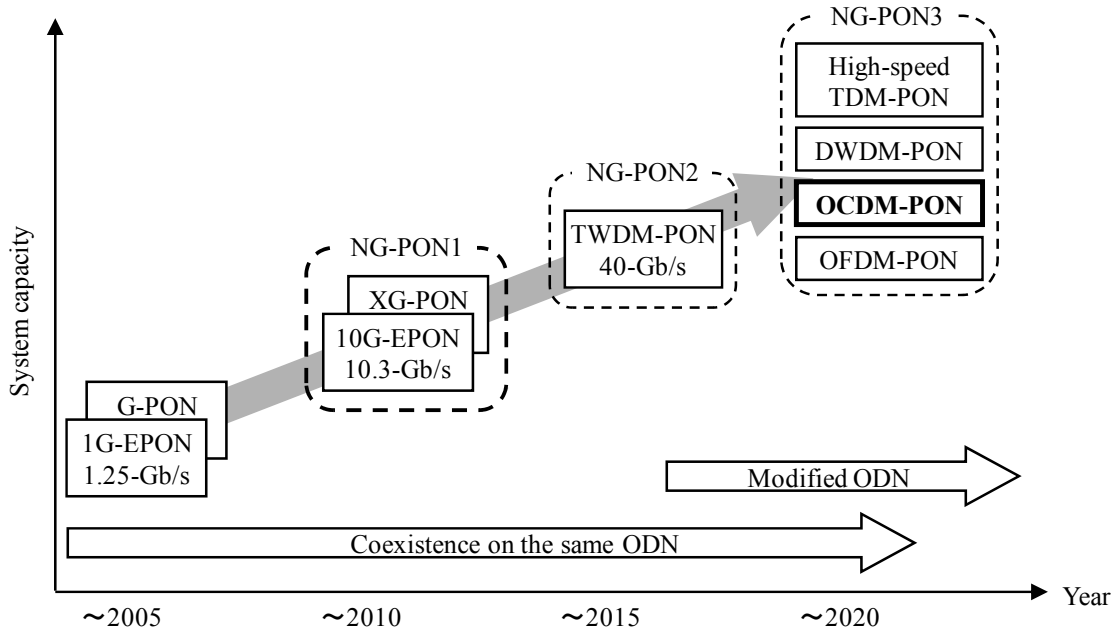

Fig. 1.4: Roadmap of optical access network technologies.

1.4 Purpose of This Study

There are three issues for realizing high-speed, high spectral efficiency, long-reach optical access systems. The first is a 10-Gb/s burst-mode transmitter/receiver. In order to launch the NG-PON1, 10-Gb/s bust-mode transceivers with a fast burst-mode response time, a high power budget, and a wide dynamic range are required. The second one is a hybrid TDM × OCDM transmission. In future optical access networks following NG-PON2, hybrid multiplexing technologies such as TWDM will become the mainstream because it will be difficult to realize high-speed, cost-effective networks by adopting only one access technology. OCDMA has huge potential to realize the high-speed and flexible optical access networks described in the previous section. Several hybrid OCDM × WDM networks have been studied [19, 97], but few OCDM × TDM hybrid networks have been reported due to the lack of a high-speed burst-mode transceiver. Feasibility studies of a 1-Gb/s TDM × OCDM hybrid system have been reported, where an SSFBG encoder/decoder and a burst-mode receiver for 1G-EPON were used [42]. However, a TDM × OCDM capable of more than 10-Gb/s has not been reported. The third issue is a long reach transmission to directly connect an existing optical access network to a metro network. Recently, a long-distance transmission over a 100-km single mode fiber (SMF) without inline dispersion compensation was achieved by tailoring the optical spectrum of the encoded signal in an OCDMA-PON system [101]. However, there still remains a long reach transmission of 10-Gb/s burst-mode optical code signal without dispersion compensation.

In this thesis, we study a 10-Gb/s burst-mode transmitter and receiver for realizing a 10-Gb/s TDM-PON system. In addition, we propose a 10-Gb/s TDM × OCDM hybrid PON system (10G-TDM-OCDM-PON) and investigate long reach 10G-TDM-OCDM-PON systems that can realize direct connections between metro and access networks.

1.5 Overview of the Dissertation

Figure 1.5 shows the organization of this thesis. Following the introduction of optical encoding and decoding schemes in OCDM networks in Chapter 2, 10-Gb/s burst-mode transmitter and receiver techniques are described in Chapter 3. The 10G-TDM-OCDM-PON and long reach 10G-TDM-OCDM-PON systems are proposed in Chapters 4 and 5, respectively. The contents of

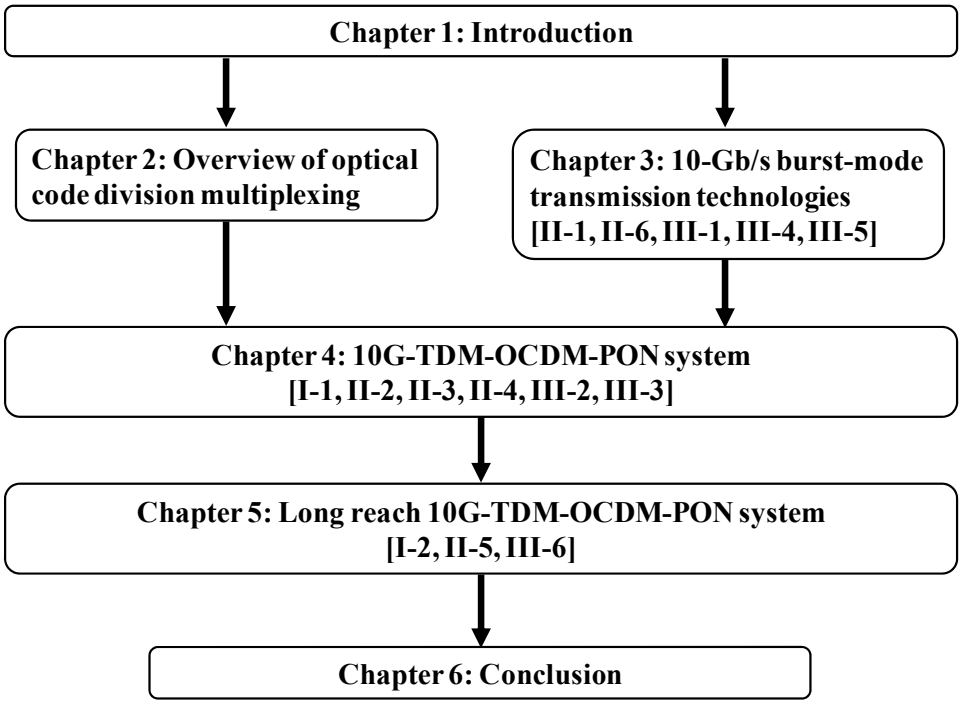

Fig. 1.5: Organization of the thesis.

each chapter are summarized as follows.

Chapter 2 describes the optical encoding and decoding techniques. The fundamentals of the optical encoding and decoding schemes adopting a planer lightwave circuit (PLC), an FBG, and an AWG are introduced in this chapter. Then, we introduce the properties of a multi-port encoder/decoder for a PSK optical code (OC). This multi-port encoder/decoder is suitable for our proposed long reach 10G-TDM-OCDM-PON systems because it can process several OCs at the same time.

In Chapter 3, the 10-Gb/s burst-mode transmitter and receiver are described. First, we show the block diagram and optical performances of the 10-Gb/s burst-mode transmitter. In order to realize fast turn-on/off time, a laser driver and a distributed feedback laser diode (DFB-LD) are connected by an impedance controlled DC coupling transmission line. Second, the configuration and performances of the 10-Gb/s burst-mode receiver are described. The 10-Gb/s burst-mode receiver can deliver a fast receiver settling time and a wide dynamic range by adopting continuous automatic gain control (AGC) and automatic threshold control (ATC) for a transimpedance amplifier and a limiting amplifier. The configuration of the dual-rate receiver, which can be realized by switching its transimpedance gain and equivalent noise bandwidth, is also described. The results described in Chapter 3 have been published in II-1, II-6, III-1, III-4, and III-5 that are shown in the list of publications by the author.

In Chapter 4, we propose a 10G-TDM-OCDM-PON system that multiplexes 10-Gb/s TDM-PON systems by using OCDMA techniques. The proposed system is able to increase the total capacity without sacrificing the uplink bandwidth currently assigned to each ONU. A 16-ONU (4-OCDMA × 4-packet) uplink burst transmission is experimentally demonstrated by using a hybrid 16-chip (200 Gchip/s), 16-phase-shifted SSFBG encoder/multi-port decoder and a burst-mode receiver along with forward error correction (FEC). Finally, we discuss how the newly introduced multi-level phase-shifted encoding/decoding, with which auto-correlation waveform can be preferably adopted in the burst-mode reception at 10-Gb/s, is the key to the proposed system. The results described in Chapter 4 have been published in I-1, II-2, II-3, II-4, III-2, and III-3 that are shown in the list of publications by the author.

In Chapter 5, we propose a long reach 10G-TDM-OCDM-PON architecture using only a multi-port encoder/decoder pair at an OLT and a remote node (RN), which eliminates the need for an encoder/decoder at each ONU. The 10G-TDM-OCDM-PON can be scaled up by aggregating 10-Gb/s TDM-PON systems with OCDMA techniques. In addition, a narrow band optical band pass filter (NB-OBPF) enables a long reach transmission of 10G-TDM-OCDM-PON systems without dispersion compensation by tailoring the optical spectrum. In the long reach 10G-TDM-OCDM-PON system, full duplex 4-packet × 4-OC transmission on a single wavelength over a 65-km SMF without dispersion compensator is demonstrated by using a 16 × 16 multi-port encoder and decoder, an NB-OBPF, and a 10-Gb/s burst-mode 3R receiver. We also discuss the sources of power penalty in the proposed long reach 10G-TDM-OCDM-PON system. The results described in Chapter 5 have been published in I-2, II-5, and III-6 that are shown in the list of publications by the author.

Chapter 6 concludes the dissertation with a summary of the overall results.

Chapter 2

Overview of Optical Code Division Multiplexing

2.1 Introduction

This chapter introduces the OCDM technologies, including optical encoding and decoding, on which the long reach 10G-TDM-OCDM-PON system proposed in this thesis are based. In Section 2.2, fundamental mechanisms of an optical encoding and decoding are described. There are several approaches to encode optical plain data in time and/or wavelength domains. Section 2.2 focuses on a time domain coherent decoding scheme that can deliver better correlation performances than other schemes. Section 2.3 describes the configuration of optical devices for optical encoding/decoding including optical delay lines, a planar lightwave circuit (PLC), a fiber Bragg grating (FBG), and an arrayed waveguide grating (AWG). In particular, the optical encoder/decoder with an AWG configuration, called a multi-port encoder/decoder, has remarkable characteristics that can process several optical codes simultaneously. Section 2.4 shows the details of the multi-port encoder/decoder configuration and correlation performances [67].

2.2 Principle of Optical Encoding/Decoding

2.2.1 Optical Encoding

An optical encoding operation optically transforms each data bit into an optical code before transmission. Optical encoding involves translating a data bit by a code sequence either in the time domain or the wavelength domain, or in a combination of the two called two-dimensional coding (2D-coding) [54]. Figure 2.1 shows an illustration of these classifications.

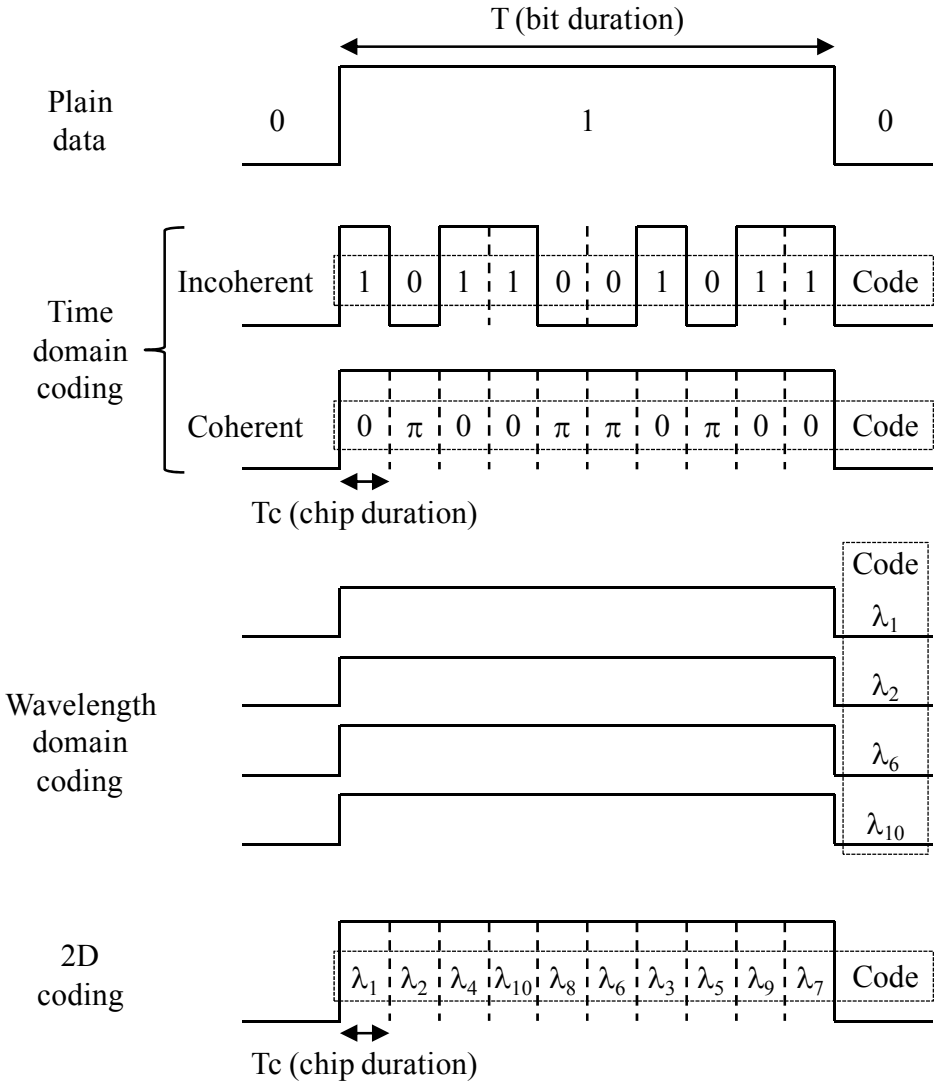

Fig. 2.1: Classification of different optical encoding schemes.

In a time-domain optical encoded signal, each bit is split into time components shorter than the original bit slot, called chips. This type of time-domain optical encoding scheme can be classified into two categories: an incoherent scheme [36, 37] and a coherent scheme [55]. In the time-domain incoherent optical encoding scheme, the optical intensity is manipulated but the phase is not. In contrast, in the time-domain coherent optical encoding scheme, the phase of the optical signal is manipulated. The benefit of the incoherent scheme is that it can be realized by an incoherent light source. However, the correlation property of the incoherent scheme is poorer than that of the coherent one because of its unipolar characteristic.

In the wavelength-domain optical encoding signal, one encoded signal consists of a unique subset of wavelengths forming the code. The encoding process is based on Fourier transform and does not require the high-speed optical modulators used in time-domain encoding systems. 2D-coding combines the above time-domain chip spreading and wavelength selection. One data bit is encoded as consecutive chips of different wavelengths, forming a unique wavelength sequence in time constituting one optical code.

2.2.2 Optical Decoding

At a receiver, an optical decoding operation reverse to the encoding process is performed to recover the original data in the optical domain. Figure 2.2 shows an example of optical decoding for a time-domain coherent binary phase shift keying (BPSK) code. The transmitted signal is encoded by an 8-chip BPSK signal as (π, π, π, π, 0, 0, 0, 0). There are two optical decoders, to which different optical code sequences are assigned, at the receiver. The optical decoder, to which the same optical code sequence of an incoming signal is assigned, outputs the auto-correlation, which has a large peak in the center of the output waveform (as shown in Fig. 2.2(a)) because of the exact matching of an incoming code sequence. The other optical decoder, to which a different optical code sequence such as (π, π, 0, 0, π, π, 0, 0) is assigned, outputs the cross-correlation, which has no large peak [55] (as shown in Fig. 2.2(b)). Note that the cross-correlation output does not vanish perfectly. This unwanted signal appears as noise in the decoder output, which is called multiple access interference (MAI) noise. MAI is the principal source of noise in OCDM systems. The larger the number of multiplexed optical codes used, the larger the MAI noise output. This MAI noise degrades the performance of OCDM systems. In order to suppress it, optical thresholding [56] and/or optical time gating [57] have been proposed. These approaches can improve the system performance, but it is costly to introduce optical thresholding devices, and

optical time gating limits the asynchronous operation. It is important for an OCDM network to choose a proper code having a good correlation performance. Several optical codes, such as M sequence and gold codes, have been proposed to meet such requirements [19]. Code length is also an important factor in system design, because a longer code length delivers a good correlation property, whereas the bit rate of plan data is limited by the product of the code length and the chip duration.

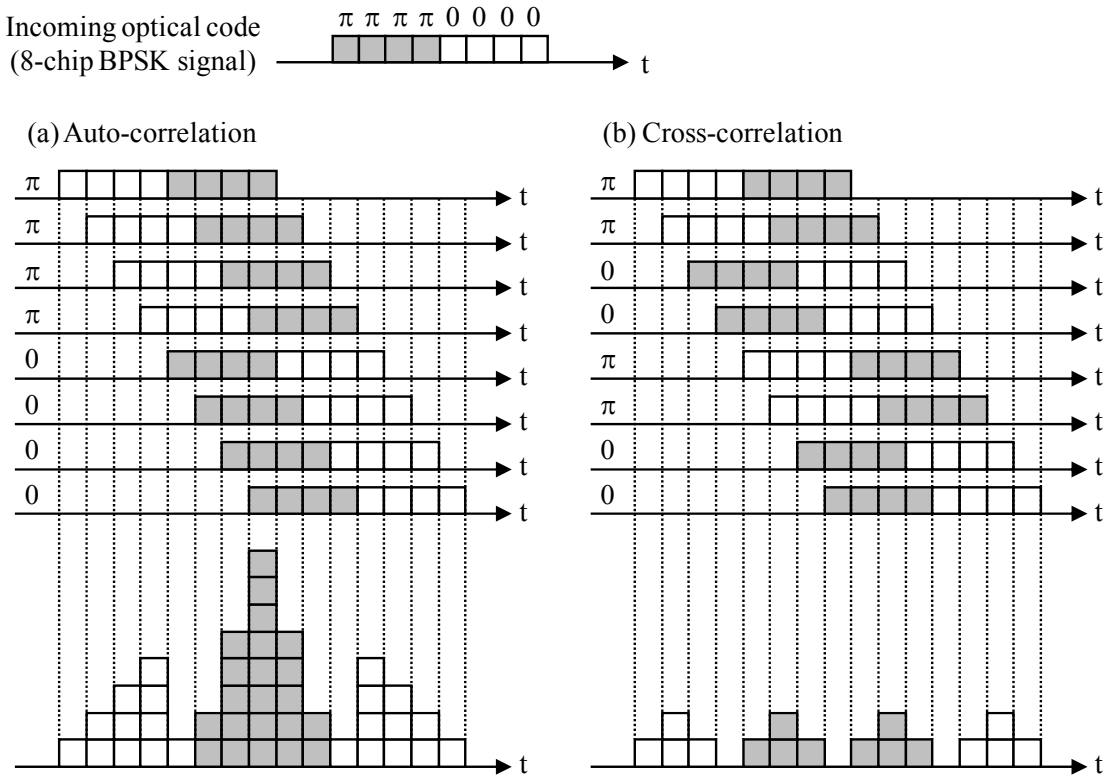

Fig. 2.2: Auto-correlation and cross-correlation output of time-domain coherent optical code.

2.3 Optical Devices for Optical Encoding/Decoding

Figure 2.3 shows several approaches for optical encoding and decoding [58–66]. In a scheme that demonstrated OCDMA for the first time, an input laser pulse is split into a set of delay lines in order to realize incoherent optical orthogonal codes (OOCs), as shown in Fig. 2.3(a). To passively generate an OOC, a bank of delay lines is placed between a splitter and a combiner. The combination of delay lines determines the optical code strain. At the receiver side, received signals are decoded in the electric domain, where a suitable clock recovery circuit is required [59]. Figure

2.3(b) shows the configuration of the spectral encoding technique using optical gratings, lenses, and a phase or amplitude mask [60, 61]. The phase or amplitude mask is placed in the Fourier plane to imprint a code sequence onto the spatial frequency spectrum. The signal is then reflected by the second diffraction grating to recombine the spectrum into one spatial mode, which is coupled into a fiber. The decoding process is reciprocal to the encoding scheme. For a time-domain coherent optical code, a PLC device consisting of tunable taps and thermo-controlled optical phase shifters has been proposed, as shown in Fig. 2.3(c) [62]. The phase shifter is an optical waveguide partly covered with a heater electrode. The optical carrier phase can be varied by changing the temperature of the waveguide that changes the waveguide refractive index. In this optical encoding, an input single pulse is duplicated to a set of chip pulses with an identical amplitude, and the optical carrier of each chip pulse is phase-shifted to either 0 or π by phase shifters. Then, the chip pulses are recombined by an optical combiner to form a bipolar signature code. In optical decoding, the same procedure as that in the encoding is performed for all incoming optical code sequences. This architecture has several benefits in terms of tunability and controllability for changing an optical code sequence. However, it does have some drawbacks, such as polarization dependency and the impossibility of realizing long code sequences due to constraints in device fabrication. Figure 2.3(d) shows the block diagram of an optical encoder with an FBG [63–65]. The FBG can easily generate a PSK optical code longer than the above PLC encoder can due to its low insertion loss. Actually, a long 511-chip 640-Gchip/s signal coded by a super-structured FBG (SSFBG) has been reported [66]. This long PSK code can realize a 10-user truly asynchronous 1.25-Gb/s coherent OCDMA network.

Figure 2.4 shows a SSFBG configuration and an OC generation scheme [64]. A SSFBG is defined as an FBG with a slowly varying refractive-index modulation profile imposed along its length [100]. In addition, a complex refractive-index modulation profile can be realized in an SSFBG by inserting phase shifts between different segments, as shown in Fig. 2.4(a). The input optical short pulse can penetrate the whole grating length, and the individual segments of the grating contribute more or less equally to the reflected response when the lengths of all segments are all the same as L_{chip} and the refractive-index modulation is constant along the whole grating. The phase-shifted SSFBG thus works as an optical transversal filter to generate a PSK OC from its impulse response, and it can also perform correlation for OC recognition. Figure 2.4(b) shows the principles of BPSK OC generation. This sort of phase-shifted SSFBG can be fabricated with a single short phase mask of length L_{chip} by continuous grating writing [100] or holographic techniques [65]. These techniques provide a high flexibility in producing different long optical code. High-precision phase control can be achieved as well for PSK OCs.

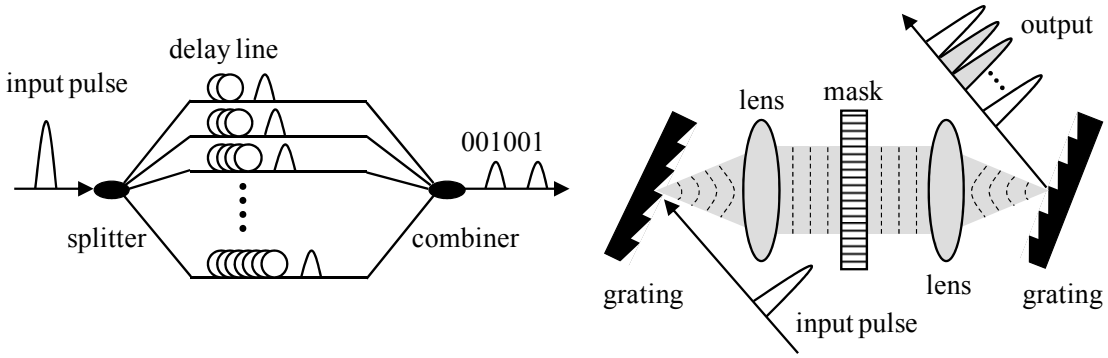

(a) A set of the delay lines for OOC (b) Gratings, lenses, and a mask for frequency spread OC

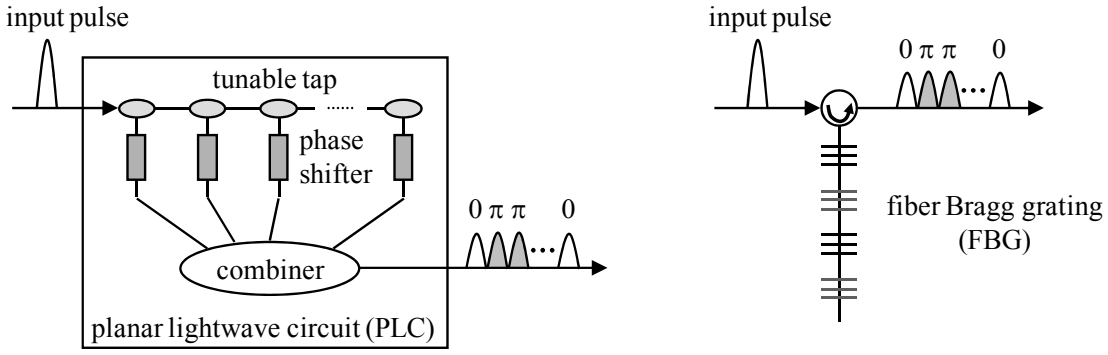

(c) PLC for PSK OC (d) FBG for long length OC

Fig. 2.3: Optical encoding/decoding devices.

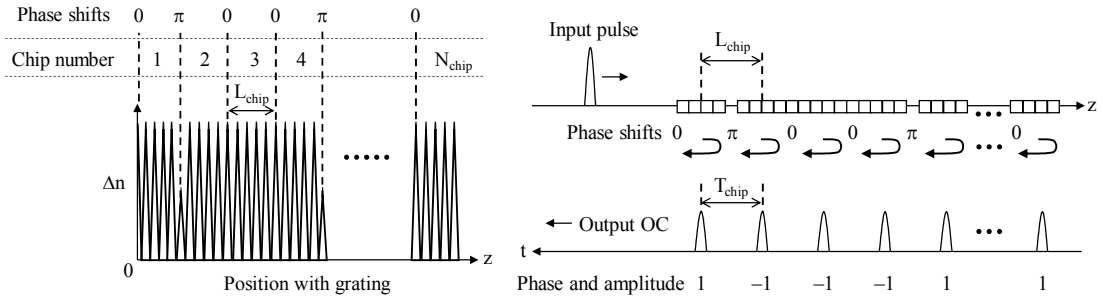

(a) SSFBG configuration (b) Working principle for BPSK OC generation

Fig. 2.4: SSFBG with phase shifts for BPSK OC.

Recently, as described in the previous chapter, most optical access networks have been constructed in a PON configuration, i.e., a point-to-multipoint network. Therefore, it is desired to generate multiple optical codes by a single optical device, especially for OLT sides. A novel multi-port optical encoder/decoder was proposed by adopting an AWG configuration, which is known as a wavelength multiplexer/demultiplexer. Figure 2.5 shows the configuration of this multi-port encoder/decoder and its operation [67]. Here, the numbers of input and output ports are equal to *N*. An incoming optical short pulse is input from an arbitrary input port. *N* copies of the

input pulse are generated in the input slab coupler. The optical pulses travel through different paths in the grating, and then the output slab coupler recombines them to build *N* copies at the device outputs. Each PSK code is composed of *N* optical chips, and the differential path delay in the grating is set to be larger than the input pulse width so that chips in the OC do not overlap in time. This multi-port encoder/decoder is able to measure the correlation between any pair of codes, simultaneously. In fact, if an OC is sent to the input port, an auto-correlation peak (ACP) appears at one of output ports and low power cross-correlation signals appear at the others, univocally determining the incoming OC.

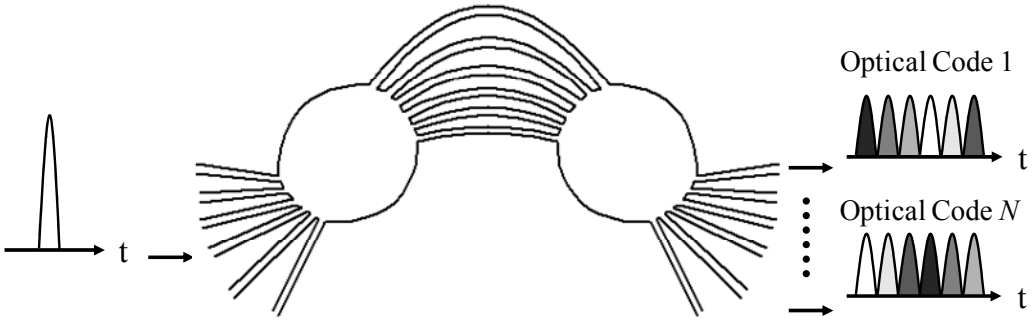

(a) Optical encoding diagram

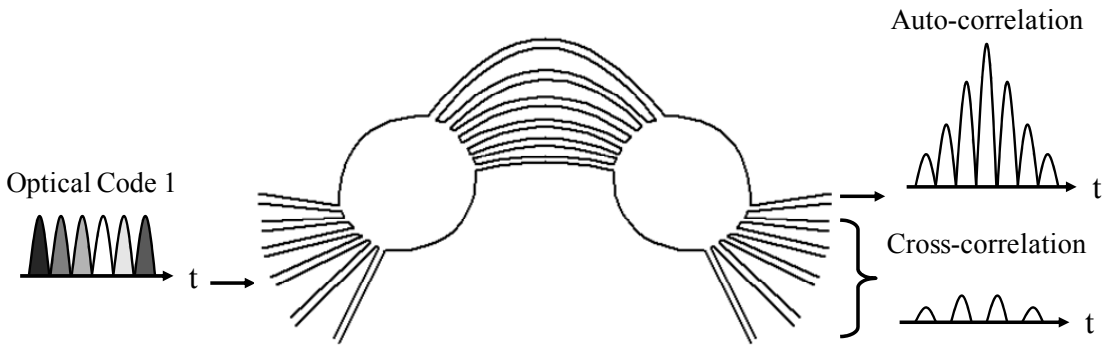

(b) Optical decoding diagram

Fig. 2.5: Multi-port encoder/decoder with AWG configuration.

2.4 Multi-Port Encoder/Decoder

2.4.1 Configuration of Multi-Port Encoder/Decoder

The mechanism to build a set of OCs can be easily described by analyzing the AWG in the time domain. Referring to Fig. 2.6 and the parameters listed in Table 2.1, the impulse response from input port *i* to output port *k* can be written as

$$h_{ik}(t) = \sum_{l=0}^{N-1} \exp\left[-\mathbf{j}\pi \frac{n_s d}{\lambda}(2l - N + 1)(\sin\theta_i + \sin\theta_o) \right] \times \delta\left(t - n_s \frac{L + l\Delta L}{c} \right)$$
$$i,k = 0,1,\ldots N-1, \quad (2.1)$$

where $\mathbf{j} = \sqrt{-1}$, $\delta(t)$ is the Dirac's delta function, L is the shortest waveguide length, and θ_i and θ_o are the diffraction angles in the input and output slab couplers, respectively

$$\sin\theta_i \cong (2i - N + 1)\frac{d_i}{2R}, \qquad \sin\theta_o \cong (2k - N + 1)\frac{d_o}{2R}. \quad (2.2)$$

For the sake of simplicity, L is assumed to be 0, as its value affects a constant time delay but not the code generation process. The chip interval, i.e., the time interval between two consecutive pulses in each code, is $\Delta\tau = n_s \Delta L / c$, which equals the inverse of the free spectrum range (FSR) of an AWG multiplexer/demultiplexer, and the correlation time is given by $(N-1)\Delta\tau$. From the parameters listed in Table 2.1, $\Delta\tau = 5$ ps.

The exponential term in Eq. (2.1) corresponds to the phase of each chip in the code. We set $d_i = d_o$, i.e., identical spacing in the input and output gratings. Equation (2.1) can then be reduced to

$$h_{ik}(t) = \sum_{l=0}^{N-1} \exp\left[-\mathbf{j}\frac{\pi}{N}(2l - N + 1)(i + k + 1) \right] \times \delta(t - l\Delta\tau)$$
$$i,k = 0,1,\ldots N-1. \quad (2.3)$$

The OCs are *N*-array PSK codes. For a given input port *i*, the code generated at output port $k = N - i - 1$ has all chips with an identical phase.

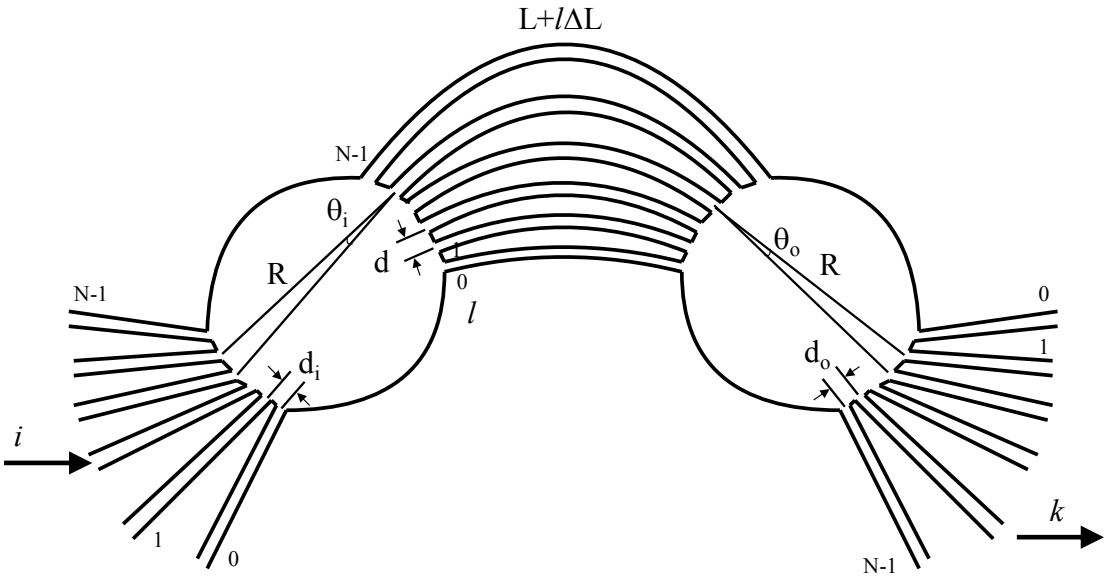

Fig. 2.6: Multi-port encoder/decoder configuration.

Table 2.1: Parameters of multi-port encoder/decoder.

Symbol	Description	Value	Unit
f_0	Carrier frequency (λ = 1550.984 nm)	193.292	THz
N	Number of ports	16	–
R	Input/output slabs focal length	20.85	mm
d	Spacing of waveguide array at the input/output slab couplers	24.6	μm
w_g	AWG waveguide width	7	μm
d_i	Input waveguide spacing at the input slab coupler	56.47	μm
d_o	Output waveguide spacing at the output slab coupler	56.47	μm
w	Waveguide width in the input/output grating	50	μm
ΔL	Differential path length	1.0316	mm
n_s	Effective refractive index	1.468	–

2.4.2 Correlation Property

According to Parseval's theorem, the correlation function between two OCs generated at output ports *k* and *k*' can be evaluated in the frequency domain as

$$h_{ik}(t) * h_{ik'}(t) = \int_{-\infty}^{\infty} H_{ik}(f) H_{ik'}(f) \exp(\mathbf{j}2\pi f t) dt$$

$$k, k' = 0,1,\ldots N-1, \quad (2.4)$$

where $*$ denotes the convolution unit and $H_{ik}(f)$ is the transfer function from the input port *i* to the output port *k*, obtained by the Fourier transform of Eq. (2.3) as

$$H_{ik}(f) = \sum_{l=0}^{N-1} \exp\left[-\mathbf{j}\pi(2l-N+1)\left(\frac{i+k+1}{N} + f\Delta\tau\right)\right]$$
$$= \exp\left[-\mathbf{j}\pi(N-1) f\Delta\tau\right] \frac{\sin\left[\pi(i+k+1+Nf\Delta\tau)\right]}{\sin\left[\pi\left(\frac{i+k+1}{N} + f\Delta\tau\right)\right]}$$

$$i, k = 0,1,\ldots N-1. \quad (2.5)$$

The power spectra of output port *k* are plotted in Fig. 2.7. Two OCs are orthogonal when the cross-correlation function of Eq. (2.4) vanishes everywhere, which happens when the two corresponding transfer functions $H_{ik}(f)$ and $H_{ik'}(f)$ do not overlap with each other and their product is zero. Therefore, Eq. (2.4) indicates the code-recognition capability of a full encoder/decoder, and the lower the crosstalk between two adjacent frequency channels, the "more orthogonal" the corresponding OCs. OCs generated at two adjacent outputs are "less orthogonal" since the crosstalk between two adjacent frequency channels is higher than the others.

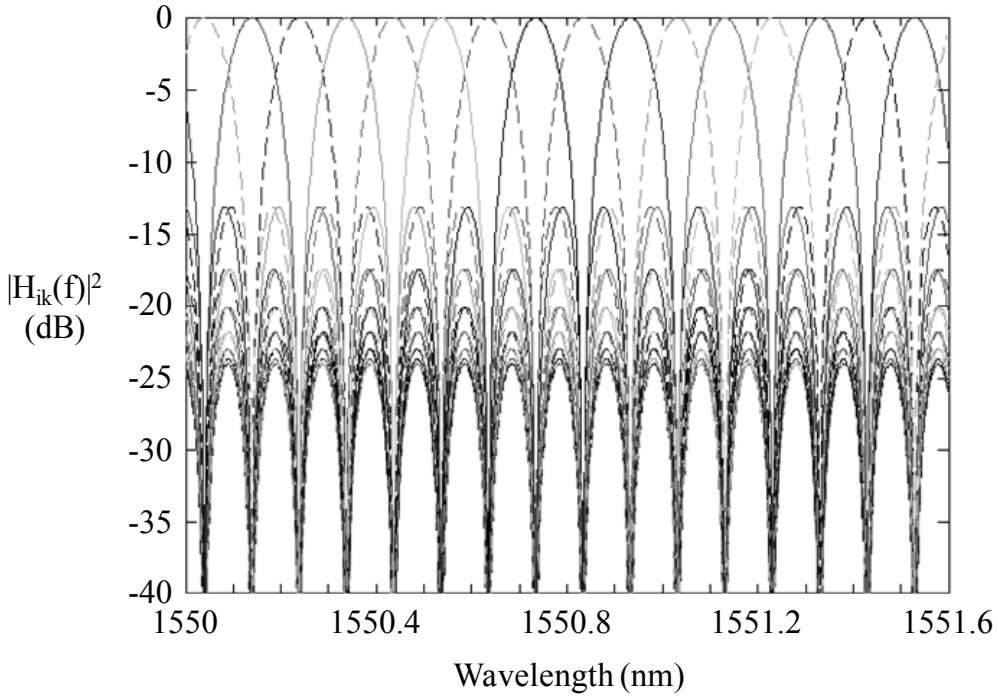

Fig. 2.7: Transfer function at two adjacent output ports.

The correlation signal is computed by substituting Eq. (2.3) into Eq. (2.4) and performing simple algebra:

$$
\begin{aligned}
h_{ik}(t) * h_{ik'}(t) = \sum_{l=0}^{N-1}\sum_{l'=0}^{N-1} & \exp\left[-\mathbf{j}\frac{\pi}{N}(2l-N+1)(i+k+1)\right] \\
& \times \exp\left[-\mathbf{j}\frac{\pi}{N}(2l'-N+1)(i+k'+1)\right] \\
& \times \delta\left[t-(l+l')\Delta\tau\right] \\
= \sum_{l=0}^{N-1} & \exp\left[-\mathbf{j}\frac{2\pi(l+1)}{N}(i+k+1)\right] \\
& \times \sum_{l'=0}^{l} \exp\left[-\mathbf{j}\frac{2\pi l'}{N}(k'-k)\right]\delta(t-l\Delta\tau) \\
& + \sum_{l=N}^{2N-2} \exp\left[-\mathbf{j}\frac{2\pi(l+1)}{N}(i+k+1)\right] \\
& \times \sum_{l'=l+1}^{2N-1} \exp\left[-\mathbf{j}\frac{2\pi l'}{N}(k'-k)\right]\delta(t-l\Delta\tau) \\
& i,k,k' = 0,1,\ldots N-1. \qquad (2.6)
\end{aligned}
$$

To evaluate the auto-correlation function, $k' = k$ is considered in Eq. (2.6):

$$h_{ik}(t) * h_{ik}(t) = \sum_{l=0}^{N-1} \exp\left[-\mathbf{j}\frac{2\pi(l+1)}{N}(i+k+1) \right](l+1)\delta(t-l\Delta\tau) + \sum_{l=N}^{2N-2} \exp\left[-\mathbf{j}\frac{2\pi(l+1)}{N}(i+k+1) \right] \times (2N-l-1)\delta(t-l\Delta\tau)$$

$$i,k = 0,1,\ldots N-1, \quad (2.7)$$

and the ACP appears at $t = (N-1)\Delta\tau$ as

$$ACP = \left| h_{ik}(t) * h_{ik}(t) \right|_{t=(N-1)\Delta\tau} = N$$

$$i,k = 0,1,\ldots N-1. \quad (2.8)$$

Furthermore, the maximum sidelobe (MSL) of the autocorrelation function is $MSL = (N-1)$. In the case of $k' \neq k$, the cross-correlation function of Eq. (2.6) becomes

$$h_{ik}(t) * h_{ik'}(t) = \exp\left[-\mathbf{j}\frac{\pi(k-k')}{2N} \right] \times \sum_{l=0}^{2N-2} \exp\left[-\mathbf{j}\frac{2\pi(l+1)}{N}\left(i+1+\frac{k-k'}{2} \right) \right] \times \frac{\sin\left[\frac{\pi(l+1)(k-k')}{N} \right]}{\sin\left[\frac{\pi(k-k')}{N} \right]}\delta(t-l\Delta\tau)$$

$$i,k,k' = 0,1,\ldots N-1, \quad (2.9)$$

and the maximum CCP appears at $t = \left[(2q+1)/2(k-k')-1\right]\Delta\tau$ with $q = 0,1,\ldots,\lfloor 2(2N-1)(k-k')/N \rfloor$, where $\lfloor\ \rfloor$ denotes the integer part, and is

$$CCP = \left| h_{ik}(t) * h_{ik'}(t) \right|_{\left[\frac{N}{2}(k-k')-1\right]\Delta\tau} = \frac{1}{\sin\left[\frac{\pi(k-k')}{N} \right]}$$

$$i,k = k' = 0,1,\ldots N-1. \quad (2.10)$$

Figure 2.8(a) shows the intensity and the phase of an OC generated by a 4-ps width Gaussian-shape pulse, and Fig. 2.8(b) shows its auto-correlation function. Figures 2.8(c) and (d) show the cross-correlation functions between OCs generated at two adjacent output ports and at two far-apart ports, respectively. As shown in Fig. 2.8, the ratio of APC and max CCP is enough to recognize auto-correlation output.

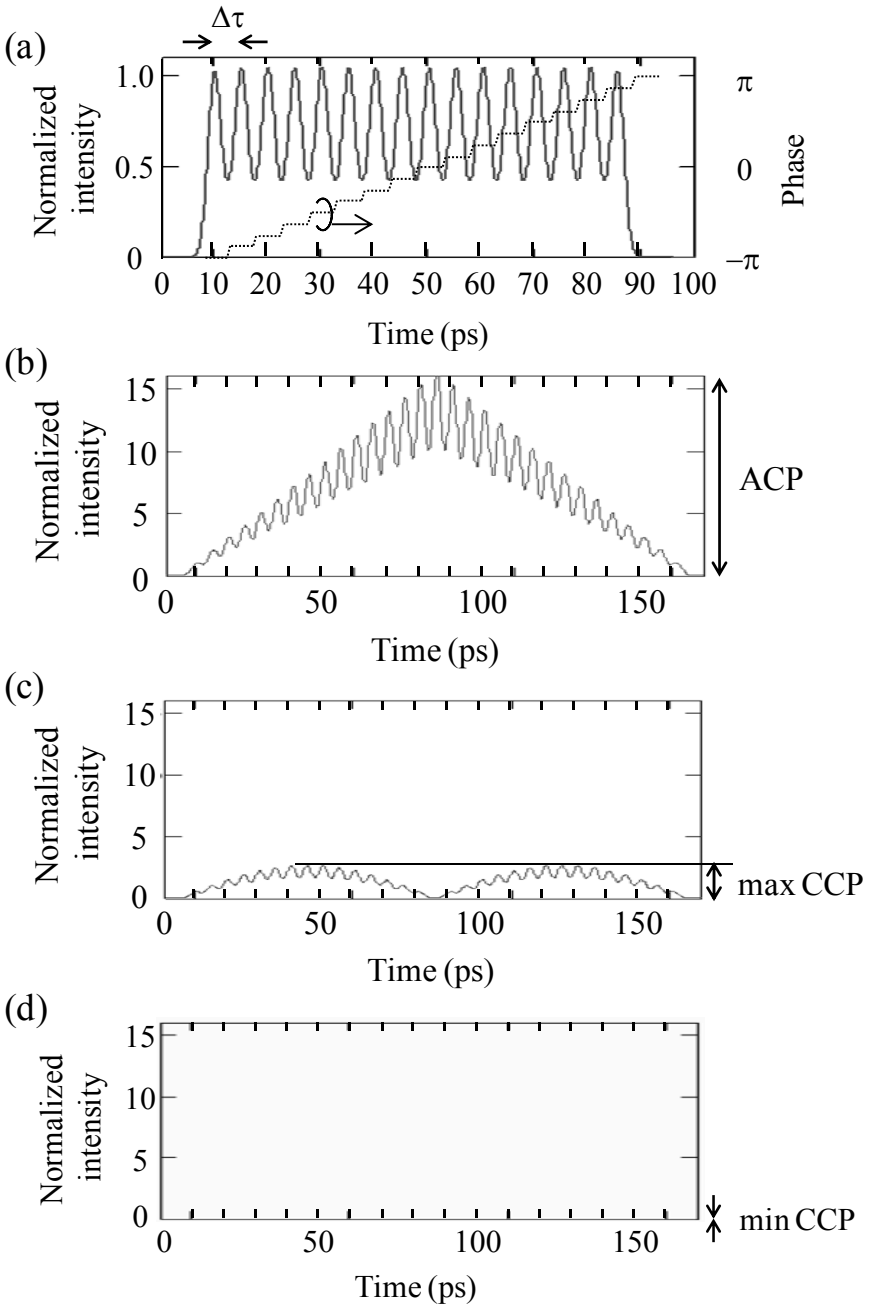

Fig. 2.8: (a) PSK code generated by the device for an input 4-ps Gaussian-shape pulse. (b) Auto-correlation waveform. (c) Maximum cross-correlation waveform. (d) Minimum cross-correlation waveform.

2.5 Conclusion

In this chapter, an overview of OCDM technologies has been described. Section 2.2 has described the fundamentals of optical encoding and decoding. We have shown that a difference in the peak power between auto- and cross-correlation signals can distinguish a desired received signal from the others. We have also explained that the output powers of cross-correlation signals do not vanish, which leads to MAI noise. In Section 2.3, optical devices for optical encoding/decoding have been discussed. Among several optical devices proposed to date, a multi-port encoder/decoder with an AWG configuration is the most suitable device for OCDMA systems in PON architectures. In Section 2.4, the configuration of a multi-port encoder/decoder and the properties of a PSK OC have been described. These devices and the OC techniques form the basis of our proposed system, which is described in the following chapters.

Chapter 3

10-Gb/s Burst-Mode Transmission Technologies

3.1 Introduction

In this chapter, the performances of a 10-Gb/s burst-mode transmitter for an ONU [68] and a 10-Gb/s burst-mode receiver for an OLT [69], both for 10G-EPON systems, are shown. The key issue for ONU and OLT transceivers is a sufficient response time to deal with fast burst modes. Section 3.2 describes the configuration and performances of our 10-Gb/s burst-mode transmitter. In order to obtain a fast response waveform in the transmitter, an impedance controlled DC-coupled transmission line is applied to the burst-mode transmitter in the ONUs. Section 3.3 shows our 10-Gb/s burst-mode receiver configuration and its performances. For smooth migration from 1-Gb/s to 10-Gb/s access systems, the OLT of the 10G-EPON must be able to receive 10-Gb/s and 1-Gb/s packets. Dual-rate burst-mode automatic gain control (AGC)/automatic threshold control (ATC) functions are applied to our OLT receiver in order to ensure a wide dynamic range for dual-rate burst-mode optical signals.

3.2 10-Gb/s Burst-Mode Transmitter Technologies

3.2.1 10-Gb/s Burst-Mode Transmitter Configuration

Figure 3.1 shows the block diagram of our 10-Gb/s burst-mode transmitter. It consists of a burst-control circuit, an LD driver, a bias circuit, a feedforward automatic power control (APC) circuit, and a 1.27-μm un-cooled DFB-LD suitable for 10-Gb/s direct modulation. The burst control circuit can generate 10.3-Gb/s burst data based on both external 10.3-Gb/s continuous data and burst gate signals. The LD driver is able to provide a modulation current (I_{mod}). The bias circuit can supply a stable bias current (I_{bias}) with a rapid on/off time. On/off switching of the burst-mode current is controlled by a pre-bias signal.

The LD modulation current and the bias current are controlled by the feedforward APC circuit with an electrically erasable and programmable read-only memory (EEPROM) that stores a lookup table of appropriate modulations and bias currents for the entire temperature range. In typical continuous-mode transmitters, the optical output power is controlled by monitoring the monitor photo detector (PD) current, which is called a feedback APC. However, it is difficult to achieve a burst-mode fast response of modulation and bias currents with the feedback APC due to a slow response time of the monitor PD current. In contrast, in the feedforward APC, the modulation and

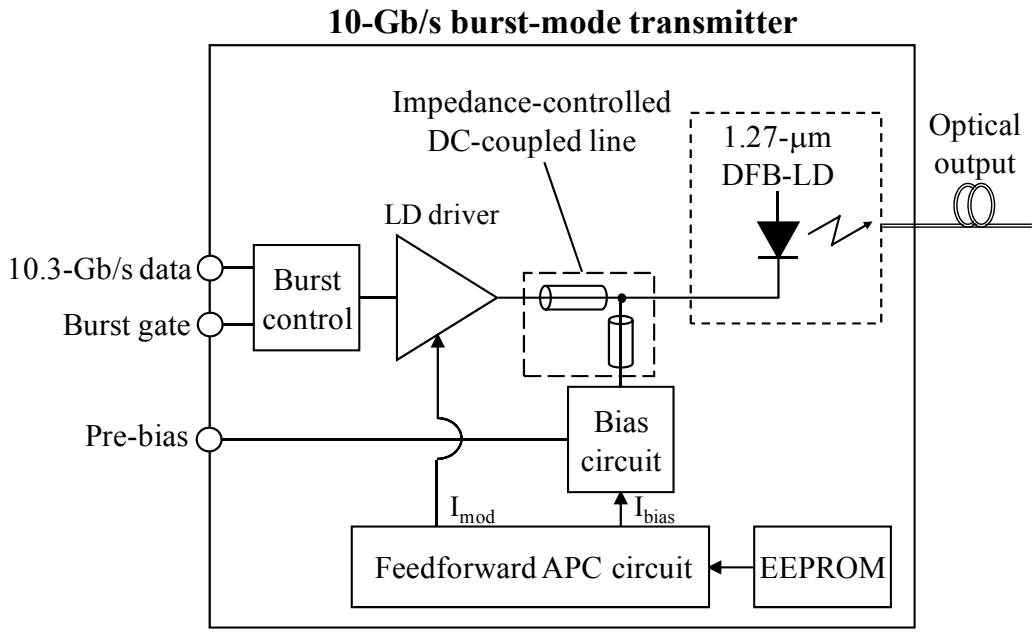

Fig. 3.1: Block diagram of 10-Gb/s burst-mode transmitter.

bias currents are uniquely determined based on the temperature. Therefore, the feedforward APC circuit is suitable for burst-mode operation and can keep the output launch power and extinction ratio constant over the full temperature range.

An impedance-controlled DC-coupled transmission line is inserted between the DFB-LD and the LD driver circuit in the optical transmitter. The transmission interface between the DFB-LD and the driver circuits includes an optimally designed RC network and a flexible strip-line cable to compensate for the parasitic inductance of the optical module. In order to realize a DC-coupled transmission line in the burst-mode transmitter, supply voltages to the output stage of the LD driver and DFB-LD are set to be as high as 5.0 V and the supply voltages to other parts are 3.3 V to reduce the power consumption. With the DC-coupled transmission line, this impedance controlled line enables both high current modulation above 10.3-Gb/s and fast burst-mode control without transmitter waveform distortion.

3.2.2 Experimental Results

Figure 3.2 shows the measured turn-on, turn-off, and optical output eye waveforms after the 4th-order 10.3-Gb/s Bessel-Thomson filter at case temperatures of Tc = 0, +25, and +75 °C. The input data pattern was PRBS 2^{31}–1. In the measurement, we applied a pre-bias burst-mode [40], and the turn-on time represents the convergence time to within 10% deviation of the first bit pulse-width distortion induced by the turn-on delay of the direct modulated DFB-LD and the transient response of the driver circuit. As shown in Fig. 3.2, a fast turn-on time of less than 10 ns and a turn-off time of 7 ns were achieved. In addition, clear eye mask margins (MM) of up to 24% higher than the IEEE802.3av standard [39] were obtained. The measured average power and the extinction ratio of the transmitter output are shown in Fig. 3.3. We confirmed that a high average output power of more than +7.0 dBm and an extinction ratio of 7.0 dB, together with very small temperature-dependent power and extinction ratio deviations of less than 0.1 dB, were achieved over a wide temperature range due to using the feedforward APC circuit. These optical output power and extinction ratios satisfy IEEE802.3av PR30 standards over the full temperature range.

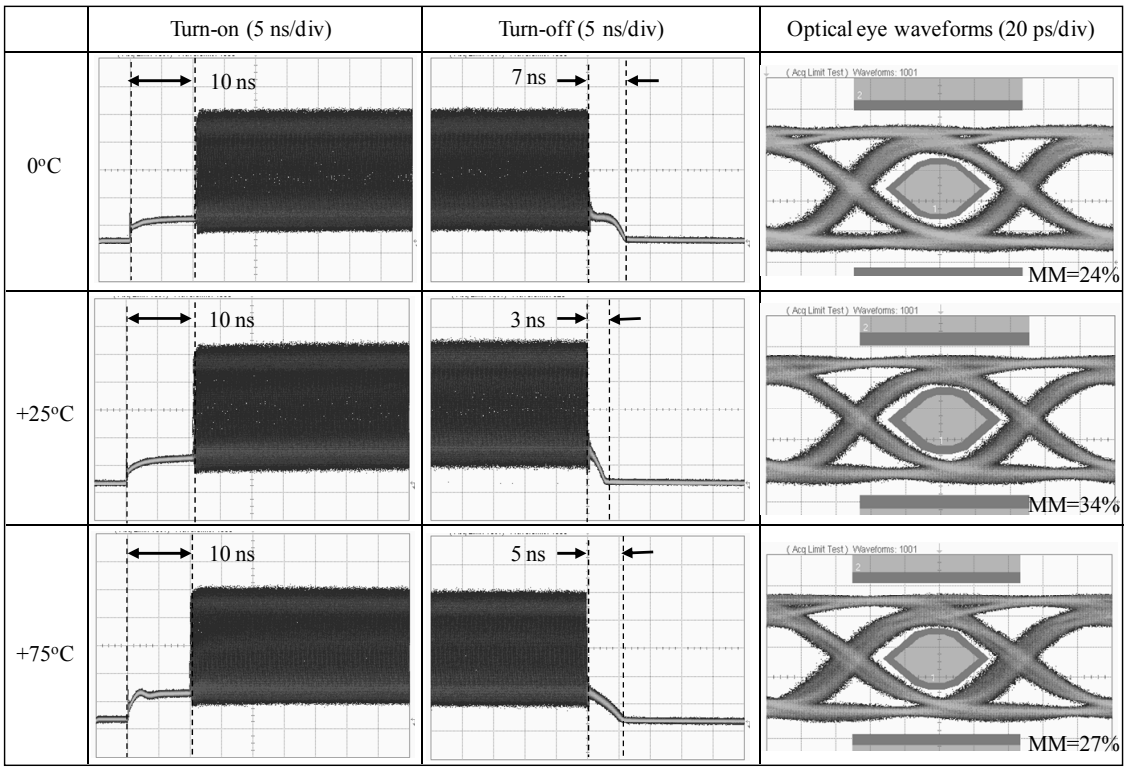

Fig. 3.2: Output waveforms of turn-on/off and optical eye waveforms.

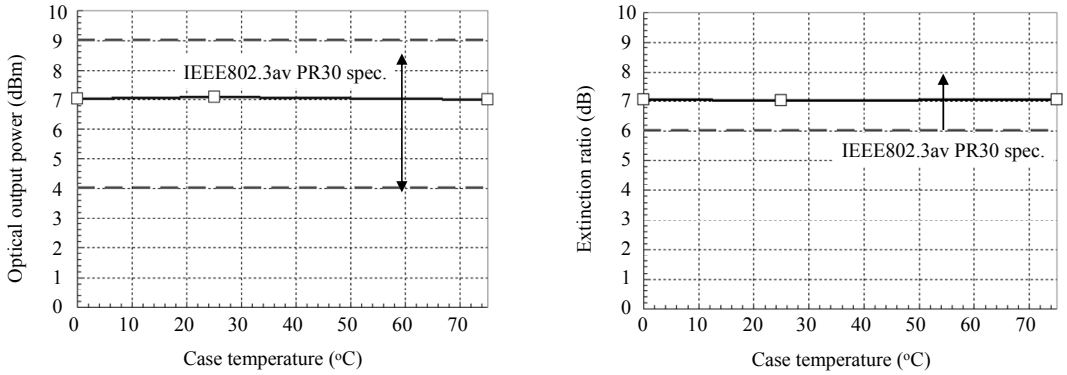

(a) Optical output power (b) Extinction ratio

Fig. 3.3: Optical output power and extinction ratio of 10-Gb/s burst-mode transmitter.

3.2.3 Analysis of Burst-Mode Performances

Figure 3.4 shows the measured and calculated pulse-width distortions versus pre-bias setting time of Tc = +25 °C. In this figure, the calculated curve uses the rate equations for the intrinsic transient response of the directly modulated DFB-LD [70]. The rate equations are as follows:

$$\frac{dN}{dt} = \frac{I}{q \cdot V_a} - G_N \cdot (N - N_0) \cdot (1 - \varepsilon \cdot P) \cdot P - \frac{N}{\tau_s}, \tag{3.1}$$

$$\frac{dP}{dt} = \Gamma \cdot G_N \cdot (N - N_0) \cdot (1 - \varepsilon \cdot P) \cdot P - \frac{P}{\tau_{ph}} + \frac{\Gamma \cdot \beta \cdot N}{\tau_s}, \tag{3.2}$$

where N is the carrier density, P is the photon density, I is the injection current, q is the elementary charge, V_a is the volume of the active region, ε is the phenomenological gain compression factor, τ_s is the carrier lifetime, G_N is the gain coefficient, Γ is the optical confinement factor, N_0 is the transparent carrier density, τ_{ph} is the photon lifetime, and β is the spontaneous emission coupling factor. It can be clearly seen in Fig. 3.4 that our burst-mode transmitter can achieve a fast LD turn-on time close to the intrinsic DFB-LD lifetime-dominated transient response because the pulse-width distortion with 3-ns pre-bias setting time is less than 10%. The difference between the measured and theoretical results can be explained by the circuit delay due to inductance in the bias line. As shown in Fig. 3.4, a pre-bias setting time of longer than 10 ns is suitable for a 10-Gb/s burst-mode transmitter to avoid pulse-width distortions.

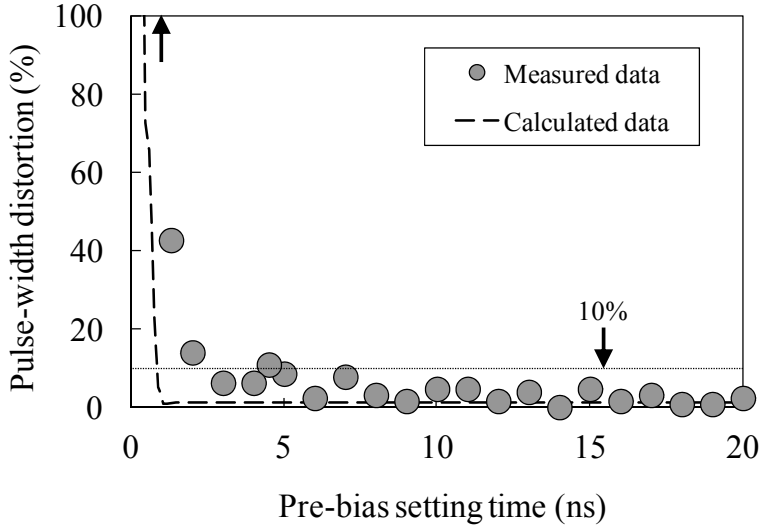

Fig. 3.4: Measured and calculated pulse-width distortions versus pre-bias setting time.

3.3 10-Gb/s Burst-Mode Receiver Technologies

3.3.1 Burst-Mode Receiver Configuration

In general, a burst-mode optical receiver consists of an avalanche photo diode (APD), a transimpedance amplifier (TIA), and a limiting amplifier (LIA) incorporating burst-mode AGC/ATC functions. Burst-mode receivers can be categorized roughly into two types: step detection and continuous detection [85]. Received burst optical packets have different power levels, so each packet should be normalized by amplification with an appropriate gain and regeneration at a proper decision threshold level in a burst-mode optical receiver, as shown in Fig. 3.5. The technical challenge for burst-mode AGC/ATC is to simultaneously support quick response to incoming burst packets and high tolerance to long consecutive identical digits (CIDs). A burst-mode receiver of the step detection sets its gain to the highest mode before receiving a packet. Then, it determines its gain and threshold according to the received power at the beginning of an incoming packet. With these operations, a burst-mode receiver of the step detection type [83, 84] can realize a receiver settling time as fast as 51 ns as well as tolerance to a long CID. However, the drawback is that it needs a reset signal input at the leading edge of each packet at the right moment. In contrast, a burst-mode receiver of the continuous detection type can vary its gain and threshold continuously according to the received power averaged over the time. As a result, a burst-mode receiver of the continuous detection type [76, 81] can realize a simple configuration and robustness against power fluctuation in a packet. However, it is difficult to achieve a fast receiver settling time shorter than 150 ns in order to retain sufficient strength for a long CID. Therefore, we adopt the continuous detection type for the 10-Gb/s burst-mode receiver.

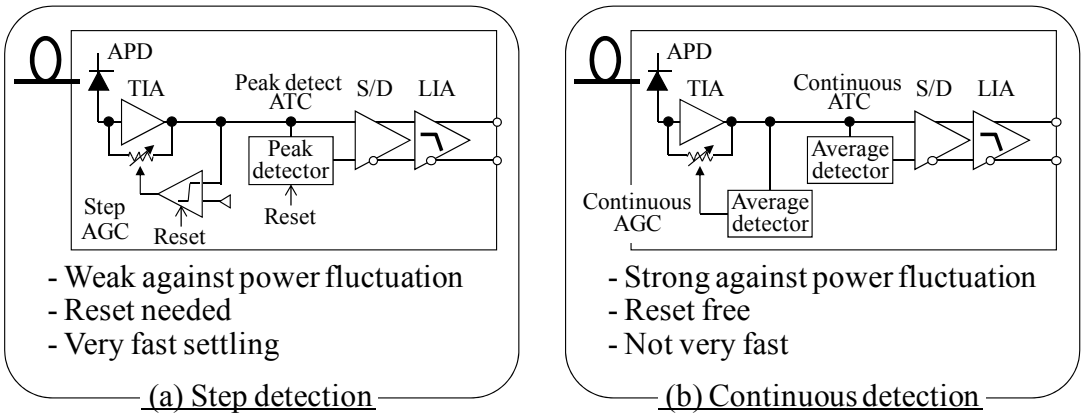

Fig. 3.5: Block diagrams of burst-mode receiver for TDM-PON.

3.3.2 Dual-Rate Receiver Configuration

In this section, the dual-rate receiver configurations that have also been proposed are discussed. In 10G-EPON systems, the upstream wavelength regions of 10-Gb/s and 1-Gb/s systems are overlapped from 1260 nm to 1280 nm. Therefore, an OLT receiver has to receive both 10-Gb/s and 1-Gb/s packets. In order to meet such demand, there are three main configurations of a dual-rate receiver. Figures 3.6(a), (b), and (c) show the block diagrams of parallel (optical splitting [75] and TIA output splitting types [76]), and serial types of a dual-rate optical receiver for a 10G-EPON OLT, respectively. In the optical splitting type, the received optical signal is divided by a 3-dB coupler and 10-Gb/s and 1-Gb/s signals are received by each data rate receiver including an APD, a TIA, and a LIA. The advantage of this method is that cost-effective 1-Gb/s optical and electrical components for 1G-EPON can be applied. However, the receiver sensitivity becomes worse than that achieved by other methods due to the 3-dB coupler. In addition, the number of components in the receiver is large. The TIA output splitting type can be realized by a single APD and 10-Gb/s TIA, as well as by parallelized 10-Gb/s LIA and 1-Gb/s LIA following a low-pass filter (LPF) with a 1-GHz cutoff frequency. This type can reduce the number of components compared with the optical splitting type, but the receiver sensitivity for the 1-Gb/s signal is not optimized due to applying a 10-Gb/s TIA, which has a transimpedance gain lower than that of a 1-Gb/s TIA. The serial type dual-rate receiver can realize optimized transimpedance gain and equivalent noise bandwidth by changing the operation mode with an external rate select signal. In addition, the number of optical components, the power consumption, and the cost can be minimized. Therefore, we adopt the serial type for the dual-rate burst-mode receiver.

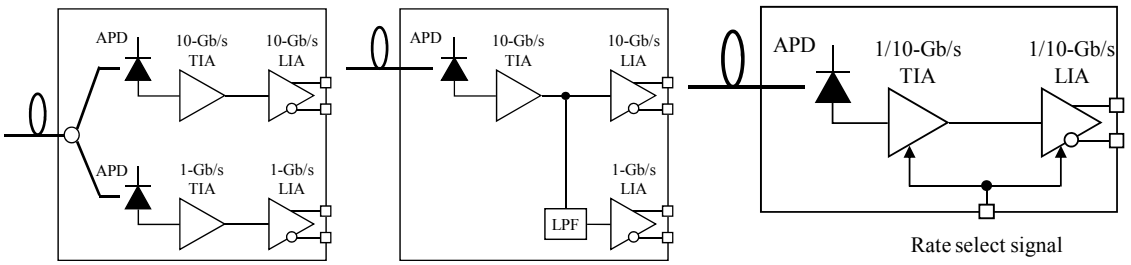

(a) Optical splitting type (b) TIA output splitting type (c) Serial type

Fig. 3.6: Block diagrams of parallel and serial types of dual-rate receiver for 10G-EPON OLT.

3.3.3 Dual-Rate Burst-Mode Transceiver Configuration

Figure 3.7 shows the block diagram of a dual-rate optical transceiver for a 10G-EPON OLT. It consists of a dual-rate burst-mode optical receiver and 10-Gb/s and 1-Gb/s downstream transmitters integrated into an XFP-E size package via a triplexer optical module [89]. The burst-mode optical receiver employs a dual-rate APD-preamplifier and a dual-rate limiting amplifier that can switch their transimpedance gain, equivalent noise bandwidth, and transient response time optimized for each 10-Gb/s and 1-Gb/s packet in order to achieve the receiver sensitivity and receiver settling time specified in the IEEE802.3av PR30 standards. These dual-rate preamplifier and limiting amplifier ICs are fabricated by the 0.13-μm SiGe BiCMOS process to realize single-core chip sets and low power consumption. The APD bias control circuit applies the optimized voltage for the APD over the entire temperature range in order to achieve a high receiver sensitivity. The 10-Gb/s and 1-Gb/s transmitters employ a cooled 10-Gb/s electro-absorption modulator integrated laser (EML), an un-cooled 1-Gb/s DFB-LD, and driver ICs to drive these light sources.

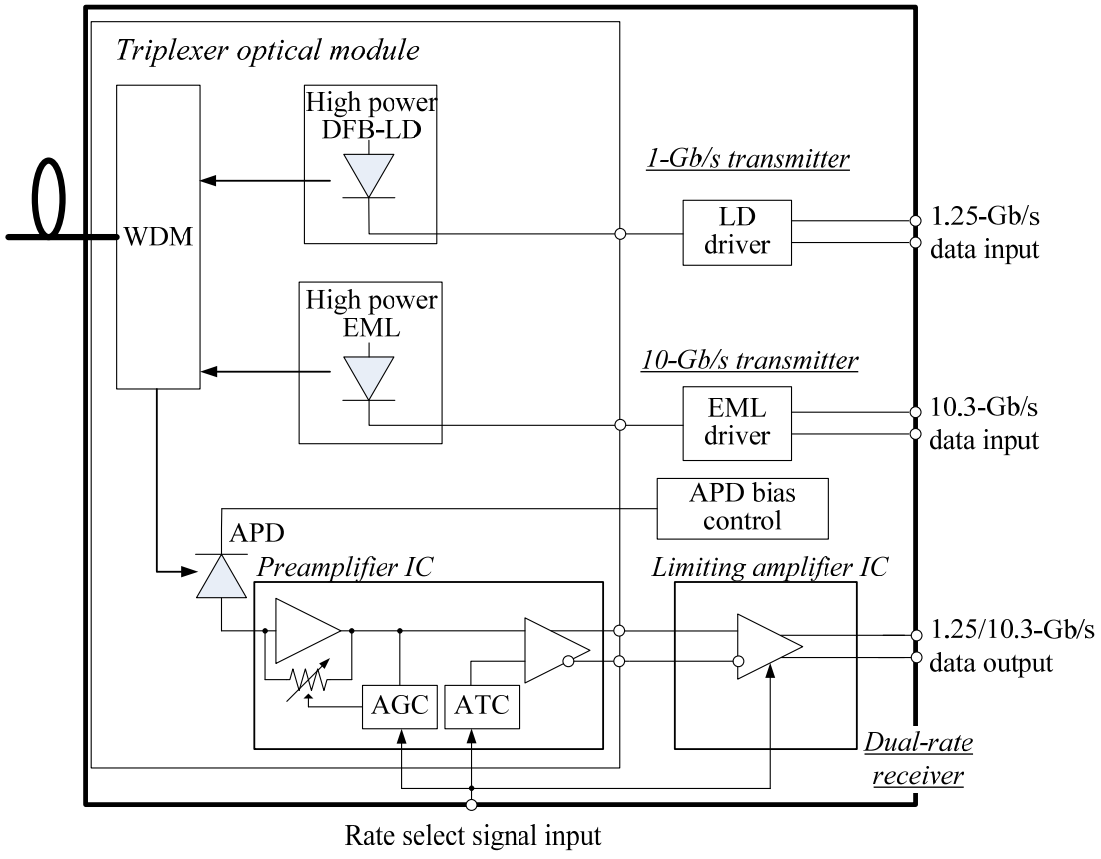

Fig. 3.7: Block diagram of dual-rate burst-mode transceiver for 10G-EPON OLT.

3.3.4 Experimental Results

The measurement results of our dual-rate burst-mode dynamic receiving response are shown in Fig. 3.8. In Fig. 3.8(a), the input signal consists of 10-Gb/s optical soft packets with an optical power of –30 dBm and 1-Gb/s loud packets with –6 dBm without guard time for the worst case condition. In Fig. 3.8(b), the input signal consists of 10-Gb/s packets with a power level of –6 dBm and 1-Gb/s packets with a power level of –35 dBm. Figure 3.8 clearly shows that the dual-rate burst-mode AGC and ATC could rapidly regenerate the received 10-Gb/s and 1-Gb/s mixed packets within 800 ns for the 10-Gb/s packet and 400 ns for the 1-Gb/s packet, which are specified as the receiver settling time in IEEE802.3av, over the entire dynamic range.

Figure 3.9 shows all of the BER measurement conditions in the 10-Gb/s and 1-Gb/s coexisting 10G-EPON systems. In the dual-rate 10G-EPON systems, there are three BER measurement

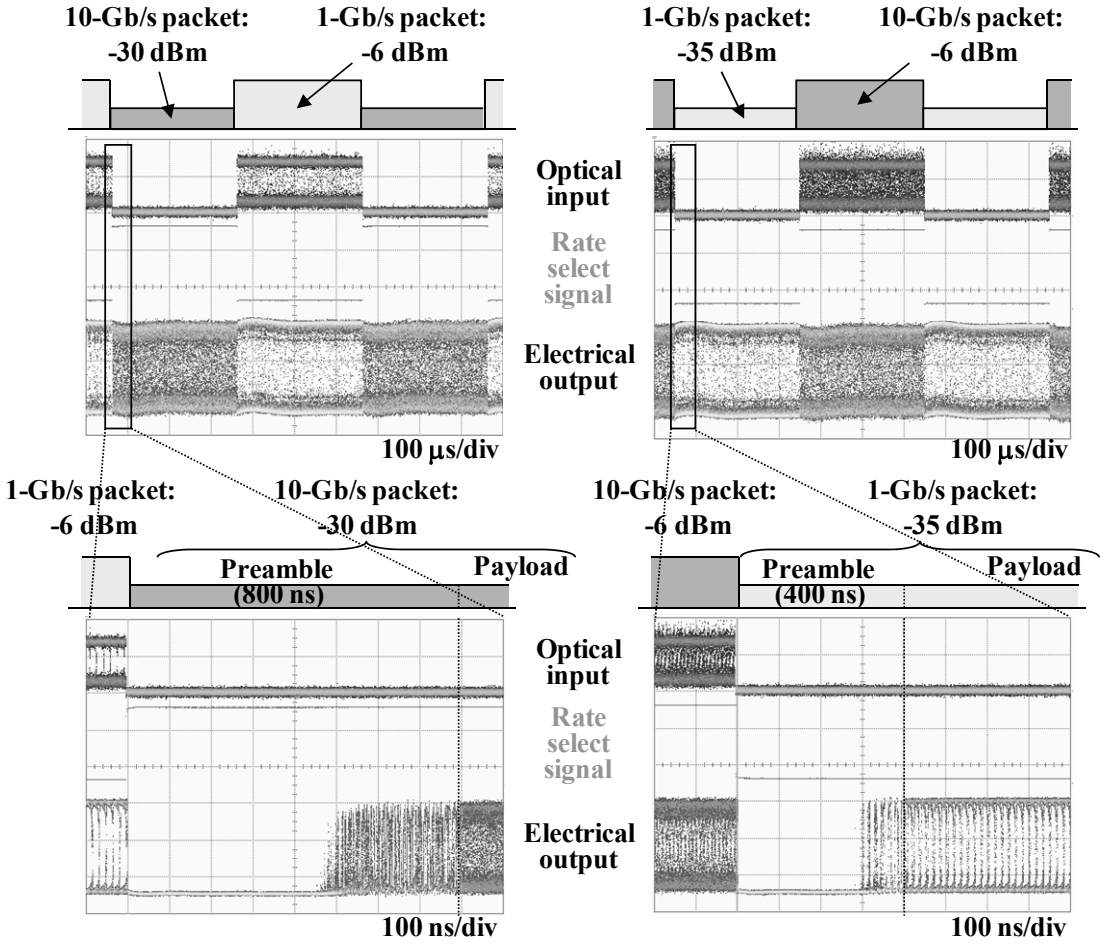

(a) 1-Gb/s loud and 10-Gb/s soft packets (b) 10-Gb/s loud and 1-Gb/s soft packets

Fig. 3.8: Dual-rate burst-mode dynamic receiving response.

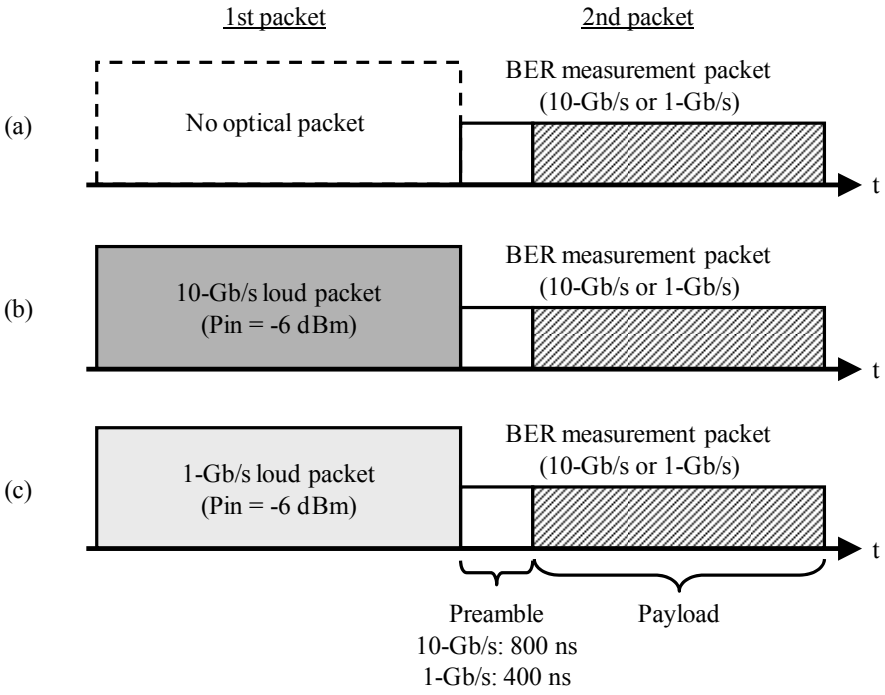

Fig. 3.9: The BER measurement conditions on dual-rate 10G-EPON.

conditions for each 10-Gb/s and 1-Gb/s optical burst packet in terms of the optical input power and the line-rate of the first (previous) packet because the dual-rate burst-mode AGC and ATC have to regenerate a second (BER measurement) packet during a preamble period under all of the first packet conditions. We measured the BER of payload in a second packet to confirm the feasibility of the dual-rate burst-mode AGC and ATC. The preamble periods of 10-Gb/s and 1-Gb/s packets are 800 ns and 400 ns, respectively, which are specified as the receiver settling time in IEEE802.3av. The guard time of the first loud packet with –6 dBm and BER measurement packet was set to 0 ns for the BER measurement condition with the widest dynamic range. The 10-Gb/s and 1-Gb/s payload data patterns were 64B/66B and PRBS 2^7–1, respectively.

The BER performances of the dual-rate burst-mode receiver are shown in Fig. 3.10. A minimum receiver sensitivity of –30.6 dBm and an overload of –5 dBm at BER = 10^{-3} for 10-Gb/s operation and a minimum receiver sensitivity of –34.6 dBm and an overload of –9 dBm at BER = 10^{-12} for 1-Gb/s operation were achieved. The receiver sensitivities in all the measurement conditions satisfied the requirements of IEEE802.3av PR30 within an appropriate margin.

A 10-Gb/s cooled EML with a wavelength of 1577 nm controlled by an APC circuit was used for an OLT 10-Gb/s downstream transmitter. A high average output power larger than +2.6 dBm and an extinction ratio higher than 8.9 dB at the case temperature range from –5 to 70 °C, both of which meet the IEEE802.3av PR30 standards, were achieved. A measured 10-Gb/s transmitted optical

waveform after a 4th-order Bessel-Thomson filter enabling a clear eye opening is shown in Fig. 3.11. In the 1-Gb/s downstream transmitter, a 1-Gb/s un-cooled DFB-LD with a wavelength of 1490 nm was used. The DFB-LD drive current was controlled by an APC controller to compensate for the transmitter output power and the extinction ratio over the entire temperature range. A high average output power larger than +5.3 dBm and a high extinction ratio larger than 14.3 dB in the case of temperatures ranging from –5 to 70 °C were obtained, both of which meet the IEEE802.3-2008/1000BASE-PX20 standards. The measured 1-Gb/s transmitted optical waveform after the 4th-order Bessel-Thomson filter enabling a clear eye opening is shown in Fig. 3.11.

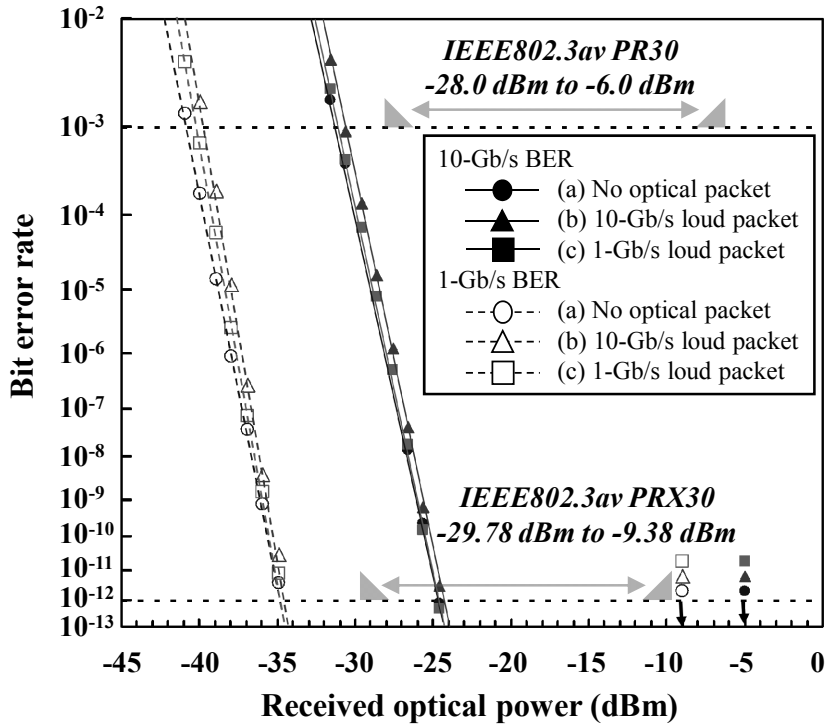

Fig. 3.10: Dual-rate BER performance.

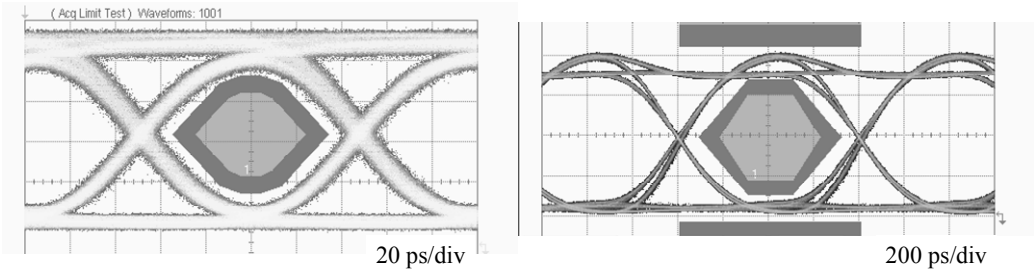

(a) 10-Gb/s transmitter (b) 1-Gb/s transmitter

Fig. 3.11: Output waveforms of (a) 10-Gb/s and (b) 1-Gb/s transmitters.

3.4 Conclusion

In this chapter, we have described the performances of our ONU and OLT transceivers for 10G-EPON systems, including 10-Gb/s burst-mode transmitting and dual-rate receiving technologies. Table 3.1 shows the summary of the burst-mode transmission performances including the ONU transmitter and the OLT transceiver. The burst-mode transmitter for the ONU could achieve a fast burst-mode response time shorter than 10 ns and a high launched optical power larger than +7.0 dBm. The OLT transceiver could achieve high receiver sensitivities of less than –30.6 dBm for 10-Gb/s packets and less than –34.6 dBm for 1-Gb/s packets, with fast receiver settling times of 800 ns for the 10-Gb/s packets and 400 ns for the 1-Gb/s packets.

Table 3.1: Summary of burst-mode transmission performances.

		Description	IEEE802.3 PR30		Results		Unit
ONU	Tx	Wavelength	1260 – 1280		1265 – 1273		nm
		Average launch power	4 – 9		7.01 – 7.02		dBm
		Extinction ratio	> 6		7.03		dB
		Turn-on/off time	< 512		< 10		ns
		Description	IEEE802.3		Results		Unit
			10-Gb/s	1-Gb/s	10-Gb/s	1-Gb/s	
OLT	Tx	Wavelength	1575 – 1580	1480 – 1500	1578.5	1488 – 1495	nm
		Average launch power	2 – 5	2 – 7	2.6 – 3	5.3 – 5.4	dBm
		Extinction ratio	> 6	> 6	8.9	14.3	dB
	Rx	Overload	> –6.0	> –9.38	–5	–9	dBm
		Receiver sensitivity	< –28	< –29.78	–30.6	–34.6	dBm
		Receiver settling time	< 800	< 400	< 800	< 400	ns
		Burst dynamic range	> 24	> 20.4	25.6	25.6	dB

Chapter 4

10G-TDM-OCDM-PON System

4.1 Introduction

In this chapter, we propose our novel 10G-TDM-OCDM-PON system that can scale up conventional 10-Gb/s TDM-PON by aggregating systems using an OCDMA technique. The proposed system is able to increase the total capacity without sacrificing the uplink bandwidth currently assigned to the individual optical network unit (ONU). Section 4.2 presents the 10G-TDM-OCDM-PON system configuration, which includes an ONU with a compact super-structured fiber Bragg grating (SSFBG) [99], an optical line terminal (OLT) with a single multi-port encoder/decoder [67], and a 10-Gb/s burst-mode receiver [75]. Section 4.3 describes a 16-ONU (4-OCDMA × 4-packet) uplink burst transmission experiment using 16-chip (200 Gchip/s), 16-phase-shifted OCs which generations and recognitions were described in Chapter 2. In Section 4.3, we discuss how the newly introduced multi-level phase-shifted encoding/decoding, whose auto-correlation waveform can be preferably adopted in the burst-mode reception at 10-Gb/s, is the key to the proposed system and the uplink throughput performances.

4.2 10G-TDM-OCDM-PON System Configuration

Figure 4.1 shows the upgrade scenario of a single 10-Gb/s TDM-PON to $n \times$ 10G-TDM-OCDM-PON systems. When n conventional 10-Gb/s TDM-PON systems including $m \times$ ONUs are accommodated, the bandwidth per user is reduced by a factor of n due to the nature of time division multiple access (TDMA), resulting in the bandwidth reduction factor of $m \times n$, that is, (10-Gb/s /m)/n per ONU. Here, the bandwidth means the data rate for each user. In contrast, the 10G-TDM-OCDM-PON system can maintain the bandwidth reduction factor of only the number of ONUs (= m) by assigning different optical codes (OCs), OCs No. 1–n, to an individual 10-Gb/s TDM-PON system. For example, OC No. 1 is shared with No. 1-1–1-m ONUs where uplink signals No.1-1–1-m in a group are time-aligned without contention. As a result, the uplink bandwidth per user can be increased by a factor of n, compared with TDM-based systems, that is, 10-Gb/s/m. From the viewpoint of the upgrade cost of 10-Gb/s TDM-PON systems, our proposed system is more expensive because OCDMA-specific components have to be additionally implemented. OCDMA-specific components additional to conventional PON systems would include an encoder/decoder as well as a special class of short pulsed lasers. However, the costs of the multi-port decoder as well as that of the short pulsed laser can be shared by a number of different ONUs, and the SSFBG type of encoder could be inexpensive if it were mass-produced.

For 10G-TDM-OCDM-PON systems, a single multi-port encoder/decoder [67] is located at an OLT, which can generate n different OCs, while each ONU uses a multi-level phase-shifted SSFBG. The multi-port encoder/decoder can lower the budget loss due to simultaneous processing of multiple OCs without splitters. It is also cost-effective because the cost can be shared between all ONUs. In contrast, an SSFBG has the ability to process an ultra-long OC, perform polarization-independent operation, has a compact structure, and also has a low-cost capability for mass production [65]. Therefore, it is appropriate to allocate a multi-port encoder/decoder to the OLT and SSFBG encoder/decoders to the ONUs, respectively. A crucial challenge of 10G-TDM-OCDM-PON systems is the detection of uplink optical “burst” signals, decoded after the transmission. To study the feasibility of 10G-TDM-OCDM-PON systems, we developed a 10-Gb/s burst-mode receiver consisting of an avalanche photodiode (APD)-preamplifier module and a limiting amplifier. This burst-mode receiver can achieve high sensitivity by adopting a high-sensitivity APD with a large gain-bandwidth product [91] and a low-noise preamplifier.

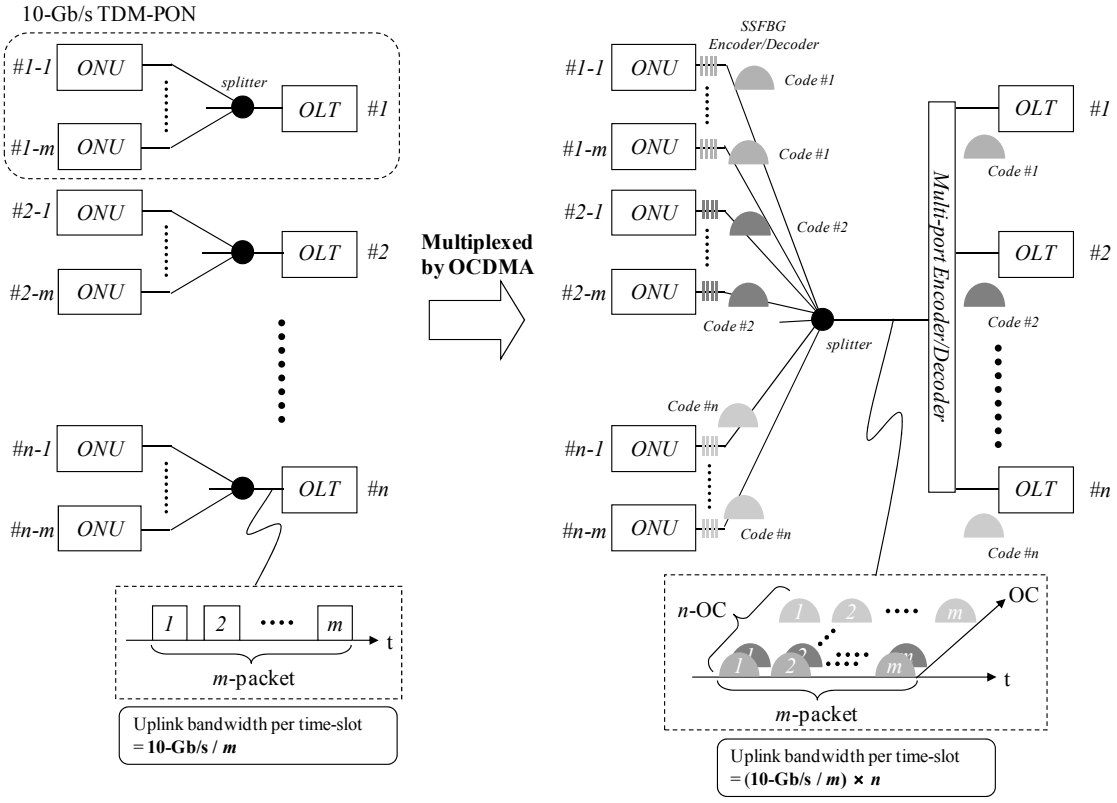

Fig. 4.1: Architectures of scalable 10-Gb/s TDM-PON system upgraded using OCDMA approach.

4.3 Burst-Mode Uplink Transmission Experiment

Figure 4.2 shows the experimental setup for the 16-ONU uplink burst-mode transmission of our 10G-TDM-OCDM-PON system. 16 ONUs can be accommodated by a 4-packet 10-Gb/s TDM-PON over 4-OC OCDMA. A 1.8-ps pulse train was generated by a mode-locked laser diode (MLLD), as shown in Fig. 4.3(a). The center wavelength was 1546 nm and the repetition rate was 9.95328 GHz. The output from the MLLD was modulated to 4 packets by optical burst-mode modulators (BM Mod.) constructed by a $LiNbO_3$ (LN) intensity modulator and an acousto-optic modulator (AOM) that worked as a burst-mode gate switch (SW). The switching speed and extinction ratio of the burst-mode gate switch were about 100 ns and over 40 dB, respectively. Therefore, the optical burst-mode modulators could simultaneously realize a fast burst turn-on/off time and sufficient power suppression during idle periods. Figure 4.3(b) shows the LN intensity modulator output data with a 2^{31}–1 pseudo random bit sequence (PRBS). Each packet length was 64 μs, which includes a 10-μs overhead, as shown in Fig. 4.3(c). Figure 4.3(d) shows the packet pattern, which had a guard

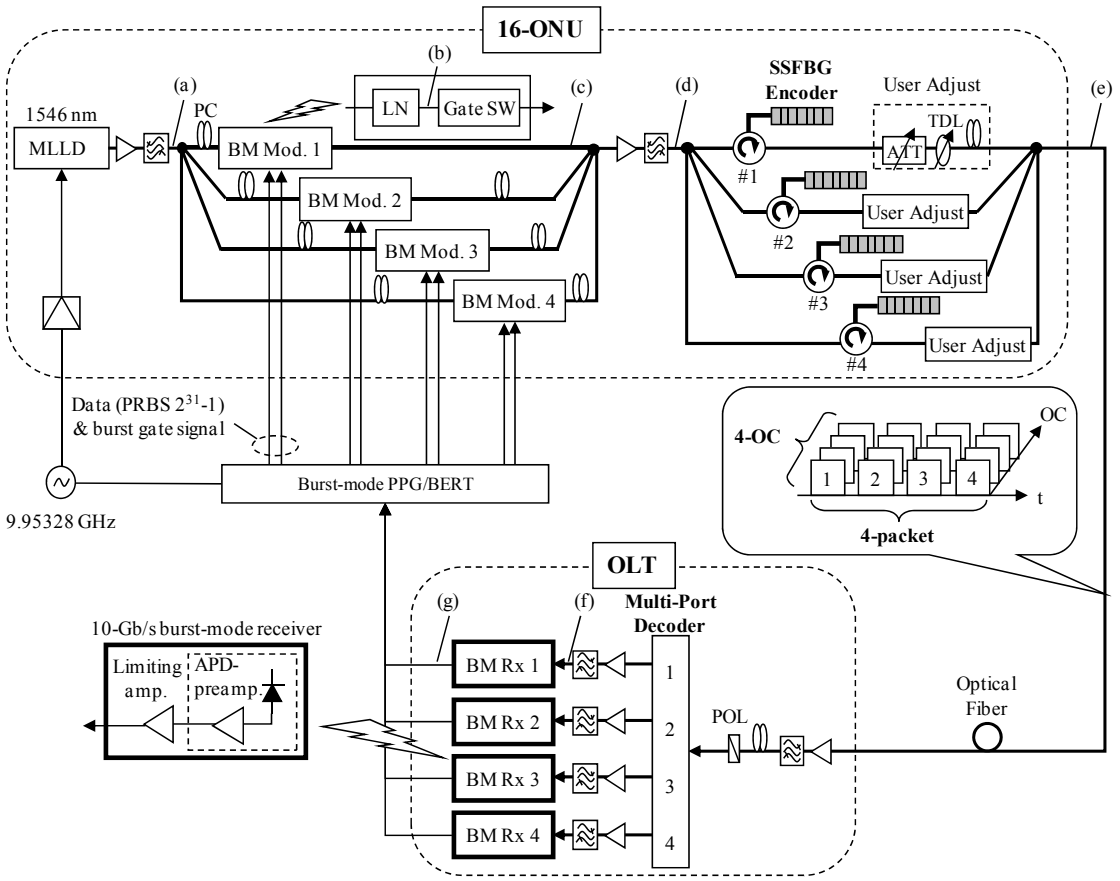

Fig. 4.2: Experimental setup of 16-ONU uplink transmission of 10G-TDM-OCDM-PON.

time of 0 ns. This no-guard time was set to cope with the most severe condition for a fast response of the burst-mode receiver. The packets were encoded by 4 different 16-chip, 16-phase-shifted SSFBGs. In the SSFBG encoder, the input optical pulse was time-spread into 16 pulses, called chip pulses, at 5-ps intervals. These chip pulses had relative phase shift with respect to each other's codes. In terms of the design parameters of the SSFBG encoder, the center wavelength was 1546 nm, the chip length was ~ 0.52 mm, the total length of the grating was 8.32 mm, and the 16 phase levels were generated by shifting the chip grating. These encoded signals were time-multiplexed into a TDM × OCDM signal. A tunable optical attenuator (ATT), a tunable delay line (TDL), and a polarization controller (PC) were inserted in each path to investigate the system performance in the worst scenario where interference would become the most serious, as shown in Fig. 4.3(e).

At the OLT side, the received signal was decoded by a 16-chip with a 5-ps interval (200 Gchip/s), 16-phase-shifted multi-port decoder that could simultaneously process the 16 OCs. We set a PC and inline polarizer (POL) at the front of the multi-port decoder due to the polarization dependence of the multi-port decoder. In the decoding process, each chip pulse was time-spread again into 16 pulses and experienced a relative phase shift with respect to the combination of the input and output

ports. The frequency deviation (channel spacing) between neighboring ports of the 16 × 16 port decoder was 12.5 GHz. Figure 4.3(f) shows the decoded signal of OC No. 1, showing a high-peaked auto-correlation waveform with multiple access interference (MAI) noise skirts. Each decoded signal was processed by our originally developed 10-Gb/s burst-mode receiver. This 10-Gb/s burst-mode receiver provides a high-sensitivity burst-mode 2R function with the optimal multiplication factor M of the APD (M = 8.0). Figure 4.3(g) shows a good electrical eye opening obtained from the decoded signal despite MAI noise thanks to the adequate bandwidth of the burst-mode receiver, which was wider than 6.0 GHz. In this experiment, erbium doped fiber amplifiers (EDFAs) were inserted to compensate for the optical loss of each component, such as the SSFBG encoders and the multi-port decoder.

Figure 4.4 shows the measured bit error rate (BER) performances for all 16-ONU of the 4-OC × 4-packet and those of the back-to-back (B-to-B) non-encoded and non-decoded signals. All packets achieved error-free (BER < 10^{-3}) operation with the FEC of Reed-Solomon (RS) (255, 223). In the 4-OC multiplexed system, a BER of less than 10^{-7} could not be measured due to MAI noise. However, the feasibility of the 10G-TDM-OCDM-PON system was clear because the 10-Gb/s TDM-PON system operates with a FEC. We obtained good eye openings for all four decoded signals of OCs No. 1–4, as evidenced by the BER measurements in Fig. 4.4. These results confirm an uplink bandwidth of 10-Gb/s/4, which is four times larger than that in conventional 10-Gb/s TDM-PON systems, e.g., 10-Gb/s/16. Figure 4.5 shows the receiver sensitivity at BER = 10^{-3} for all 16-ONU uplink data. Receiver sensitivity of less than –29.9 dBm was successfully achieved by adopting the high-sensitive burst-mode receiver, and the power penalties between 4-OC × 4-packet and back-to-back were less than 2.0 dB and were caused by degradation of optical signal-to-noise ratio (OSNR) due to amplified spontaneous emission (ASE) from each EDFA and the MAI noise. A small deviation in the receiver sensitivities would be caused by the characteristic mismatch of correlation properties and the extinction ratio of each packet.

In this experiment, BER results by changing the received optical power of each packet and the length of guard time are not shown due to the lack of a burst-mode optical amplifier [95]. However, the system feasibility was demonstrated by using the burst-mode receiver, which can process 10-Gb/s uplink packets with different optical power [75].

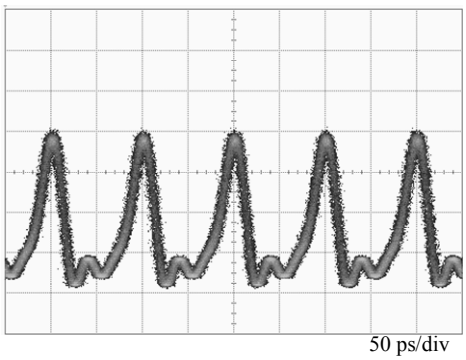

(a) MLLD output

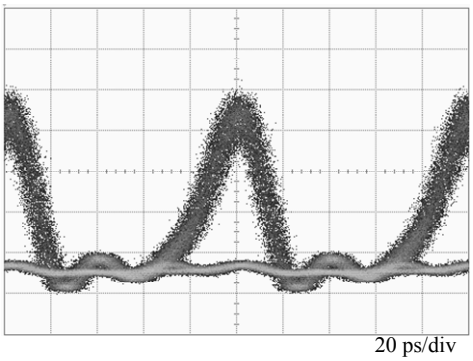

(b) LN intensity modulator output

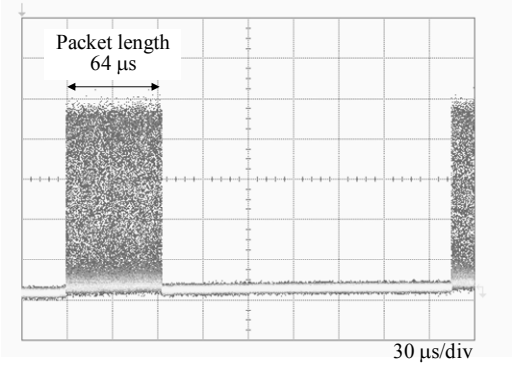

(c) BM mod. output

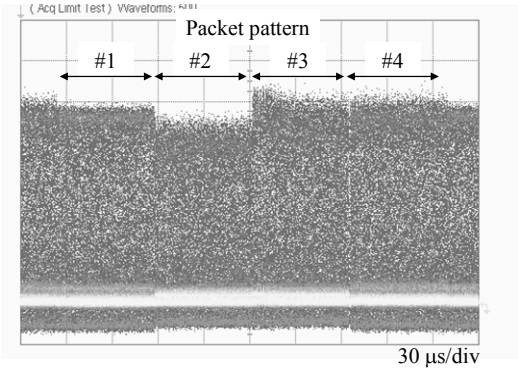

(d) Packet pattern of 4 packets

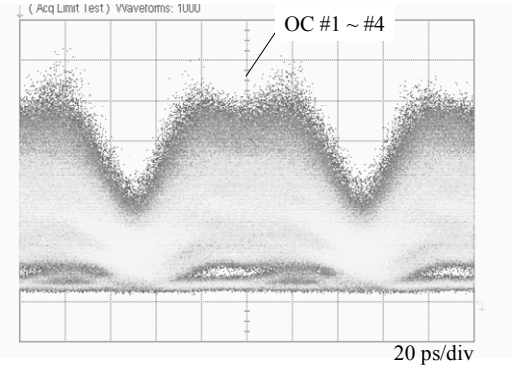

(e) 4-OCDM

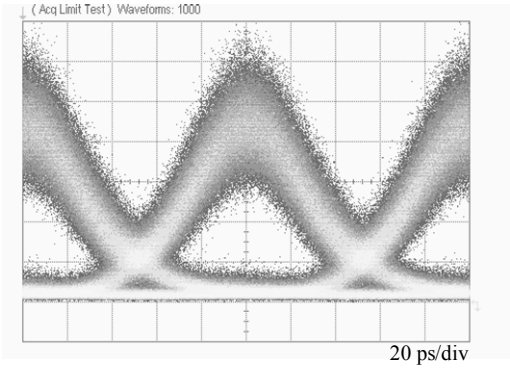

(f) Multi-port decoder output

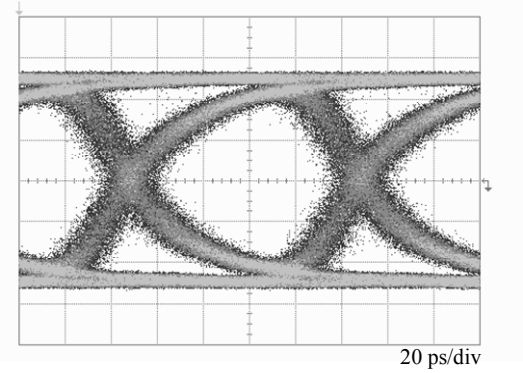

(g) BM Rx output

Fig. 4.3: Waveforms of burst-mode OC transmission signals.

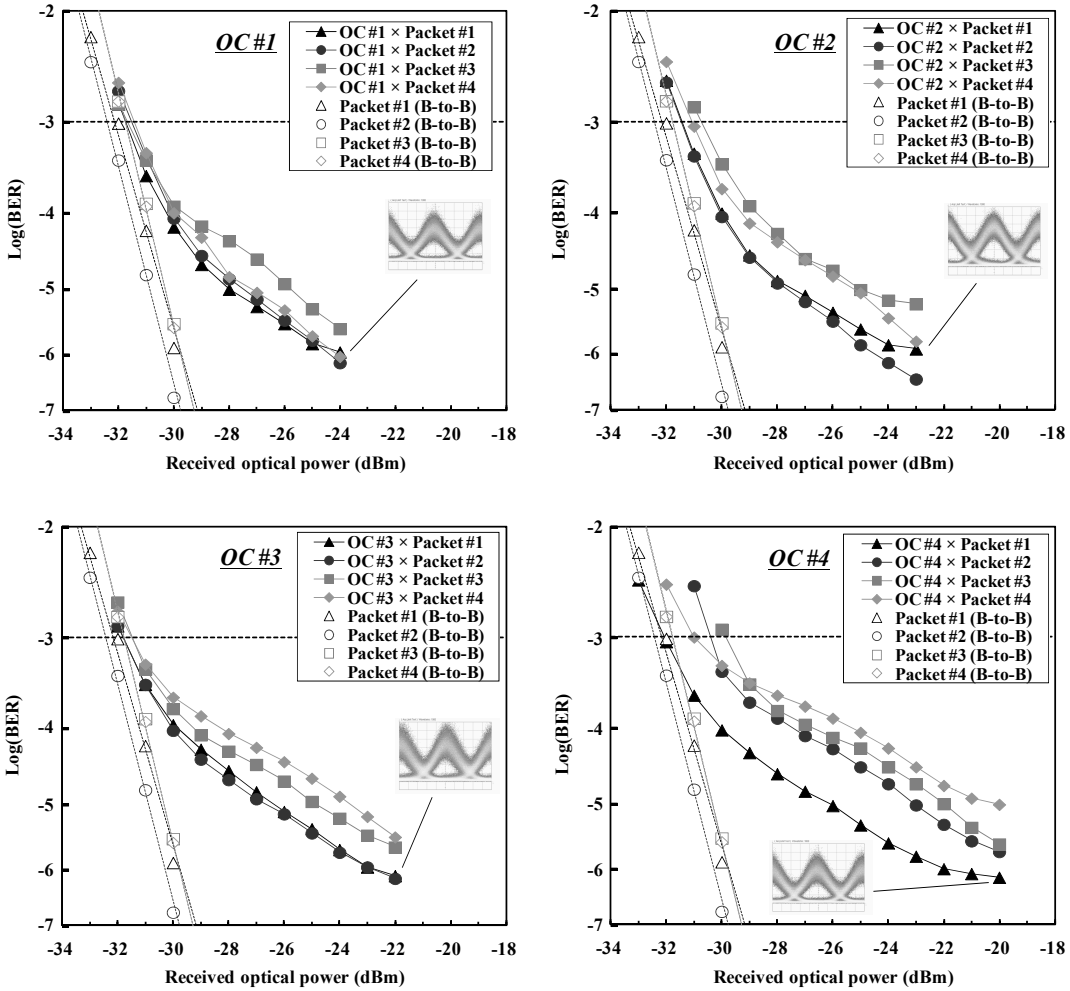

Fig. 4.4: Measured bit error rate performances of all 16 ONUs.

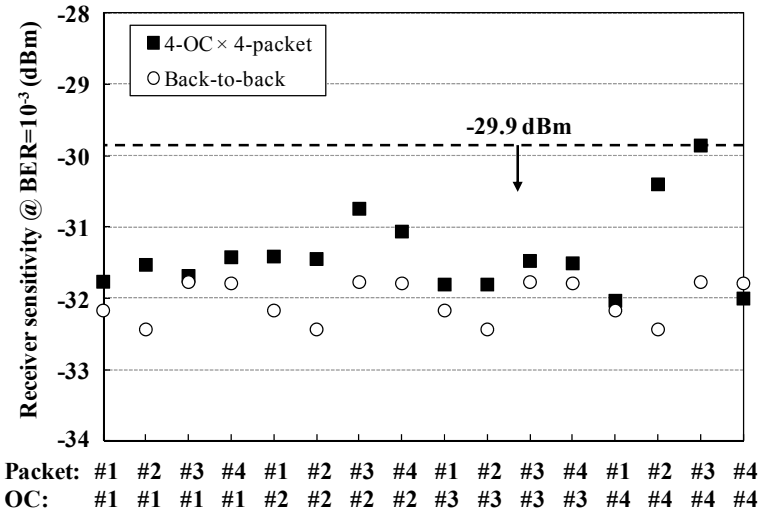

Fig. 4.5: Measured receiver sensitivity of all data at BER = 10^{-3}.

4.4 Discussion

4.4.1 Correlation Performances for 10-Gb/s Burst-Mode Reception

A burst-mode reception is a “must” for PON systems and has never been realized at 10-Gb/s in any OCDMA system. This is because the auto-correlation waveforms in optical decoding have a sharp peak, requiring tens of gigahertz bandwidth of the burst-mode receiver at 10-Gb/s. This requirement can be met by narrowing the bandwidth of the decoded signal, and so this is the approach that we have taken. Two different phase-shifted encoding schemes for coherent TS-OCDMA have previously been proposed and demonstrated [93]. One is bipolar phase-shifted encoding (0, π) by using an SSFBG [65]. The other is multi-level phase-shifted encoding by using a multi-port encoder/decoder [67]. Figures 4.6(a) and (b) compare the auto-correlation waveforms of the bipolar and the 16-level phase-shifted encodings used in the transmission experiments, respectively. The pulse width of the auto-correlation signal of the bipolar phase-shifted code (63 chips and 640 Gchip/s) is a few picoseconds with side-lobe suppression while the envelope width of the 16-level phase-shifted auto-correlation signal is approximately 80 ps (= 16 chip/200 Gchip/s). The difference in the pulse width is the key to successful burst-mode reception at 10-Gb/s. For 1G-TDM-OCDM-PON [42], the bipolar phase-shifted encoding has been adopted for the burst-mode reception, but this narrow pulse width was a stumbling block at 10-Gb/s. This is because it is difficult to receive the bipolar phase-shifted auto-correlation signal without OSNR degradation, and a wide bandwidth receiver (tens of gigahertz) is required. Currently, it is not feasible to achieve both high-bandwidth and high-gain burst-mode reception under the condition that the gain-bandwidth product remains constant. In addition, the bipolar phase-shifted encoding has another issue resulting from use of long OCs. The longer the code length becomes for a high bit rate, the narrower the auto-correlation waveform because the chip pulse width has to become narrower. This property indicates that the bipolar phase-shifted encoding is inadequate for our proposed systems. This is why we employed the multi-level phase-shift encoder, which provides a broad and smooth auto-correlation temporal waveform. It is noteworthy that the multi-level phase-shifted encoding can generate a larger number of codes than the bipolar phase-shifted encoding with an identical number of chips. Regarding inter-symbol interference (ISI), the ISI noise has the same effect as the MAI and results in the power penalty in systems [96]. The auto-correlation pulse widths of the 63-chip bipolar (640 Gchip/s) and the 16-chip multi-level (200 Gchip/s) are 200 and 160 ps, respectively. Therefore, the 16-chip multi-level phase-shifted code can reduce the influence of ISI more effectively than the

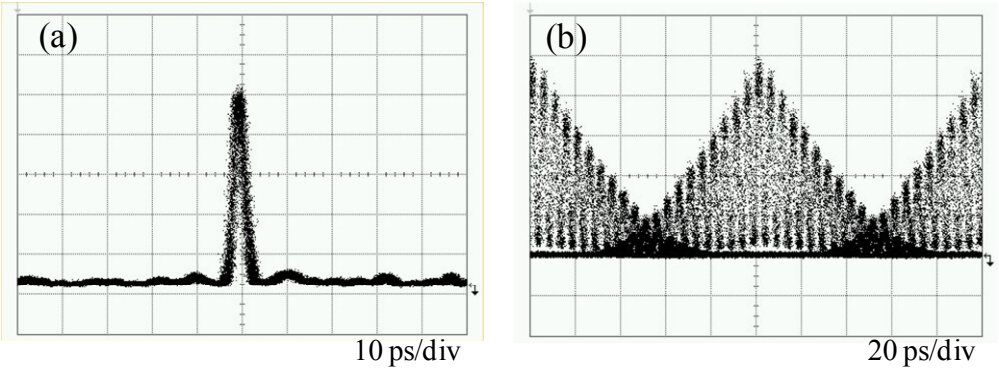

Fig. 4.6: The auto-correlation waveforms of (a) bipolar and (b) 16-level phase-shifted encoding.

63-chip bipolar code. In addition, the multi-level phase-shifted code has a better power contrast ratio (PCR) characteristic than the bipolar code [97]. It can suppress both the coherent beat noise and the MAI noise. Therefore, the multi-level phase-shifted encoding is the best solution for 10G-TDM-OCDM-PON uplink burst transmission because a burst-mode receiver with a wide bandwidth is not required for processing the multi-level phase-shifted auto-correlation signal.

4.4.2 Uplink Throughput Performances

The uplink performances of the proposed system are discussed in this subsection. Figure 4.7 shows the uplink burst frame model discussed here. In a case in which the data payload is fully loaded, uplink bandwidth per user can be written as

$$BW = BR \times \frac{GP - (m \times OH_{PMD})}{GP} \times \frac{100 - OH_{FEC}}{100} \times \frac{n}{m}, \tag{4.1}$$

where BW is the bandwidth per user, BR is the bit rate of the system, GP is the grant period equal to the optical burst frame length, m is the number of ONUs belonging to a 10-Gb/s TDM-PON system, OH_{PMD} is the PMD overhead consisting of burst-mode turn-on/off and sync times, OH_{FEC} is the FEC overhead ratio after the FEC frame mapping, and n is the number of systems multiplexed by using OCDMA techniques. Table 4.1 shows the parameter values assumed in calculating the throughput of the proposed system. In this calculation, we assume that OH_{PMD} includes the burst-mode CDR lock time because burst-mode CDR can realize a quick burst-mode data recovery [87]. In addition, OH_{FEC}

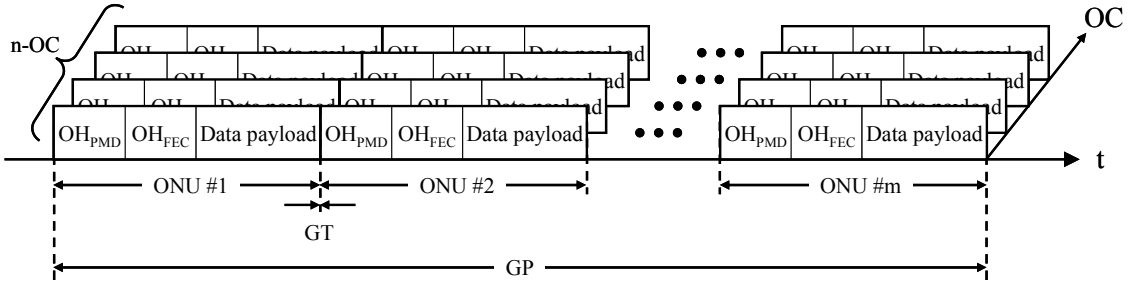

Fig. 4.7: Uplink transmission optical burst frame model.

Table 4.1: Parameters of throughput calculation.

Quantity	Symbol	Value	Unit
Bit rate	BR	9.95328	Gb/s
PMD overhead time	OH_{PMD}	10	μs
FEC overhead	OH_{FEC}	12.9	%
Guard time	GT	0	ns
Grant period	GP	1	ms
Number of optical codes	n	4	–

and GT are assumed to be 12.9% [94] and 1 ms, respectively. Other parameters are set on the basis of the experimental conditions.

Figure 4.8 shows the calculation results of the uplink bandwidth per user. Here, the number of users is $n \times m$. The uplink bandwidth per user of conventional 10-Gb/s TDM-PON systems is given by Eq. (4.1) with $n = 1$. The proposed system achieves a capacity four times larger than that in conventional 10-Gb/s TDM-PON systems. Therefore, an uplink bandwidth of 1 Gb/s per user is achieved even if the system accommodates 32 users, and all users can use symmetric gigabit-bandwidth applications by applying OCDMA techniques. In addition, the increase in network capacity by using OCDMA techniques can be adapted to additional subscribers. For example, the number of users in this system can be increased to 128 without throughput degradation, which is in contrast to a 10-Gb/s TDM-PON system that can only accommodate 32 users.

The maximum number of users can be increased to more than 32 in the 10G-TDM-OCDM-PON system because the optical power ratio between the burst signal and the idle period is more than 40 dB. According to the theoretical analysis of the maximum number in this coherent OCDMA system [98], provided that encoding/decoding is properly performed, 32 users and more can be accommodated at any bit rate, and the number of active users depends on the coherency of the light source. As the coherence goes higher, the beat noise becomes more dominant than the MAI noise.

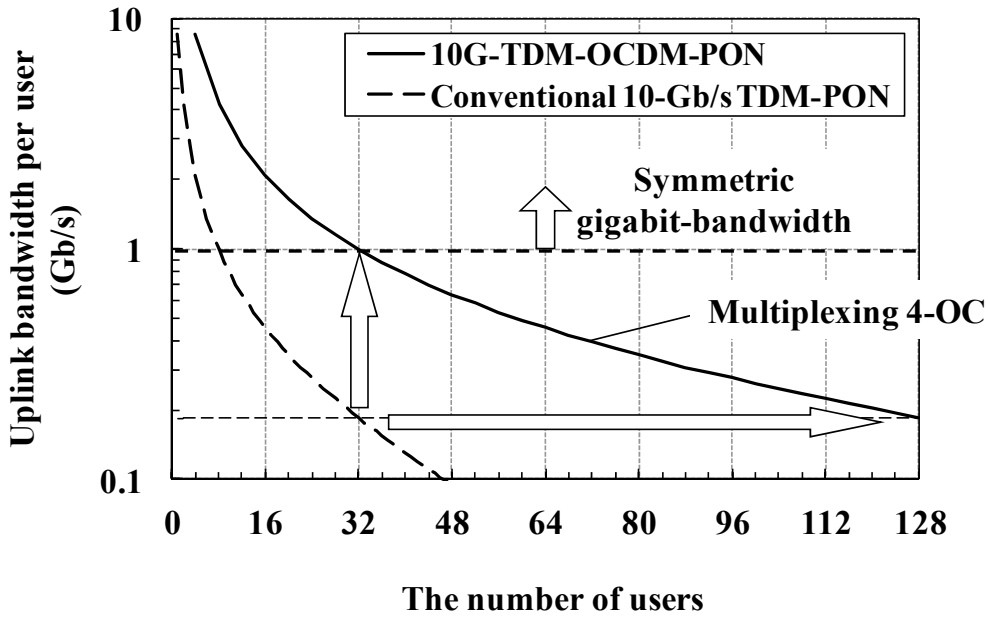

Fig. 4.8: 10G-TDM-OCDM-PON uplink bandwidth calculation result.

4.5 Conclusion

In this chapter, a novel 10G-TDM-OCDM-PON system that does not sacrifice the currently assigned uplink bandwidth per user has been described. The uplink burst-data transmission of 4 × 10-Gb/s TDM-PON systems over 4 × OC has been demonstrated by using a 16-chip (200 Gchip/s), 16-level phase-shifted SSFBG encoder at ONUs and a single multi-port decoder at an OLT. With the assistance of FEC, error-free operation could be achieved in all 16 ONUs of the 10G-TDM-OCDM-PON, resulting in a total capacity four times larger than the conventional 10-Gb/s TDM-PON. Finally, we have revealed that the key to unprecedented symmetric uplink bandwidth is a newly introduced 16-level phase-shifted encoding/decoding, of which an auto-correlation waveform can be preferably adopted in a burst-mode reception at 10-Gb/s. We have also showed that 32 users can be accommodated by being provided with an up/down link of symmetric gigabit-bandwidth in 10G-TDM-OCDM-PON systems.

Chapter 5

Long Reach 10G-TDM-OCDM-PON System

5.1 Introduction

In this chapter, we propose a novel long reach 10G-TDM-OCDM-PON architecture using only a multi-port encoder/decoder pair at an optical line terminal (OLT) and a remote node (RN), thus eliminating the need for an encoder/decoder at each optical network unit (ONU) [103]. This long reach 10G-TDM-OCDM-PON can realize cost-effective configuration by removing the dispersion compensator for long reach transmission. Section 5.1 shows the general architecture of the long reach 10G-TDM-OCDM-PON. The three key devices required for long reach transmission without dispersion compensation—a single multi-port encoder/decoder pair, a narrow band optical band pass filter (NB-OBPF), and a 10-Gb/s burst-mode 3R receiver—are described. In section 5.2, an experimental demonstration of full duplex 4-packet × 4-OC transmission on a single wavelength over a 65-km SMF without dispersion compensator is described. In section 5.3, we discuss the sources of the power penalty in the proposed system [104].

5.2 Long Reach 10G-TDM-OCDM-PON System Configuration

Figure 5.1 shows the general architecture of the long reach 10G-TDM-OCDM-PON, which can be scaled up by aggregating 10-Gb/s TDM-PON systems with the OCDMA technique. We realize our long reach 10G-TDM-OCDMA-PON, $m \times n$ -ONU (m-TDM packet × n-OCDMA), by eliminating the need for an encoder/decoder at each ONU and dispersion compensator. Instead, only the NB-OBPF and the multi-port encoder/decoder are introduced at both the OLT and the RN. Thus, a dispersion compensation-free long reach can be realized by narrowly tailoring the optical code (OC) spectrum. In downlink, each 10.3-Gb/s piece of data is encoded by the multi-port encoder to aggregate 10-Gb/s TDM-PON downlink signals. The OC spectrum is tailored by using NB-OBPF to mitigate the chromatic dispersion effect. Therefore, encoded signals can be transmitted over a trunk span and decoded at the RN. Furthermore, each decoded signal is transmitted over an access span and received by each ONU, while in uplink, 10.3-Gb/s burst data from each ONU is multiplexed as TDM signals and transmitted over an access span. Then, uplink m-TDM signals are encoded with different OCs, followed by tailoring their spectra at the RN. After the trunk span transmission, uplink signals are decoded and recovered at the OLT. As a result, the proposed system is able to gather central offices and directly connect to the metro/core networks, leading to a cost-effective, high-capacity 10-Gb/s TDM-PON. The three key technologies for long reach 10G-TDM-OCDM-PON—a single multi-port encoder/decoder pair, an NB-OBPF, and a 10-Gb/s burst-mode 3R receiver—will be introduced in the next section.

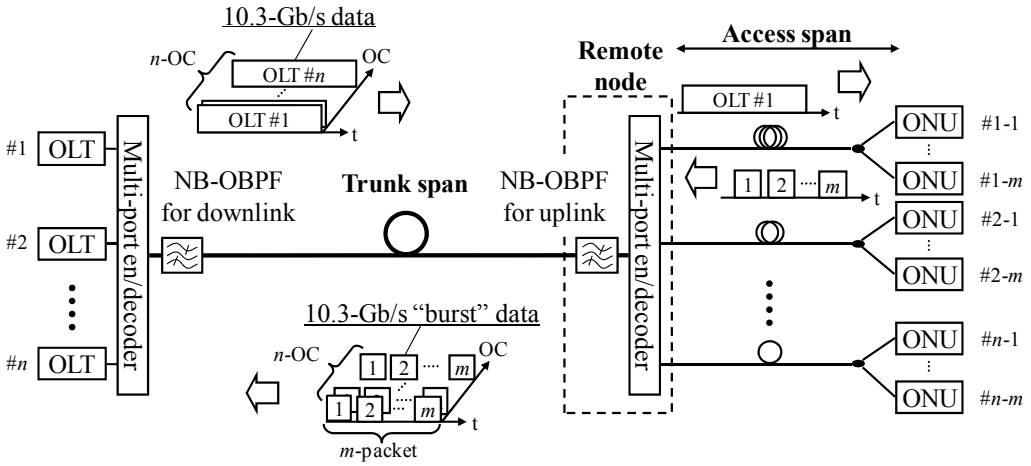

Fig. 5.1: The architecture of long reach 10G-TDM-OCDM-PON.

5.2.1 Multi-Port Encoder/Decoder Pair at OLT and RN

We applied a 16-chip with 5-ps interval (200 Gchip/s), 16-phase-shifted multi-port encoder/decoder pair, which can simultaneously process the 16 OCs, in the 10G-TDM-OCDM-PON. The insertion loss of this multi-port encoder/decoder is about 10 dB. This insertion loss might be smaller by eliminating device mismatches such as coupling loss because the insertion loss of a typical AWG achieves only a few dB. An optical amplifier is inserted at an input port in order to compensate for the insertion loss. From the insertion loss point of view, the multi-port encoder/decoder can increase the number of ports to more than 16. However, we only applied a 16 × 16 port encoder/decoder pair because we prepared only this one device for the experiment. In addition, a thermal controller for the multi-port encoder/decoder, whose control accuracy was less than 0.1 °C, is necessary to obtain good correlation performances. In order to use this multi-port encoder/decoder for an outdoor component, athermal technologies which are adopted for a part of AWG will be required.

By using just an encoder/decoder pair at an OLT and an RN, long reach 10G-TDM-OCDM-PON can be scaled up by aggregation with 10-Gb/s TDM-PON systems. The configuration of ONU becomes simpler than the 10G-TDM-OCDM-PON by eliminating the need for an encoder/decoder at each ONU, as shown in Fig. 5.1. Note that the multi-port encoder/decoder can be located anywhere on the SMF transmission line between the OLT and ONUs because the nonlinear effect is negligible. As a result, our proposed system is able to gather central offices and directly connect to metro/core networks, leading to a cost-effective high-capacity 10-Gb/s TDM-PON.

5.2.2 Extended Reach by NB-OBPF

For realizing long-reach transmission of OC signals without dispersion compensation, the NB-OBPF can tailor the OCs spectrum. In conventional OCDMA systems, the encoded signals cannot be transmitted more than a few km on the SMF without dispersion compensation because the spectral width of a non-filtered OC is about 3 nm due to applying an optical short pulse source. However, N. Kataoka et al. proposed 10-Gb/s OCDMA systems capable of SMF transmission without dispersion compensation by tailoring the extra spectrum components of the OC [53].

Figure 5.2 shows the ideal principle operation of tailoring OC spectrum components produced by the 16 × 16 port encoder/decoder. This encoder/decoder has the free spectral range (FSR) of 200 GHz, which is nearly equal to 1.6 nm at 1550 nm. Note that the output wavelength component of the

multi-port encoder/decoder has a cyclic nature due to the AWG configuration, as shown in Fig. 5.2. Here, only one FSR component filtered by NB-OBPF can keep the signal information and decrease the effect of chromatic dispersion. Figure 5.3 shows the wavelength response of the rectangular shaped NB-OBPF. The bandwidth of NB-OBPF is set to the FSR of the multi-port encoder/decoder in order to tailor the OCs spectrum. The tailored spectrum has a bandwidth of just 1.6 nm that can be obtained by adapting a rectangular shaped NB-OBPF. As a result, the NB-OBPF output spectrum includes only 4-OC components. If the bandwidth of NB-OBPF is larger than FSR, the received optical signal to noise ratio (OSNR) is decreased because of the chromatic dispersion [53]. On the other hand, if the bandwidth of NB-OBPF is narrower than FSR, the correlation performance degradation occurs because each OC can't keep the orthogonal relation.

Figure 5.4 shows the 10.3-Gb/s decoded optical eye diagrams of one OC functioning as 4 multiplexing OCs whose spectra are tailored by the NB-OBPF. The back-to-back decoded eye diagram with a multiple access interference (MAI) noise skirt can achieve a clear eye opening because of the excellent correlation characteristic of the multi-port encoder/decoder and adequate spectrum tailoring, as shown in Fig. 5.4(a). Figure 5.4(b) shows the decoded optical eye diagram after 65-km transmission of SMF as 4 OCs multiplexing. This eye diagram has more inter-symbol interference (ISI) compared with the back-to-back one due to the chromatic dispersion. However, the receiver can process the transmitted signal because the decoded OC signal can obtain a sufficient eye opening. This demonstrates that the combination of a multi-port encoder/decoder and NB-OBPF can achieve over 65-km transmission on SMF without dispersion compensation.

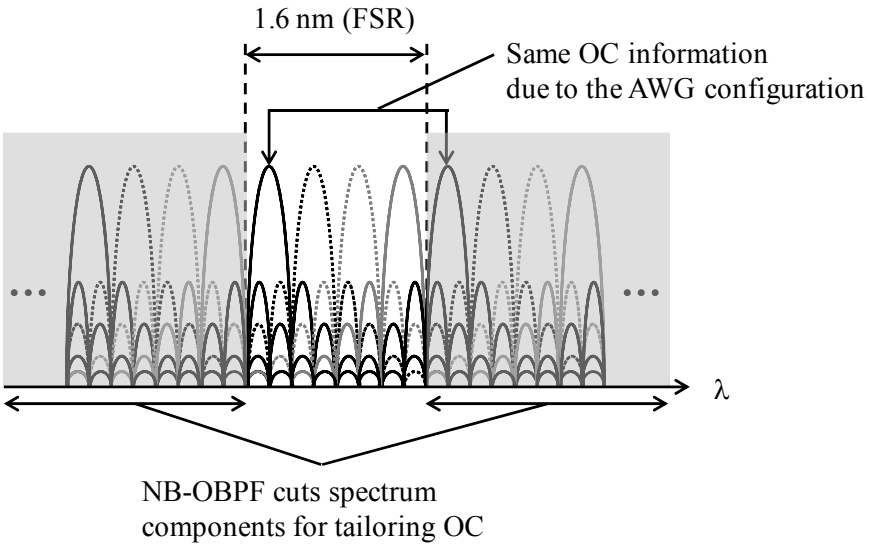

Fig. 5.2: Ideal operation principle of tailoring OC by 16 × 16 port encoder.

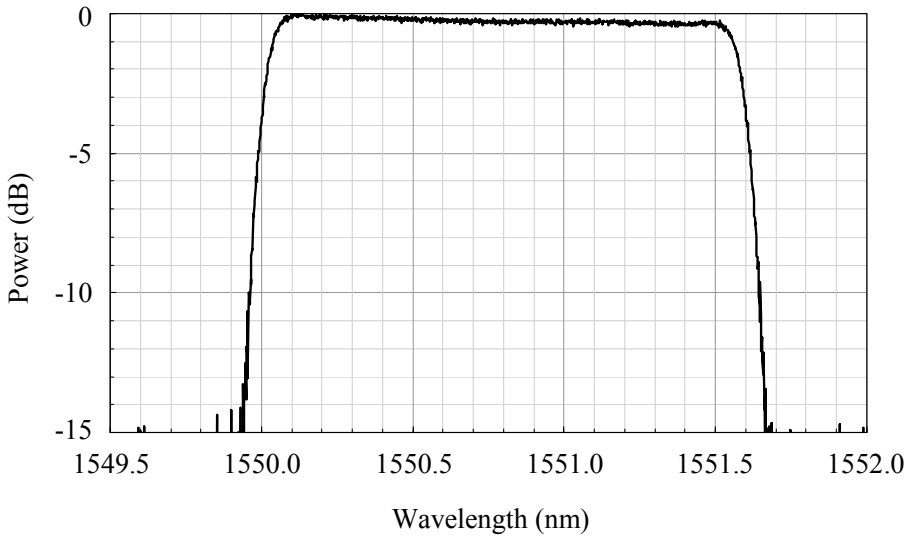

Fig. 5.3: Wavelength response of the rectangular shaped NB-OBPF.

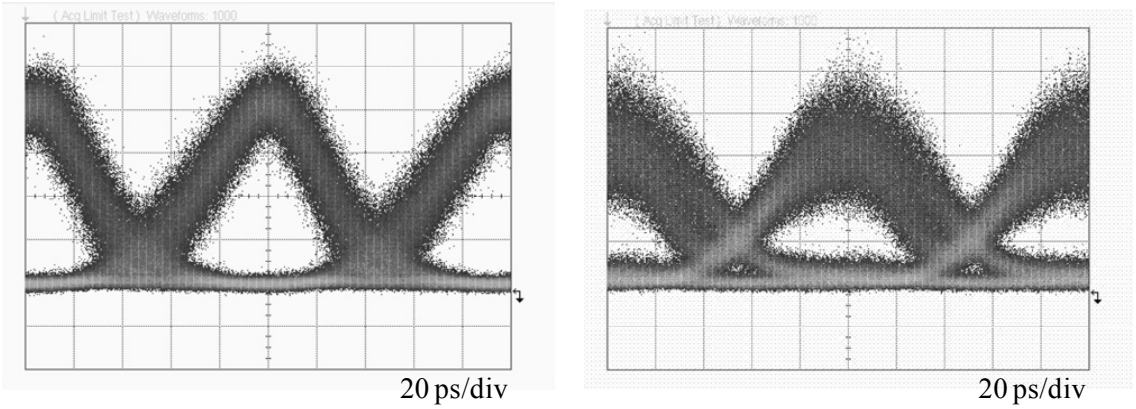

(a) Back-to-back (b) 65-km SMF transmission

Fig. 5.4: Decoded optical eye diagrams as 4 multiplexing OCs whose spectra are tailored by the NB-OBPF.

5.2.3 10-Gb/s Burst-Mode 3R Receiver

10-Gb/s burst-mode receiving techniques are one of the most crucial challenges after long-reach transmission without dispersion compensation. Due to the degradation of OSNR after long-reach transmission, it is necessary for the OLT receiver to have both good receiver sensitivity and high pulse width distortion tolerance. In order to study the feasibility of the 10G-TDM-OCDM-PON systems, we developed the 10-Gb/s burst-mode 3R receiver incorporating a burst-mode automatic gain control (AGC) optical receiver and an 82.5 Gsample/s (8 × 10.3125 GHz) over-sampling

burst-mode CDR to fully comply with IEEE802.3av 10G-EPON PR30 standards [78]. Figure 5.5 shows the block diagram of the 10-Gb/s burst-mode 3R receiver. The 10-Gb/s burst-mode 3R receiver is constructed by an APD-preamplifier IC, a limiting amplifier IC, and an 82.5 Gsample/s sampling CDR [87]. The function of the burst-mode AGC/ATC receiver has been described in Chapter 3. The 82.5 GSample/s over-sampling CDR produces eight 10.3-GHz multi-phase clocks. These eight clocks are sequentially shifted by 45 degrees per phase. Thus, incoming data can be successfully captured by the sampling IC at the sampling resolution of a high 12-ps, which is equal to 45° in phase at 10.3-Gb/s. This very high speed sampling resolution can elevate the pulse-width distortion tolerance of the oversampling based CDR [21] because it can sample a very narrow eye opening region of data. The incoming burst-mode data can be retimed by selecting the adequate phase at an 82.5 GSample/s equivalent rate by eight 45° phase-shifted clocks. The burst-mode receiver can realize high sensitivity as well as a fast response by adapting in combination with the burst-mode AGC, ATC, and 82.5 GSample/s over-sampling techniques.

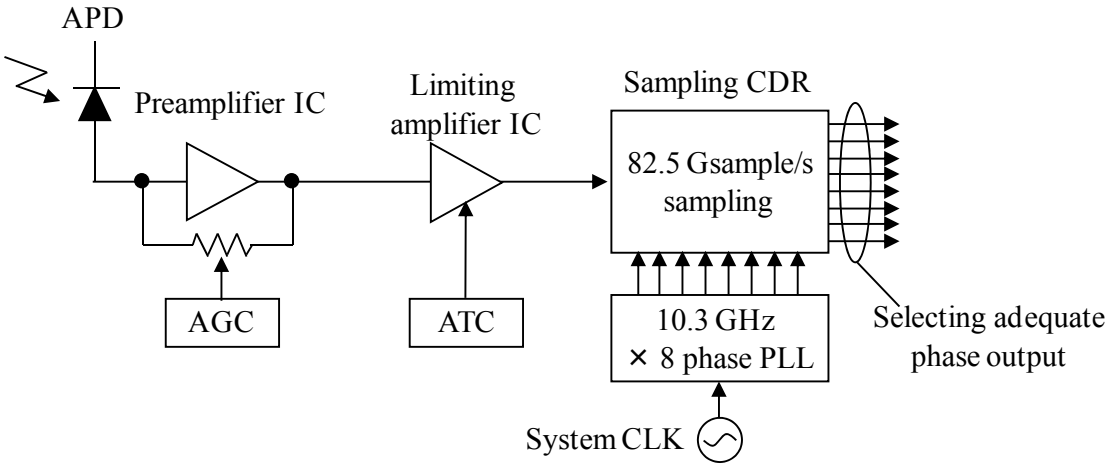

Fig. 5.5: Block diagram of 10-Gb/s burst-mode 3R receiver.

5.3 Full-Duplex Transmission Experiment without Dispersion Compensation

5.3.1 Experimental Setup and Transmission Performance

The transmission performances of our proposed long reach 10G-TDM-OCDM-PON systems were measured in two stages. First, the total transmission performance was evaluated under the condition of fixing the port numbers of multi-port encoder/decoders. Figure 5.6 shows the experimental setup and results of full duplex 4-packet × 4-OC transmission over a 65-km SMF without dispersion compensation on a single wavelength. Four different transmission lengths (25, 15, 10, and 1 km) between an RN and ONUs were tested because the practical 10-Gb/s TDM-PON system is operated under various access spans within 20 km [39]. For BER measurements of different transmission distances, the connections between access spans and ONUs were changed at the connection points for the first experiment, as shown in Fig. 5.6. In this experiment, a 16 × 16 port encoder/decoders pair was adopted as the multi-port encoder/decoder. Port names of D1, D2, D3, D4, U1, U2, U3, U4, D, and U were set to port numbers No. 1, 5, 9, 13, 3, 7, 11, 15, 8, and 6, respectively. Mode-locked laser diodes (MLLDs) with a 10.3125 GHz repetition rate and 1551 nm center wavelength were used for the OLT and ONUs, respectively. The 10-Gb/s burst-mode 3R receivers (BM-Rxs) were placed at the OLT. Use of the same wavelength for both uplink and downlink was the most serious condition due to reflections from each component.

In the downlink, the MLLD output a 2.4-ps pulse train, as shown in Fig. 5.6(a). It was modulated to the continuous data with PRBS 2^{31}–1 by a $LiNbO_3$ intensity modulator (LN-IM). The modulated data was split into 4 branches and encoded by the 16-chip (200 Gchip/s), 16-phase-shifted multi-port encoder with 200-GHz FSR, as shown in Fig. 5.6(b). In order to reduce the chromatic dispersion effect, the spectrum of each OC signal was tailored by filtering out the sideband components by using the rectangular shaped NB-OBPF with a 1.6 nm bandwidth, as shown in Fig. 5.6(c). Figure 5.6(d) shows the completely closed eye diagram of 4-OC data after 40-km SMF transmission due to the chromatic dispersion. However, a good eye opening was obtained from the multi-port decoder, which has the same structure as the OLT multi-port encoder, at the RN (Fig. 5.6(e)) because the decoded signal has a single spectrum component. At the ONU, a clear eye diagram after the total 65-km SMF transmission was achieved, as shown in Fig. 5.6(f). For the BER measurement, the transmitted signal was recovered by the 3R receiver, as shown in Fig. 5.6(g). In this experiment, the

10-Gb/s burst-mode 3R receiver for the OLT was also applied for ONUs to measure the penalty between uplink and downlink.

In the uplink, 3.2-ps optical pulses were generated by the MLLD, as shown in Fig. 5.6(h). The output of the MLLD was modulated to 4 optical packets with PRBS 2^{31}–1 data by the burst-mode modulators. Each burst-mode modulator was constructed by both a LN-IM and an acousto-optic modulator (AOM). The switching speed and the extinction ratio of the AOMs were about 100 ns and over 45 dB, respectively. Therefore, the burst-mode modulators could simultaneously achieve a fast burst turn-on/off time and sufficient power suppression during idle periods. The packet length was 100 μs with an overhead length of 800 ns, which is compliant with IEEE802.3av standards (Fig. 5.6(i)). These optical packets were combined and each guard time between packets was set to less than 300 ns. Other uplink signals were also modulated to the continuous data with PRBS 2^{31}–1 due to a lack of equipment. However, this experimental setup is sufficient to demonstrate the feasibility of this system. Figure 5.6(j) shows the pulse broadening waveform after 25-km SMF transmission due to the chromatic dispersion. However, the envelope of the multi-port encoder output was shaped like a downlink optical encoded waveform, as shown in Fig. 5.6(k). Figure 5.6(l) shows that the spectrum of 4-OC data was limited to only 4 spectrum components as the downlink. After 40-km SMF transmission, 4-OC data were decoded and recovered for BER measurement by the multi-port decoder and burst-mode 3R receiver at the OLT, as shown in Figs. 5.6(m) and (n), respectively. The 10-Gb/s burst-mode 3R receiver can provide a burst-mode 3R function with 82.5 Gsample/s over-sampling.

Figures 5.7 and 5.8 show the BER measurement results of the downlink and uplink, respectively. The solid and dashed lines indicate SMF transmission and B-to-B results, respectively. In all cases, a BER of less than 10^{-7} could be achieved. This demonstrates that the system can realize error-free operation with the forward error correction (FEC) of RS (255, 223). In the cases of both downlink and uplink, the power penalties increased with further SMF transmission due to the increase of cumulative chromatic dispersion as well as optical signal to noise ratio (OSNR) degradation. In contrast, in the uplink, the power penalty between packets for the same OC at BER = 10^{-3} was as low as 0.3 dB because the burst-mode 3R receiver could recover the received packet data quickly. A receiver sensitivity of less than –29.8 dBm at BER = 10^{-3} was also achieved.

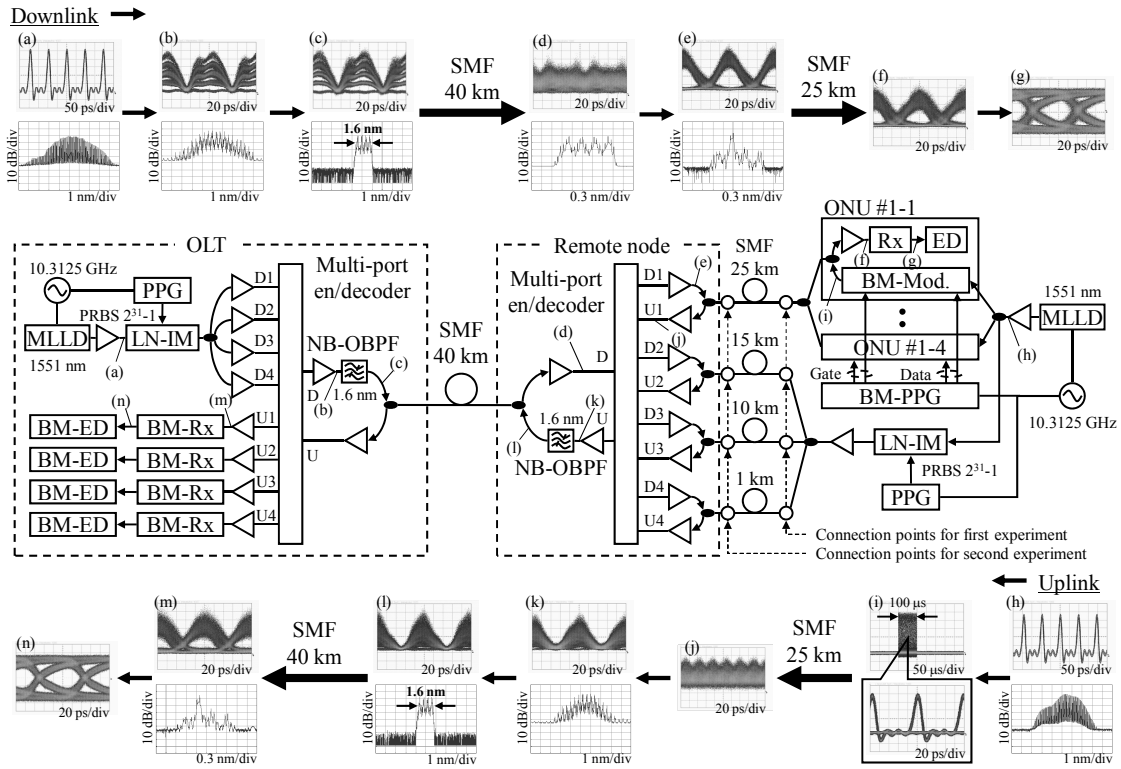

Fig. 5.6: Experimental setup and results of 10G-TDM-OCDM-PON full-duplex transmission over 65-km SMF.

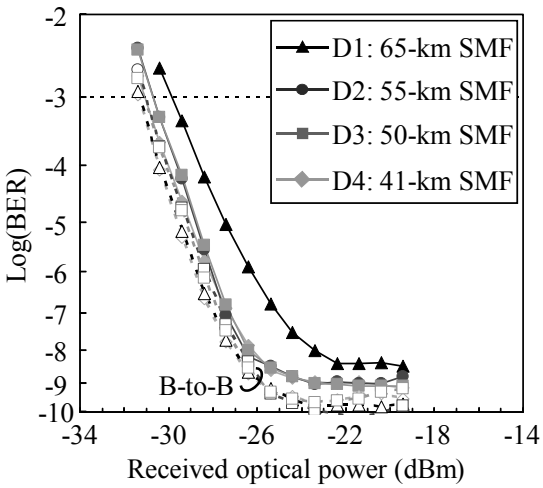

Fig. 5.7: Measured BER performances of downlink 4-OC data.

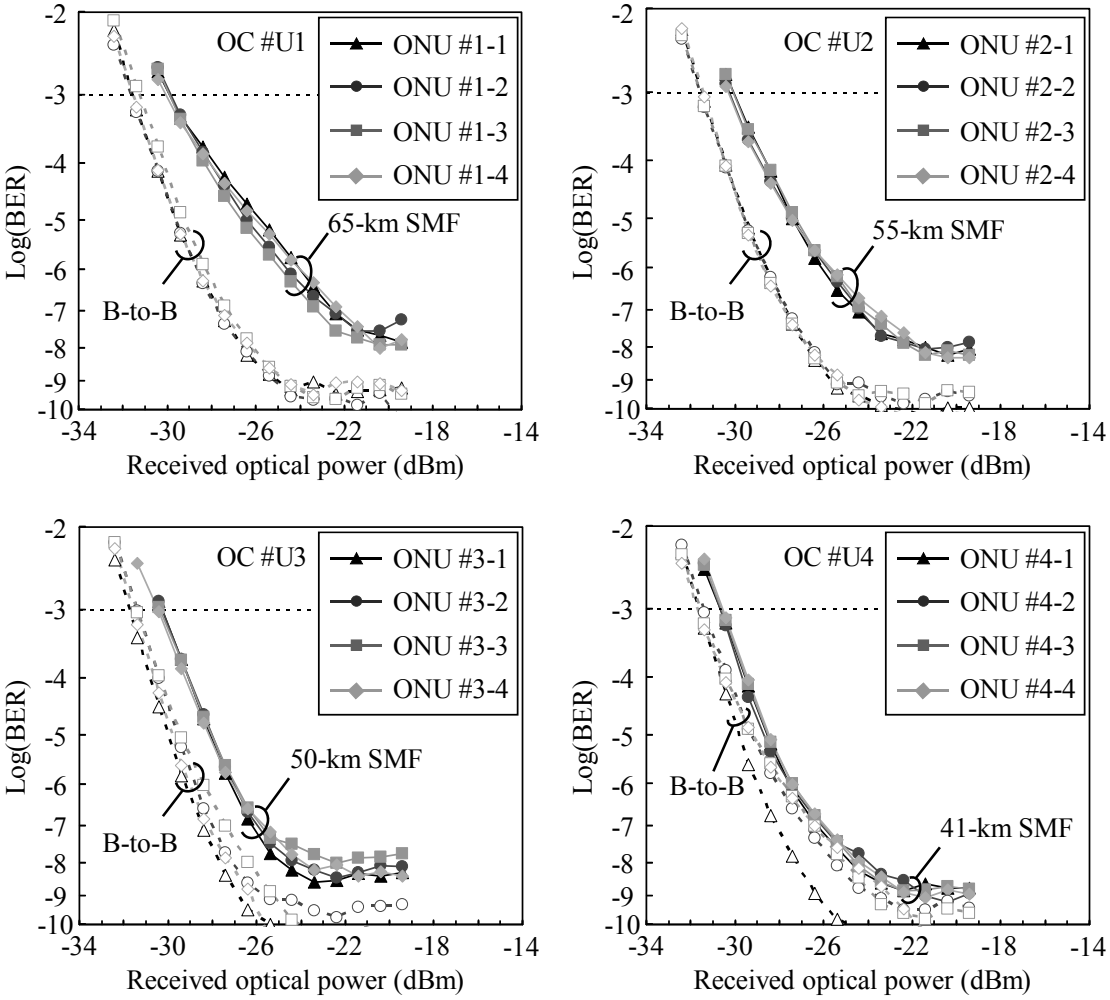

Fig. 5.8: Measured BER performances of uplink 4-packet × 4-OC data.

5.3.2 65-km SMF Transmission without Dispersion Compensation

In the next step, we studied the feasibility of the multi-port encoder/decoder over 65-km SMF transmission in the long reach 10G-TDM-OCDM-PON system. We additionally measured the BER performances of all encoder/decoder ports after the transmission because the multi-port encoder/decoder might have some performance deviations depending on the port. Although the performance of the multi-port encoder/decoder varied port by port to some extent, the overall data will confirm the 65-km transmission even for the worst case. We also measured the crosstalk between uplink and downlink and the MAI with 4-OC.

Figure 5.9 shows the measured total chromatic dispersions of the 65-km, 55-km, 50-km, and 41-km SMFs, which at 1551 nm were around 1258 ps/nm, 1098 ps/nm, 1008 ps/nm, and 867 ps/nm,

respectively. In this experiment, the total chromatic dispersions of all transmission lines were larger than those adopting standard SMF, which had a dispersion parameter of about 17 ps/nm/km at 1550 nm, because the dispersion parameter of the 40-km SMF was about 21.4 ps/nm/km at 1551 nm in this experiment. Therefore, the total transmission length can be extended to about 74 km by adapting a standard SMF to all transmission lines.

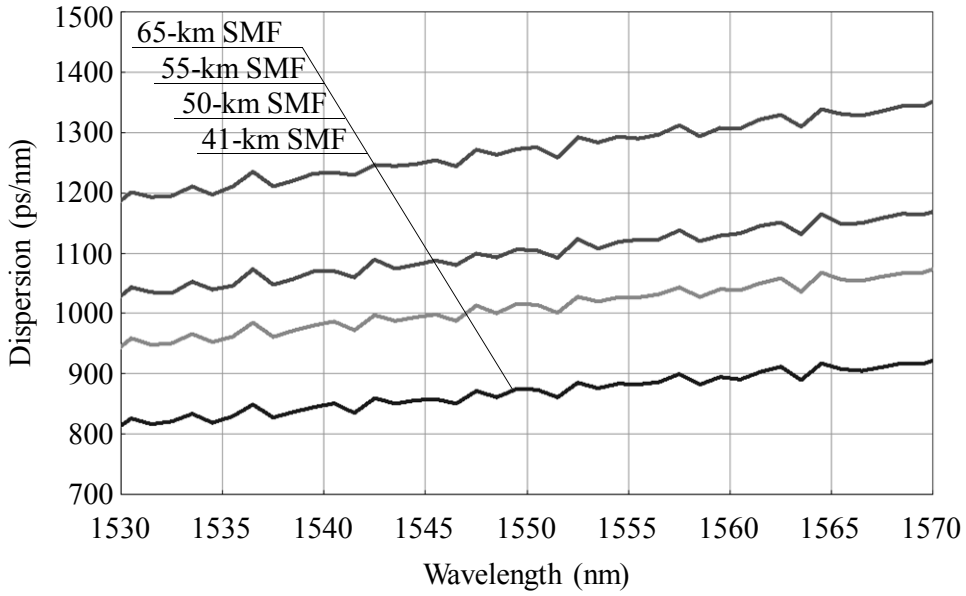

Fig. 5.9: Measured total chromatic dispersion of all transmission lines.

Figure 5.10 shows the measured BER of the downlink and uplink after 65-km SMF transmission. In all cases, a BER of less than 10^{-7} could be achieved, similar to the result of the first experiment. This confirms that all data after 65-km SMF transmission can realize error-free operation with the FEC of RS (255, 223). In the downlink, the deviation of the measured receiver sensitivities of all OCs at BER = 10^{-3} was less than 0.4 dB. In contrast, in the uplink, that of all 16-data (4-packet × 4-OC) was less than 0.8 dB. These deviations of receiver sensitivity were caused by a mismatch of the correlation characteristics between the multi-port encoder/decoder ports. The receiver sensitivity of the downlink was better than that of the uplink, and the power penalty between uplink and downlink was about 0.4 dB. This power penalty may be caused by the burst transmission in the uplink. However, an uplink receiver sensitivity of less than –29.2 dBm at BER = 10^{-3} was achieved by adapting the high-sensitivity burst-mode 3R receiver. These results of low deviations and high receiver sensitivity confirm the feasibility of the proposed long reach 10G-TDM-OCDM-PON system.

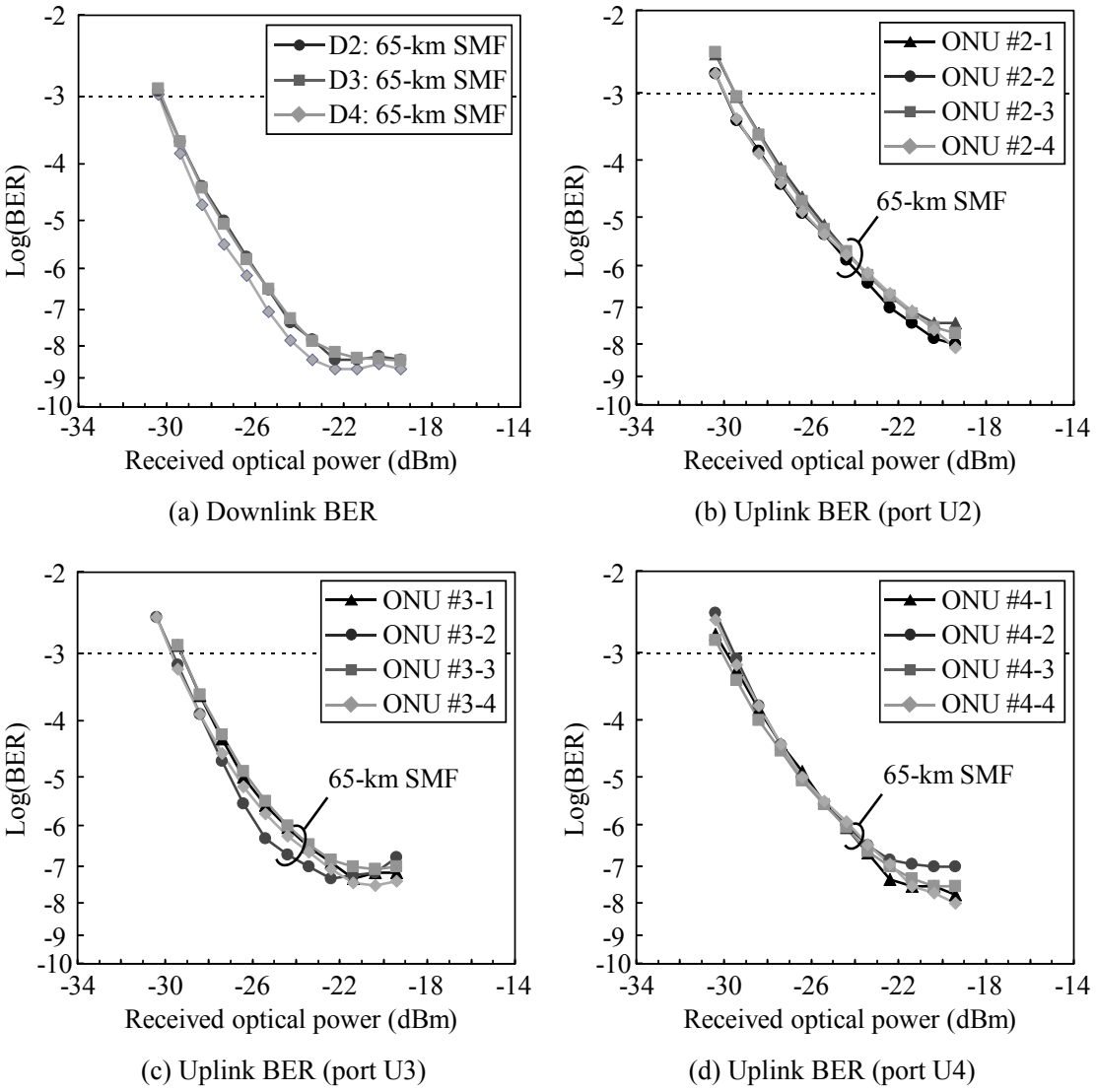

(a) Downlink BER (b) Uplink BER (port U2)

(c) Uplink BER (port U3) (d) Uplink BER (port U4)

Fig. 5.10: Measured BER performances of (a) downlink and (b), (c), and (d) uplink 4-packet × 4-OC data after 65-km SMF transmission.

None of the experiments showed any dynamic range dependence between packets and guard time dependence due to the lack of a burst-mode optical amplifier [105]. However, the system feasibility can be demonstrated by using the 10-Gb/s burst-mode receiver, which can process 10-Gb/s uplink packets with different optical powers, as discussed in Chapter 3.

5.4 Discussion on Power Penalty

Figure 5.11 shows the measured BER performances of uplink from ONU No. 1-1 after 65-km SMF transmission. The filled circle, open circle, and cross mark indicate the BER results under conditions of bi-directional 4-OC multiplexing, uni-directional (only uplink) 4-OC multiplexing, and uni-directional 1-OC, respectively. As shown in the figure, the crosstalk between uplink and downlink was negligible because of the minimization of reflections from each component and the different code assignment for uplink and downlink. Moreover, the MAI of 4-OC was about 0.6 dB at BER = 10^{-3} due to the good correlation properties of the multi-port encoder/decoder. Figure 5.12 shows the SMF transmission distance versus minimum receiver sensitivity at BER = 10^{-3} for all 4 combinations of uplink/downlink and bi-directional × 4-OC / uni-directional × 1-OC. The maximum burst penalty between uplink and downlink was only 0.4 dB. This small penalty was thanks to the fast response of the burst-mode receiver. However, the power penalty was proportional to the SMF transmission distance due to the increase of the cumulative chromatic dispersion. As a result, the maximum transmission penalty was 1.8 dB compared with the difference in the receiver sensitivity between 0-km and 65-km transmission of uplink bi-directional × 4-OC. Table 5.1 shows the comparison of the power penalty. The sensitivity variations and power penalties other than transmission penalty were less than 0.6 dB. This indicates that the variations of the TDM and OCDM signals were small enough to ignore. The power penalty of the 65-km SMF transmission was the largest of the power penalty sources, meaning that the transmission penalty is the most significant parameter in the construction of long reach 10G-TDM-OCDM-PON systems. T. Kodama et al. showed the theoretical analysis for the ultimate distance of this dispersion compensation-free transmission by using the NB-OBPF [106]. In this analysis, 100-km standard SMF transmission is the maximum distance without dispersion compensation by using a 16 × 16 port encoder/decoder.

In addition, we would like to discuss the number of OCs using the 16 × 16 port encoder/decoder. In this experiment, we applied only 4 OCs for both uplink and downlink due to the beat noise and MAI. In a coherent OCDMA, the required power contrast ratio (PCR) of the cross-correlation to the auto-correlation is more than 15 dB in order to suppress the beat noise and the MAI noise [102]. The 16 × 16 port encoder/decoder can achieve the PCR more than 15 dB when neighboring output ports are not used. However, the PCR of neighboring output ports was only about 6 dB [102]. Half-ports of the 16 × 16 port encoder/decoder have already been used for duplex 4-OC systems. Therefore, the BER performance will be degraded by adopting more optical codes even if the chromatic dispersion effect is perfectly compensated. However, the port count of the optical multi-port encoder/decoder

can be increased up to more than 50 [107]. This indicates that the proposed long reach 10G-TDM-OCDM-PON can scale up the number of OCs by adopting the high port count multi-port encoder/decoder.

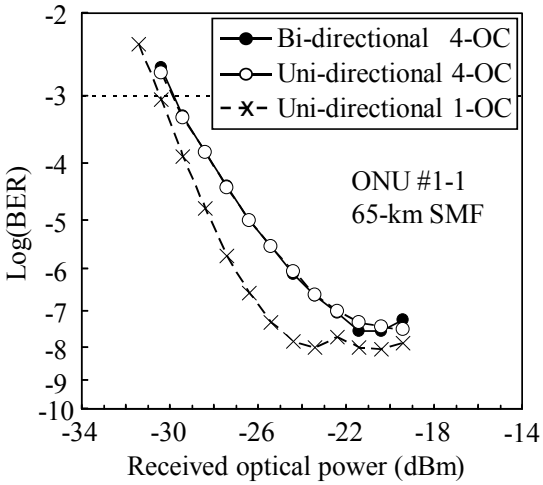

Fig. 5.11: Measured BER performances of uplink from ONU No. 1-1 with 65-km SMF.

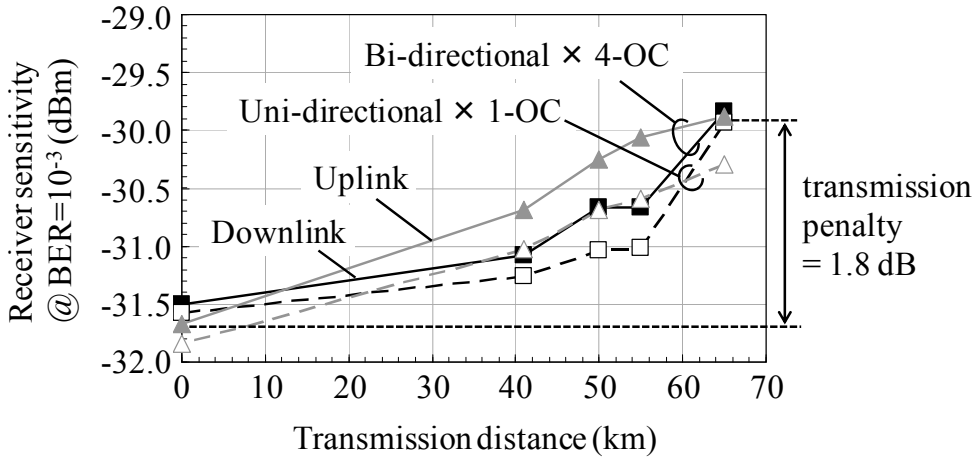

Fig. 5.12: Transmission distance vs. receiver sensitivity of all 4 combinations of up/down link and bi-directional × 4-OC/uni-directional × 1-OC.

Table 5.1: Comparison of power penalties.

No.	Sources of power penalty	Max. penalty	Unit
1	Packet variation	0.5	dB
2	OC variation	0.4	dB
3	Bi-directional transmission	0.1	dB
4	4-OC MAI	0.6	dB
5	Burst-mode transmission	0.4	dB
6	65-km SMF transmission	1.8	dB

5.5 Conclusion

In this chapter, we have proposed a novel 10G-TDM-OCDM-PON system using only a multi-port encoder/decoder pair both at the OLT and RN. This configuration enables us to increase the total capacity of existing 10-Gb/s TDM-PON by a factor of OC count by mitigating the system complexity. Use of a full duplex, 4-packet × 4-OC 10G-TDM-OCDM-PON transmission on a single wavelength over 65-km SMF without dispersion compensation using 200 Gchip/s OC was successfully demonstrated by tailoring the OC spectrum and adapting a 10-Gb/s burst-mode 3R receiver. We have also explored the sources of power penalty and found that the transmission penalty is the most delicate parameter for long reach 10G-TDM-OCDM-PON systems because it is the largest power penalty source.

Chapter 6

Conclusion

This dissertation has presented our study on a long reach hybrid 10-Gb/s TDM-PON system and OCDMA (10G-TDM-OCDM-PON) systems for the purpose of achieving a high-speed, high spectral efficiency, long-reach optical access network. A detailed discussion of the validity of the proposed scheme has been presented. The main results obtained in this dissertation can be summarized as follows.

In Chapter 3, we have focused a 10-Gb/s burst-mode transmitter for an ONU and a 10-Gb/s burst-mode receiver for an OLT. The burst-mode transmitter could achieve a fast burst-mode response of less than 10 ns and high-launched optical power of more than +7.0 dBm by adopting an impedance controlled DC-coupled transmission line between an LD driver and a DFB-LD. In addition, to meet the demand for wide dynamic range and good receiver sensitivity, the continuous-mode AGC and ATC functions were used for a preamplifier and a limiting amplifier of a burst-mode receiver. We also described the configuration of a dual-rate burst-mode receiver that can be realized by using a serial type preamplifier and limiting amplifier that switch their transimpedance gain, noise equivalent bandwidth, and transient response time by an external rate select signal. As a result, the OLT burst-mode receiver could achieve a high receiver sensitivity for 10-Gb/s and 1-Gb/s of less than –30.6 dBm and –34.6 dBm, respectively, with fast receiver settling times of 800 ns for 10-Gb/s packets and 400 ns for 1-Gb/s packets.

In Chapter 4, we have proposed 10G-TDM-OCDM-PON systems that enable the total capacity of

existing 10-Gb/s TDM-PON to be increased by a factor of OC count by mitigating the system complexity. The uplink burst-data transmission of 4 × 10-Gb/s TDM-PON systems over 4 × OC was demonstrated using a 16-chip (200 Gchip/s), 16-level phase-shifted SSFBG encoder at ONUs and a single multi-port decoder at an OLT. With the assistance of FEC, error-free operation could be achieved in all 16 ONUs of the 10G-TDM-OCDM-PON while maintaining a four times larger total capacity than the conventional 10-Gb/s TDM-PON. Finally, we have shown that the key to unprecedented symmetric uplink bandwidth is a newly introduced 16-level phase-shifted encoding/decoding whose auto-correlation waveform can be preferably adopted in the burst-mode reception at 10-Gb/s. In addition, we have also shown that the 10G-TDM-OCDM-PON system can accommodate 32 users with symmetric gigabit-bandwidth.

In Chapter 5, we have proposed the long reach 10G-TDM-OCDM-PON system. Three key devices for achieving long reach transmission are described: a single multi-port encoder/decoder pair at an OLT and a RN, an NB-OBPF, and a 10-Gb/s burst-mode 3R receiver. Use of a full duplex, 4-packet × 4-OC 10G-TDM-OCDM-PON, transmission on a single wavelength over 65-km SMF without dispersion compensation using 200 Gchip/s OCs was successfully demonstrated by tailoring the OC spectrum and adopting the 10-Gb/s burst-mode 3R receiver. In addition, we have discussed the sources of power penalty. The transmission penalty is the most delicate parameter in terms of constructing long reach 10G-TDM-OCDM-PON systems because it has the largest power penalty.

All the results shown in Chapters 3, 4, and 5 demonstrate the high reliability of the proposed long reach 10G-TDM-OCDM-PON systems. We have also discussed the three key technologies for future optical access networks: 10-Gb/s burst-mode transmitter and receiver technologies, 10-Gb/s burst-mode optical code transmission technologies, and long-reach 10-Gb/s TDM × OCDM transmission technologies without dispersion compensation.

In the future development of the system, the maturity of optical devices is an important issue. Currently, optical amplifiers are inserted to compensate for the insertion loss of each optical encoder/decoder device. In addition, other immature devices such as MLLD are currently used in the proposed system, making it more complex and expensive. The maturity of optical and electrical devices crucially depends on several technological innovations in the future.

Finally, from all the obtained results and findings, the author hopes that the work in this thesis will contribute to the development of future optical access networks.

Bibliography

[1] G. P. Agrawal, *Fiber-Optic Communication Systems*, 3rd ed. New York, NY: John Wiley & Sons, 2002.

[2] S. Shimada and N. Uchida, "Field trial of medium/small capacity optical fiber transmission systems," *ECL Technical Journal, NTT, Japan*, vol. 30, no. 9, pp. 2121–2132, 1981.

[3] E. Yamazaki, S. Yamanaka, Y. Kisaka, T. Nakagawa, K. Murata, E. Yoshida, T. Sakano, M. Tomizawa, Y. Miyamoto, S. Matsuoka, J. Matsui, A. Shibayama, J. Abe, Y. Nakamura, H. Noguchi, K. Fukuchi, H. Onaka, K. Fukumitsu, K. Komaki, O. Takeuchi, Y. Sakamoto, H. Nakashima, T. Mizuochi, K. Kubo, Y. Miyata, H. Nishimoto, S. Hirano, and K. Onohara, "Fast optical channel recovery in field demonstration of 100-Gbit/s Ethernet over OTN using real-time DSP," *Optics Express*, vol. 19, no. 14, pp. 13179–13184, July 2011.

[4] F. Chang, K. Onohara, and T. Mizuochi, "Forward error correction for 100 G transport networks," *IEEE Commun. Mag.*, vol. 48, no. 3, pp. S45–S55, Mar. 2010.

[5] L. E. Nelson, G. Zhang, M. Birk, C. Skolnick, R. Isaac, Y. Pan, C. Rasmussen, G. Pendock, and B. Mikkelsen, "A robust real-time 100G transceiver with soft-decision forward error correction [Invited]," *IEEE/OSA J. Opt. Commun. Netw.*, vol. 4, no. 11, pp. B131–B141, Nov. 2012.

[6] *Carrier Sense Multiple Access With Collision Detection (CSMA/CD) Access Method and Physical Layer Specifications*, IEEE Std 802.3™-2008, 2008.

[7] Ministry of Internal Affairs and Communications Japanese Government Report.

[8] *Asymmetric digital subscriber line (ADSL) transceivers*, ITU-T Recommendation G. 992.1, 1999.

[9] *Splitterless asymmetric digital subscriber line (ADSL) transceivers*, ITU-T Recommendation

G. 992.2, 1999.

[10] J. A. Chiddix, H. Laor, D. M. Pangrac, L. D. Williamson, and R. W. Wolfe, “AM video on fiber in CATV systems: need and implementation,” *IEEE J. Select. Areas Commun.*, vol. 8, no. 7, pp. 1229–1239, Sept. 1990.

[11] P. W. Shumate, “Fiber-to-the-home: 1977–2007,” *IEEE/OSA J. Lightw. Technol.*, vol. 26, no. 9, pp. 1093–1103, May 2008.

[12] 3GPP TS 36.300, “Evolved Universal Terrestrial Radio Access (E-UTRA) and Evolved Universal Terrestrial Radio Access Network (E-UTRAN); Overall description; Stage 2,” 2008. [Online]. Available: http://www.3gpp.org/ftp/Specs/html-info/36300.htm

[13] *IEEE Standard for Air Interface for Broadband Wireless Access Systems*, IEEE Std 802.16™-2012, 2012.

[14] C.-H. Lee, W. V. Sorin, and B. Y. Kim, “Fiber to the home using a PON infrastructure,” *IEEE/OSA J. Lightw. Technol.*, vol. 24, no. 12, pp. 4568–4583, Dec. 2006.

[15] T. Koonen, “Fiber to the home/fiber to the premises: what, where, and when?,” *Proceedings of the IEEE*, vol. 94, no. 5, pp. 911–934, May 2006.

[16] F. J. Effenberger, H. Ichibangase, and H. Yamashita, “Advances in broadband passive optical networking technologies,” *IEEE Commun. Mag.*, vol. 39, no. 12, pp. 118–124, Dec. 2001.

[17] A. Banerjee, Y. Park, F. Clarke, H. Song, S. Yang, G. Kramer, K. Kim, and B. Mukherjee, “Wavelength-division-multiplexed passive optical network (WDM-PON) technologies for broadband access: a review [Invited],” *J. Opt. Networking*, vol. 4, no. 11, pp. 737–758, Nov. 2005.

[18] D. Qian, N. Cvijetic, J. Hu, and T. Wang, “108 Gb/s OFDMA-PON with polarization multiplexing and direct detection,” *IEEE/OSA J. Lightw. Technol.*, vol. 28, no. 4, pp. 484–493, Feb. 2010.

[19] K. Kitayama, X. Wang, and N. Wada, “OCDMA over WDM PON—Solution path to gigabit-symmetric FTTH,” *IEEE/OSA J. Lightw. Technol.*, vol. 24, no. 4, pp. 1654–1662, Apr. 2006.

[20] J. Nakagawa, M. Nogami, M. Noda, Y. Kato, T. Uo, and K. Motoshima, “Newly developed OLT optical transceiver for GE-PON systems compliant with IEEE802.3ah,” in *Proc. 30th European Conference on Optical Communication (ECOC 2004)*, We4.P.139, Stockholm, Sweden, Sept. 2004.

[21] H. Tagami, S. Kozaki, K. Nakura, S. Kohama, M. Nogami, and K. Motoshima, “A burst-mode bit-synchronization IC with large tolerance for pulse-width distortion for gigabit Ethernet PON,” *IEEE J. Solid-State Circuits*, vol. 41, no. 11, pp. 2555–2565, Nov. 2006.

[22] M. Nakamura, S. Nishihara, T. Ito, T. Kurosaki, M. Nogawa, and Y. Ohtomo, "Burst-mode optical receiver ICs for broadband access networks," in *Proc. IEEE Bipolar/BiCMOS Circuits and Technology Meeting (BCTM 2010)*, 2.1, Austin, TX, Oct. 2010.

[23] J. R. Stern, J. W. Ballance, D. W. Faulkner, S. Hornung, D. B. Payne and K. Oakley, "Passive optical local networks for telephony applications and beyond," *Electron. Lett.*, vol. 23, no. 24, pp. 1255–1257, Nov. 1987.

[24] N. Tokura, K. Oguchi, and T. Kanada, "A broadband subscriber network using optical star couplers," in *Proc. IEEE/IEICE Global Telecommunications Conf. (GLOBECOM'87)*, Paper 37.1, Tokyo, Japan, Nov. 1987.

[25] K. Kumozaki, "Optical access systems: present state and future directions," *NTT Technical Review*, vol. 6, no. 5, May 2008. [Online]. Available: https://www.ntt-review.jp/archive/ntttechnical.php?contents=ntr200805sf2.html

[26] *Broadband Optical Access Systems Based on Passive Optical Networks (PON)*, ITU-T Recommendation G. 983 Series 2001.

[27] *Gigabit-Capable Passive Optical Networks (G-PON)*, ITU-T Recommendation G. 984 Series 2004.

[28] H. L. Zhang, G.W. Pickrell, Z. Morbi, Y. Wang, M. Ho, K. A. Anselm, and W.-Y. Hwang, "32-channel, injection-locked WDM-PON SFP transceivers for symmetric 1.25 Gbps operation," in *Proc. Optical Fiber Communication Conference and National Fiber Optic Engineers Conference (OFC/NFOEC 2011)*, NTuB4, Los Angeles, CA, Mar. 2011.

[29] K. Y. Cho, Y. Takushima, and Y. C. Chung, "10-Gb/s operation of RSOA for WDM PON," *IEEE Photon. Technol. Lett.*, vol. 20, no. 18, pp. 1533–1535, Sept. 2008.

[30] K. Y. Cho, K. Tanaka, T. Sano, S. P. Jung, J. H. Chang, Y. Takushima, A. Agata, Y. Horiuchi, M. Suzuki, and Y. C. Chung, "Long-reach coherent WDM PON employing self-polarization-stabilization technique," *IEEE/OSA J. Lightw. Technol.*, vol. 29, no. 4, pp. 456–462, Feb. 2011.

[31] D. Qian, J. Hu, J. Yu, P. N. Ji, L. Xu, Ting Wang, M. Cvijetic, and T. Kusano, "Experimental demonstration of a novel OFDM-A based 10Gb/s PON architecture," in *Proc. 33rd European Conference on Optical Communication (ECOC 2007)*, paper 5.4.1, Berlin, Germany, Sept. 2007.

[32] D. Qian, T. T. Kwok, N. Cvijetic, J. Hu, and T. Wang, "41.25 Gb/s real-time OFDM receiver for variable rate WDM-OFDMA-PON transmission," in *Proc. Optical Fiber Communication Conference and National Fiber Optic Engineers Conference (OFC/NFOEC 2010)*, PDPD9, San Diego, CA, Mar. 2010.

[33] Y. Yoshida, K. Ishii, A. Maruta, Y. Akiyama, T. Yoshida, N. Suzuki, K. Koguchi, J. Nakagawa, T. Mizuochi, and K. Kitayama, "Experimental demonstration of 2xONU 30Gbps digitally- supported-coherent IFDMA-PON uplink," in *Proc. Optical Fiber Communication Conference and National Fiber Optic Engineers Conference (OFC/NFOEC 2012)*, OW3B.5, Los Angeles, CA, Mar. 2012.

[34] K. Kitayama, Y. Yoshida, A. Maruta, K. Ishii, Y. Akiyama, M. Noda, K. Koguchi, M. Nogami, K. Onohara, and T. Mizuochi, "Elastic and green optical access based upon coherent interleaved frequency division multiple access (IFDMA)," in *Proc. Optical Fiber Communication Conference and National Fiber Optic Engineers Conference (OFC/NFOEC 2013)*, OM2A.4, Anaheim, CA, Mar. 2013.

[35] S. Hara and R. Prasad, "Overview of multicarrier CDMA," *IEEE Commun. Mag.*, vol. 35, no. 12, pp. 126–133, Dec. 1997.

[36] P. R. Prucnal, M. A. Santoro, and T. R. Fan, "Spread spectrum fiber-optic local area network using optical processing," *IEEE/OSA J. Lightw. Technol.*, vol. LT-4, no. 5, pp. 547–554, May 1986.

[37] J. A. Salehi and C. A. Brackett, "Code division multiple-access technique in optical fiber networks, part I: Fundamental principles and part II: Systems performance analysis," *IEEE Trans. Commun.*, vol. 37, no. 8, pp. 824–842, Aug. 1989.

[38] R. Matsumoto, T. Kodama, S. Shimizu, R. Nomura, K. Omichi, N. Wada, and K. Kitayama, "Cost-effective, asynchronous 4 x 40Gbps full-duplex OCDMA demonstrator using apodized SSFBGs and a multi-port encoder/decoder," in *Proc. Optical Fiber Communication Conference and National Fiber Optic Engineers Conference (OFC/NFOEC 2013)*, OW4D.7, Anaheim, CA, Mar. 2013.

[39] IEEE P802.3av Task Force [Online]. Available: http://www.ieee802.org/3/av

[40] *10-Gigabit-Capable Passive Optical Networks (XG-PON)*, ITU-T Recommendation G.987 Series, 2010.

[41] FSAN NGA [Online]. Available: http://www.fsanweb.org/

[42] N. Nakagawa, S. Yoshima, N. Suzuki, M. Noda, M. Nogami, H. Ichibangase, J. Nakagawa, and K. Kitayama, "Scalable GE-PON over OCDMA without sacrifice of upstream bandwidth: principle and its experimental demonstration of 2xGE-PON systems over 2x63-chip code," in *Proc. 34th European Conference on Optical Communication (ECOC 2008)*, We.1.F.7, Brussels, Belgium, Sept. 2008.

[43] K. Tanaka, A. Agata, and Y. Horiuchi, "IEEE 802.3av 10G-EPON standardization and its research and development status," *IEEE/OSA J. Lightw. Technol.*, vol. 28, no. 4, pp. 651–661,

Feb. 2010.

[44] F. J. Effenberger, "The XG-PON system: cost effective 10 Gb/s access," *IEEE/OSA J. Lightw. Technol.*, vol. 29, no. 4, pp. 403–409, Feb. 2011.

[45] J. Kani, F. Bourgart, A. Cui, A. Rafel, M. Campbell, R. Davey, and S. Rodrigues, "Next-generation PON part I—Technology roadmap and general requirements," *IEEE Commun. Mag.*, vol. 47, no. 11, pp. 43–49, Nov. 2009.

[46] F. J. Effenberger, H. Mukai, S. Park, and T. Pfeiffer, "Next-generation PON part II—Candidate systems for next-generation PON," *IEEE Commun. Mag.*, vol. 47, no. 11, pp. 50–57, Nov. 2009.

[47] F. J. Effenberger, H. Mukai, J. Kani, and M. Rasztovits-Wiech, "Next-generation PON part III—System specifications for XG-PON," *IEEE Commun. Mag.*, vol. 47, no. 11, pp. 58–64, Nov. 2009.

[48] P. P. Iannone and K. C. Reichmann, "Optical access beyond 10 Gb/s PON," in *Proc. 36th European Conference on Optical Communication (ECOC 2010)*, Tu.3.B.1, Torino, Italy, Sept. 2010.

[49] P. Chanclou, A. Cui, F. Geilhardt, H. Nakamura, and D. Nesset, "Network operator requirements for the next generation of optical access networks," *IEEE Network*, vol. 26, no. 2, pp. 8–14, Mar./Apr. 2012.

[50] P. Vetter, "Next generation optical access technologies," in *Proc. 38th European Conference on Optical Communication (ECOC 2012)*, Tu.3.G.1, Amsterdam, Netherlands, Sept. 2012.

[51] Y. Luo, X. Zhou, F. J. Effenberger, X. Yan, G. Peng, Y. Qian, and Y. Ma, "Time- and wavelength-division multiplexed passive optical network (TWDM-PON) for next-generation PON stage 2 (NG-PON2)," *IEEE/OSA J. Lightw. Technol.*, vol. 31, no.4. pp. 587–593, Feb. 2013.

[52] F. J. Effenberger, "XG-PON1 versus NG-PON2: which one will win?," in *Proc. 38th European Conference on Optical Communication (ECOC 2012)*, Tu.4.B.1, Amsterdam, Netherland, Sept. 2012.

[53] N. Kataoka, N. Wada, X. Wang, G. Cincotti, and K. Kitayama, "Demonstration of 10Gbps, 4-user, OCDMA transmission over 59km single mode fiber without inline dispersion compensation," in *Proc. Optical Fiber Communication Conference and National Fiber Optic Engineers Conference (OFC/NFOEC 2010)*, OThW1, San Diego, CA, Mar. 2010.

[54] K. Fouli and M. Maier, "OCDMA and optical coding: principles, applications, and challenges," *IEEE Commun. Mag.*, vol. 45, no. 8, pp. 27–34, Aug. 2007.

[55] K. Kitayama, "Code division multiplexing lightwave networks based upon optical code

conversion," *IEEE J. Select. Areas Commun.*, vol. 16, no. 7, pp. 1309–1319, Sept. 1998.

[56] T. Hamanaka, X. Wang, N. Wada, and K. Kitayama, "Compound data rate and data-rate-flexible 622 Mb/s–10 Gb/s OCDMA experiments using 511-Chip SSFBG and cascaded SHG-DFG-based PPLN waveguide optical thresholder," *IEEE J. Select. Topics Quantum Electron.*, vol. 13, no. 5, pp. 1516–1521, Sept./Oct. 2007.

[57] P. Petropoulos, N. Wada, P. C. Teh, M. Ibsen, W. Chujo, K. Kitayama, and D. J. Richardson, "Demonstration of a 64-chip OCDMA system using superstructured fiber gratings and time-gating detection," *IEEE Photon. Technol. Lett.*, vol. 13, no. 11, pp. 1239–1241, Nov. 2001.

[58] G. Manzacca, A. M. Vegni, X. Wang, N. Wada, G. Cincotti, and K. Kitayama, "Performance analysis of a multiport encoder/decoder in OCDMA scenario," *IEEE J. Select. Topics Quantum Electron.*, vol. 13, no. 5, pp. 1415–1421, Sept./Oct. 2007.

[59] A. Keshvarzian and J. A. Salehi, "Multiple-shift code acquisition of optical orthogonal codes in optical CDMA systems," *IEEE Trans. Commun.*, vol. 53, no. 4, pp. 687–697, Apr. 2005.

[60] A. M. Weiner, J. P. Heritage, and J. A. Salehi, "Encoding and decoding of femtosecond pulses," *Opt. Lett.*, vol. 13, no. 4, pp. 300–302, Apr. 1988.

[61] J. P. Heritage, A. M. Weiner, and R. N. Thurston, "Picosecond pulse shaping by spectral phase and amplitude manipulation," *Opt. Lett.*, vol. 10, no. 12, pp. 609–611, Dec. 1985.

[62] K. Kitayama, N. Wada, and H. Sotobayashi, "Architectural considerations for photonic IP router based upon optical code correlation," *IEEE/OSA J. Lightw. Technol.*, vol. 18, no. 12, pp. 1834–1844, Dec. 2000.

[63] P. C. Teh, P. Petropoulos, M. Ibsen, and D. J. Richardson, "Phase encoding and decoding of short pulses at 10 Gb/s using superstructured fiber Bragg gratings," *IEEE Photon. Technol. Lett.*, vol. 13, no. 2, pp. 154–156, Feb. 2001.

[64] X. Wang, K. Matsushima, A. Nishiki, N. Wada, and K. Kitayama, "High reflectivity superstructured FBG for coherent optical code generation and recognition," *Optics Express*, vol. 12, no. 22, pp. 5457–5468, Nov. 2004.

[65] X. Wang, K. Matsushima, K. Kitayama, A. Nishiki, N. Wada, and F. Kubota, "High-performance optical code generation and recognition by use of a 511-chip, 640-Gchip/s phase-shifted superstructured fiber Bragg grating," *Opt. Lett.*, vol. 30, no. 4, pp. 355–357, Feb. 2005.

[66] T. Hamanaka, X. Wang, N. Wada, A. Nishiki, and K. Kitayama, "Ten-user truly asynchronous gigabit OCDMA transmission experiment with a 511-chip SSFBG en/decoder," *IEEE/OSA J. Ligthw. Technol.*, vol. 24, no. 1, pp. 95–102, Jan. 2006.

[67] G. Cincotti, N. Wada, and K. Kitayama, “Characterization of a full encoder/decoder in the AWG configuration for code-based photonic routers—Part I: modeling and design,” *IEEE/OSA J. Lightw. Technol.*, vol. 24, no. 1, pp. 103–112, Jan. 2006.

[68] S. Yoshima, M. Nogami, S. Shirai, N. Suzuki, M. Noda, H. Ichibangase, and J. Nakagawa, “A 10.3 Gbit/s LAN-PHY based burst-mode transmitter with a fast 6 ns turn-on/off time for 10 Gbps-based PON systems,” in *Proc. Optical Fiber Communication Conference and National Fiber Optic Engineers Conference (OFC/NFOEC 2008)*, OWL4, San Diego, CA, Feb. 2008.

[69] S. Yoshima, M. Noda, E. Igawa, S. Shirai, K. Ishii, M. Nogami, and J. Nakagawa, “Recent progress of high-speed burst-mode transceiver technologies for TDM-PON systems,” in *Proc. 21st Annual Wireless and Optical Communications Conference (WOCC 2012)*, N3_3, Kaohsiung, Taiwan, Apr. 2012.

[70] R. S. Tucker, “High-speed modulation of semiconductor lasers,” *IEEE/OSA J. Lightw. Technol.*, vol. 3, no. 6, pp. 1180–1192, Dec. 1985.

[71] H. Nakamura, S. Kimura, K. Hara, N. Yoshimoto, M. Tsubokawa, M. Nakamura, K. Nishimura, A. Okada, and Y. Ohtomo, “AC-coupled burst-mode transmitter using baseline-wander common-mode-rejection technique for 10-Gbit/s-class PON systems,” *IEEE/OSA J. Lightw. Technol.*, vol. 27, no. 3, pp. 336–342, Feb. 2009.

[72] E. Igawa, M. Nogami, N. Ohata, N. Suzuki, and J. Nakagawa, “Symmetric 10G-EPON ONU transceiver integrated with newly-developed burst-mode pre-bias timing control IC,” in *Proc. Optical Fiber Communication Conference and National Fiber Optic Engineers Conference (OFC/NFOEC 2010)* , NMC1, San Diego, CA, Mar. 2010.

[73] E. Igawa, M. Nogami, and J. Nakagawa, “Symmetric 10G-EPON ONU burst-mode transceiver employing dynamic power save control circuit,” in *Proc. Optical Fiber Communication Conference and National Fiber Optic Engineers Conference (OFC/NFOEC 2011)*, NTuD5, Los Angeles, CA, Mar. 2011.

[74] S. Nishihara, S. Kimura, T. Yoshida, M. Nakamura, J. Terada, K. Nishimura, K. Kishine, K. Kato, Y. Ohtomo, N. Yoshimoto, T. Imai, and M. Tsubokawa, “A burst-mode 3R receiver for 10-Gbit/s PON systems with high sensitivity, wide dynamic range, and fast response,” *IEEE/OSA J. Lightw. Technol.*, vol. 26, no. 1, pp. 99–107, Jan. 2008.

[75] Y. Hotta, A. Tsuji, K. Sugimura, S. Kozaki, N. Suzuki, J. Nakagawa, and K. Shimokasa, “The demonstration of symmetric 10G-EPON system for coexistence with 1G-EPON,” in *Proc. Optical Fiber Communication Conference and National Fiber Optic Engineers Conference (OFC/NFOEC 2009)*, OWH4, San Diego, CA, Mar. 2009.

[76] S. Takahashi, K. Shiba, E. Mizuki, K. Makita, and A. Tajima, “Over 25-dB dynamic range

10-/1-Gbps optical burst-mode receiver using high-power-tolerant APD," in *Proc. Optical Fiber Communication Conference and National Fiber Optic Engineers Conference (OFC/NFOEC 2009)*, NME2, San Diego, CA, Mar. 2009.

[77] P. Ossieur, T. Ridder, J. Bauwelinck, C. Mélange, B. Baekelandt, X.-Z. Qiu, J. Vandewege, G. Talli, C. Antony, P. Townsend, and C. Ford, "A 10 Gb/s burst-mode receiver with automatic reset generation and burst detection for extended reach PONs," in *Proc. Optical Fiber Communication Conference and National Fiber Optic Engineers Conference (OFC/NFOEC 2009)* , OWH3, San Diego, CA, Mar. 2009.

[78] J. Nakagawa, M. Nogami, N. Suzuki, M. Noda, S. Yoshima, and H. Tagami, "10.3Gb/s burst-mode 3R receiver incorporating full AGC optical receiver and 82.5GS/s sampling CDR for 10G-EPON systems," in *Proc. 35th European Conference on Optical Communication (ECOC 2009)*, Paper 7.5.3, Vienna, Austria, Sept. 2009.

[79] J. Nakagawa, M. Noda, N. Suzuki, S. Yoshima, K. Nakura, and M. Nogami, "First demonstration of 10G-EPON and GE-PON co-existing system employing dual-rate burst-mode 3R transceiver," in *Proc. Optical Fiber Communication Conference and National Fiber Optic Engineers Conference (OFC/NFOEC 2010)*, PDPD10, San Diego, CA, Mar. 2010.

[80] J. Sugawa, D. Mashimo, and H. Ikeda, "10.3Gbps burst-mode receiver capable of upstream transmission with short overhead for 10G-EPON," in *Proc. 36th European Conference on Optical Communication (ECOC 2010)*, Mo.2.B.4, Torino, Italy, Sept. 2010.

[81] K. Hara, S. Kimura, H. Nakamura, N. Yoshimoto, and H. Hadama, "New AC-coupled burst-mode optical receiver using transient-phenomena cancellation techniques for 10 Gbit/s-class high-speed TDM-PON systems," *IEEE/OSA J. Lightw. Technol.*, vol. 28, no. 19, pp. 2775–2782, Oct. 2010.

[82] K. Hara, S. Kimura, H. Nakamura, N. Yoshimoto, and H. Hadama, "1.25/10.3-Gbit/s dual-rate burst-mode receiver with automatic bit-rate discrimination circuit for coexisting PON systems," in *Proc. 8th International Conference on Optical Internet (COIN 2010)*, TuC1-5, Jeju, Korea, July 2010.

[83] T. Ito, T. Kurosaki, M. Nakamura, S. Nishihara, Y. Ohtomo, A. Okada, and M. Yoneyama, "A burst-mode APD-ROSA using reset signal with less than 100 ns response for 1G/10G-EPON dual-rate optical transceivers," *IEEE/OSA J. Lightw. Technol.*, vol. 29, no. 14, pp. 2089–2101, July 2011.

[84] J. Put, X. Yin, X.-Z. Qiu, J. Gillis, J. Verbrugghe, J. Bauwelinck, J. Vandewege, F. Blache, D. Lanteri, M. Achouche, H.-G. Krimmel, D. Veen, and P. Vetter, "DC-coupled burst-mode

receiver with high sensitivity, wide dynamic range and short settling time for symmetric 10G-GPONs," *Optics Express*, vol. 19, no. 26, pp. B594–B603, Dec. 2011.

[85] M. Noda N. Suzuki, S. Yoshima, M. Nogami, and J. Nakagawa, "Technology progress of high-speed burst-mode 3R receiver for PON applications," in *Proc. Optical Fiber Communication Conference and National Fiber Optic Engineers Conference (OFC/NFOEC 2012)*, OTh4G.6, Los Angels, CA, Mar. 2012.

[86] J. Terada, Y. Ohtomo, K. Nishimura, H. Katsurai, S. Kimura, and N. Yoshimoto, "Jitter-reduction and pulse-width-distortion compensation circuits for a 10Gb/s burst-mode CDR circuit," in *Proc. IEEE International Solid-State Circuits Conference (ISSCC) Dig. Tech. Papers*, pp. 104–106, San Francisco, CA, Feb. 2009.

[87] N. Suzuki, K. Nakura, S. Kozaki, H. Tagami, M. Nogami, and J. Nakagawa, "82.5 Gsample/s (10.3125 GHz × 8 phase clocks) burst-mode CDR for 10G-EPON systems," *Electron. Lett.*, vol. 45, no. 24, pp. 1261–1263, Dec. 2009.

[88] N. Suzuki, K. Nakura, S. Kozaki, H. Tagami, M. Nogami, and J. Nakagawa, "Single platform 10G-EPON 10.3-Gbps/1.25-Gbps dual-rate CDR with fast burst-mode lock time employing 82.5 GS/s sampling IC and bit-rate adaptive decision logic circuit," in *Proc. 36th European Conference on Optical Communication (ECOC 2010)*, Mo.2.B.3, Torino, Italy, Sept. 2010.

[89] S. Shirai, N. Ohata, H. Aruga, N. Okada, M. Noda, E. Ishimura, and A. Sugitatsu, "High coupling efficiency optical triplexer module for 10G-EPON OLT transceiver," *IEEE Photon. Technol. Lett.*, vol. 23, no. 20, pp. 1529–1531, Oct. 2011.

[90] S. Kimura, "10-Gbit/s TDM-PON and over-40-Gbit/s WDM/TDM-PON systems with OPEX-effective burst-mode technologies," in *Proc. Optical Fiber Communication Conference and National Fiber Optic Engineers Conference (OFC/NFOEC 2009)*, OWH6, San Diego, CA, Mar. 2009.

[91] E. Yagyu, E. Ishimura, M. Nakaji, H. Itamoto, T. Aoyagi, K. Yoshiara, and Y. Tokuda, "Recent advances in AlInsAs Avalanche photodiodes," in *Proc. Optical Fiber Communication Conference and National Fiber Optic Engineers Conference (OFC/NFOEC 2007)*, OThG2, Anaheim, CA, Mar. 2007.

[92] S. Yoshima, N. Nakagawa, N. Kataoka, N. Suzuki, M. Noda, M. Nogami, J. Nakagawa, and K. Kitayama, "10 Gb/s-based PON over OCDMA uplink burst transmission using SSFBG encoder/multi-port decoder and burst-mode receiver," *IEEE/OSA J. Lightw. Technol.*, vol. 28, no. 4, pp. 365–371, Feb. 2010.

[93] X. Wang, N. Wada, T. Miyazaki, G. Cincotti, and K. Kitayama, "Asynchronous multiuser coherent OCDMA system with code-shift-keying and balanced detection," *IEEE J. Sel.*

Topics. Quantum Electron., vol. 13, no. 5, pp. 1463–1470, Sept./Oct. 2007.

[94] F. Daido, T. Okamura, and Y. Miyata, "Considerations on FEC code," in *Presentation Materials, IEEE P802.3av 10G-EPON Task Force, IEEE802 Plenary Meeting*, July 2007 [Online]. Available: http://www.ieee802.org/3/av/public/2007_07/index.html

[95] Y. Awaji, H. Furukawa, and N. Wada, "Adaptive regeneration of optical packet suffering from gain transient of EDFA by using NOLM discriminator," in *Proc. Optical Fiber Communication Conference and National Fiber Optic Engineers Conference (OFC/NFOEC 2008)*, JWA73, San Diego, CA, Feb. 2008.

[96] X. Wang, N. Wada, and K. Kitayama, "Inter-symbol interference and beat noise in flexible data-rate coherent OCDMA and the BER improvement by using optical thresholding," *Optics Express*, vol. 13, no. 26, pp. 10469–10474, Dec. 2005.

[97] X. Wang, N. Wada, T. Miyazaki, G. Cincotti, and K. Kitayama, "Field trial of 3-WDM × 10-OCDMA × 10.71-Gb/s asynchronous WDM/DPSK-OCDMA using hybrid E/D without FEC and optical thresholding," *IEEE/OSA J. Lightw. Technol.*, vol. 25, no. 1, pp. 207–215, Jan. 2007.

[98] X. Wang and K. Kitayama, "Analysis of beat noise in coherent and incoherent time-spreading OCDMA," *IEEE/OSA J. Lightw. Technol.*, vol. 22, no. 10, pp. 2226–2235, Oct. 2004.

[99] X. Wang, N. Kataoka, N. Wada, G. Cincotti, and K. Kitayama, "Flexible 10 Gbps, 8-user DPSK-OCDMA system with 16×16 ports encoder and 16-level phase-shifted SSFBG decoders," in *Proc. Optical Fiber Communication Conference and National Fiber Optic Engineers Conference (OFC/NFOEC 2008)*, OMR2, San Diego, CA, Feb. 2008.

[100] P. C. Teh, P. Petropoulos, M. Ibsen, and D. J. Richardson, "A comparative study of the performance of seven- and 63-chip optical code-division multiple-access encoders and decoders based on superstructured fiber Bragg gratings," *IEEE/OSA J. Lightw. Technol.*, vol. 19, no. 9, pp. 1352–1365, Sept. 2001.

[101] N. Kataoka, G. Cincotti, N. Wada, and K. Kitayama, "100km transmission of dispersion-compensation-free, extended-reach OCDMA-PON system with passive remote node," in *Proc. 15th OptoeElectronics and Communications Conference (OECC 2010)*, 9A3-2, Sapporo, Japan, July 2010.

[102] N. Kataoka. N. Wada, X. Wang, G. Cincotti, A. Sakamoto, Y. Terada, T. Miyazaki, and K. Kitayama, "Field trial of duplex, 10 Gbps × 8-user DPSK-OCDMA system using a single 16 × 16 multi-port encoder/decoder and 16-level phase-shifted SSFBG encoder/decoders," *IEEE/OSA J. Lightw. Technol.*, vol. 27, no. 3. pp. 299–305, Feb. 2009.

[103] S. Yoshima, Y. Tanaka, N. Kataoka, N. Wada, J. Nakagawa, and K. Kitayama, "Full-duplex,

extended-reach 10G-TDM-OCDM-PON system without en/decoder at ONU," *IEEE/OSA J. Lightw. Technol.*, vol. 31, no. 1, pp. 43–49, Jan. 2013.

[104] S. Yoshima, Y. Tanaka, N. Kataoka, N. Wada, J. Nakagawa, and K. Kitayama, "A study on the optical receiver characteristics of long-reach 10G-TDM-OCDM-PON systems," in *Proc. IEICE General Conference*, B-10-71, Gifu, Japan, Mar. 2013.

[105] M. Fujiwara, K. Suzuki, K. Hara, T. Imai, K. Taguchi, H. Ishii, N. Yoshimoto, and H. Hadama, "Burst-mode compound optical amplifier with automatic level control circuit that offers enhanced setting flexibility in a 10 Gb/s-class PON," in *Proc. 36th European Conference on Optical Communication (ECOC 2010)*, PD3.2, Torino, Italy, Sept. 2010.

[106] T. Kodama, Y. Tanaka, S. Yoshima, N. Kataoka, J. Nakagawa, S. Shimizu, N. Wada, and K. Kitayama, "Scaling the system capacity and reach of a 10G-TDM-OCDM-PON system without an en/decoder at an ONU," *IEEE/OSA J. Opt. Commun. Netw.*, vol. 5, no. 2, pp. 134–143, Feb. 2013.

[107] X. Wang, N. Wada, N. Kataoka, T. Miyazaki, G. Cincotti, and K. Kitayama, "100 km field trial of 1.24 Tbit/s, spectral efficient asynchronous 5 WDM×25 DPSK-OCDMA using one set of 50×50 ports large scale en/decoder," in *Proc. Optical Fiber Communication Conference and National Fiber Optic Engineers Conference (OFC/NFOEC 2007)*, PDP14, Anaheim, CA, Mar. 2007.

Acronyms

ACP	autocorrelation peak
ADSL	asynchronous digital subscriber line
AGC	automatic gain control
AOM	acousto-optic modulator
APC	automatic power control
APD	avalanche photo diode
ASE	amplified spontaneous emission
ATC	automatic threshold control
ATM	asynchronous transfer mode
ATT	attenuator
AWG	arrayed waveguide grating
BER	bit error rate
BM	burst-mode
B-PON	broadband passive optical network
BPSK	binary phase shift keying
b/s	bit per second
B-to-B	back-to-back
BWA	broadband mobile access
CATV	cable television
CCP	cross-correlation peak
CDR	clock and data recovery
CID	consecutive identical digit

CLK	clock
CO	central office
DEC	decoder
DFB-LD	distributed feedback laser diode
DML	direct modulated laser
DQPSK	differential quadrature phase shift keying
DSL	digital subscriber line
DSP	digital signal processing
DWDM	dense wavelength division multiplexing
EDFA	erbium-doped fiber amplifier
EEPROM	electrically erasable and programmable read-only memory
ENC	encoder
EML	electro-absorption modulator integrated laser
FBG	fiber Bragg grating
FEC	forward error correction
FFT	fast Fourier transform
FPGA	field programmable gate array
FSAN	full service access network
FSR	free spectral range
FTTH	fiber-to-the-home
FTTX	fiber-to-the-x
G-PON	Gigabit-capable passive optical network
HFC	hybrid fiber and coaxial
IC	integrated circuit
IFDMA	interleaved frequency division multiple access
IFFT	inverse fast Fourier transform
ISDN	integrated services digital network
ISI	inter-symbol interference
LAN	local area network
LD	laser diode
LIA	limiting amplifier
LN	$LiNbO_3$
LN-IM	$LiNbO_3$ intensity modulator
LPF	low pass filter

LTE	long term evolution
MAI	multiple access interference
MM	mask margin
MLLD	mode-locked laser diode
MSL	maximum sidelobe
NB-OBPF	narrow band optical band pass filter
NG-PON	next generation passive optical network
OBPF	optical band pass filter
OC	optical code
OCDM	optical code division multiplexing
OCDMA	optical code division multiple access
ODN	optical distribution network
OFDM	orthogonal frequency division multiplxing
OFDMA	orthogonal frequency division multiple access
OLT	optical line terminal
ONU	optical network unit
OOC	optical orthogonal code
PC	personal computer
PC	polarization controller
PCR	power contrast ratio
PD	photo detector
PLC	planar lightwave circuit
PLL	phase locked loop
POL	polarizer
PON	passive optical network
PPG	pulse pattern generator
PRBS	pseudo-random bit sequence
PSK	phase shift keying
P2MP	point-to-multipoint
P2P	point-to-point
QAM	quadrature amplitude modulation
OSNR	optical signal-to-noise ratio
RN	remote node
RS	Reed-Solomon

RSOA	reflective semiconductor optical amplifier
SMF	single mode fiber
sample/s	sample per second
SSFBG	super-structured fiber Bragg grating
STM	synchronous transfer mode
SW	switch
TDL	tunable delay line
TDM	time division multiplexing
TDMA	time division multiple access
TIA	transimpedance amplifier
TS	time-spreading
TWDM	time and wavelength division multiplexing
WDM	wavelength division multiplexing
WDMA	wavelength division multiple access
XG-PON	10-Gigabit-capable passive optical network
1G-EPON	Gigabit Ethernet passive optical network
10G-EPON	10-Gigabit Ethernet passive optical network
2-D	two-dimensional

List of Publications by the Author

I. Journals

1. S. Yoshima, N. Nakagawa, N. Kataoka, N. Suzuki, M. Noda, M. Nogami, J. Nakagawa, and K. Kitayama, “10 Gb/s-based PON over OCDMA uplink burst transmission using SSFBG encoder/multi-port decoder and burst-mode receiver,” *IEEE/OSA J. Lightw. Technol.*, vol. 28, no. 4, pp. 365–371, Feb. 2010.
2. S. Yoshima, Y. Tanaka, N. Kataoka, N. Wada, J. Nakagawa, and K. Kitayama, “Full-duplex, extended-reach 10G-TDM-OCDM-PON system without en/decoder at ONU,” *IEEE/OSA J. Lightw. Technol.*, vol. 31, no. 1, pp. 43–49, Jan. 2013.

II. International Conferences

1. S. Yoshima, M. Nogami, S. Shirai, N. Suzuki, M. Noda, H. Ichibangase, and J. Nakagawa, “A 10.3 Gbit/s LAN-PHY based burst-mode transmitter with a fast 6 ns turn-on/off time for 10 Gbps-based PON systems,” in *Proc. Optical Fiber Communication Conference and National Fiber Optic Engineers Conference (OFC/NFOEC 2008)*, OWL4, San Diego, CA, Feb. 2008.
2. S. Yoshima, N. Nakagawa, N. Suzuki, M. Noda, M. Nogami, J. Nakagawa, and K. Kitayama, “Demonstration of burst transmission of multiple capacity 10G-PON over

OCDMA uplink using hybrid SSFBG encoder / multi-port decoder and 10 Gbps burst-mode receiver," in *Proc. Optical Fiber Communication Conference and National Fiber Optic Engineers Conference (OFC/NFOEC 2009)*, PDPD4, San Diego, CA, Mar. 2009.

3. S. Yoshima, N. Nakagawa, N. Suzuki, M. Noda, M. Nogami, J. Nakagawa, and K. Kitayama, "10G-PON over OCDMA uplink using hybrid SSFBG encoder / multi-port decoder and 10 Gbps burst-mode receiver," in *Proc. 2009 IEEE/LEOS Summer Topical Meeting (LEOSST '09)*, MA1.3, Newport Beach, CA, July 2009.
4. S. Yoshima, N. Nakagawa, J. Nakagawa, and K. Kitayama, "10G-TDM-OCDMA-PON systems," in *Proc. 15th OptoElectronics and Communications Conference (OECC 2010)*, 9A3-1, Sapporo, Japan, July 2010.
5. S. Yoshima, Y. Tanaka, N. Kataoka, N. Wada, J. Nakagawa, and K. Kitayama, "Full-duplex 10G-TDM-OCDMA-PON system using only a pair of en/decoder," in *Proc. 36th European Conference on Optical Communication (ECOC 2010)*, Tu.3.B.6, Torino, Italy, Sept. 2010.
6. S. Yoshima, M. Noda, E. Igawa, S. Shirai, K. Ishii, M. Nogami, and J. Nakagawa, "Recent progress of high-speed burst-mode transceiver technologies for TDM-PON systems," in *Proc. 21st Annual Wireless and Optical Communications Conference (WOCC 2012)*, N3_3, Kaohsiung, Taiwan, Apr. 2012.

III. Domestic Conferences

1. S. Yoshima, M. Nogami, S. Shirai, N. Suzuki, M. Noda, H. Ichibangase, and J. Nakagawa, "A study on turn-on / off time in a burst-mode optical transmitter for 10Gbps PON," in *Proc. IEICE General Conference*, B-10-56, Fukuoka, Japan, Mar. 2008.
2. S. Yoshima, N. Nakagawa, N. Suzuki, M. Noda, M. Nogami, J. Nakagawa, and K. Kitayama, "A study on multiple 10G-PON system using an OCDMA approach," in *Proc. IEICE Society Conference*, B-10-72, Niigata, Japan, Sept. 2009.
3. S. Yoshima, N. Nakagawa, N. Suzuki, M. Noda, M. Nogami, J. Nakagawa, and K. Kitayama, "A study on uplink burst transmission for 10G-PON over OCDMA systems," in *IEICE Technical Report*, vol. 109, no. 400, OCS2009-101, pp. 9–12, Yamaguchi, Japan, Jan. 2010.

4. S. Yoshima, N. Suzuki, K. Nakura, M. Tanaka, M. Nogami, and J. Nakagawa, “A study on loss budget of dual-rate 10G-EPON systems,” in *Proc. IEICE Society Conference*, B-10-38, Osaka, Japan, Sept. 2010.
5. S. Yoshima, K. Ishii, S. Shirai, M. Noda, N. Suzuki, M. Nogami, and J. Nakagawa, “10.3G/1.25G dual-rate OLT optical transceiver for 10G-EPON systems,” in *IEICE Technical Report*, vol. 110, no. 291, OCS2010-93, pp. 23–28, Osaka, Japan, Nov. 2010.
6. S. Yoshima, Y. Tanaka, N. Kataoka, N. Wada, J. Nakagawa, and K. Kitayama, “A study on the optical receiver characteristics of long-reach 10G-TDM-OCDM-PON systems,” in *Proc. IEICE General Conference*, B-10-71, Gifu, Japan, Mar. 2013.